11. X-RAY MINERALOGY STUDIES – LEG 9

H. E. Cook and I. Zemmels, University of California, Riverside, California

INTRODUCTION

The semi-quantitative determination of mineral composition has been performed according to the methods described in the reports of Legs 1 and 2 and in Appendix III of Volume IV.

Sediments from the equatorial Pacific commonly contain large quantities of volcanic glass, biogenous opaline silica and iron-manganese colloids. These materials, which are X-ray amorphous, tend to dilute and mask the crystalline minerals. The percentage *amorphous scattering* is a measure of the amount of amorphous material in the sample (Rex *et al.*, 1971). In samples which have a very high amorphous scattering value, the number of minerals reported is apt to be small because the weakly diffracting minerals and minerals in low concentrations cannot be detected. Furthermore, the precision of the semi-quantitative determination of those minerals which are detected is lower because of the reduced intensity of diffraction.

In the tables of results of X-ray diffraction analyses (Tables 1 to 9), dashes (–) are used to indicate that a mineral was not detected. The dashes replace the designation 00.0 per cent which was used in the Legs 1 to 7 X-ray mineralogy reports.

No semi-quantitative determinations of the mineral concentrations were made for the 2 to 20 micron fractions. Instead, selected minerals which commonly have an authigenic origin were sought and are reported in Tables 1 to 9 on a ranked scale. The minerals sought were: barite, phillipsite, clinoptilolite, erionite, dolomite, siderite, rhodochrosite, goethite, hematite, magnetite, cristobalite, pyrite and apatite. The minerals were ranked according to whether they constitute the major crystalline phase present (M), whether they are present (P) or whether they are present in trace (barely detectable) amounts (T). Currently, authigenic K-feldspar standards are being processed to assist in the discrimination between allogenic and authigenic K-feldspar.

Goethite was detected in several <2 micron samples from Leg 9 (Hole 76A, Cores 1 and 2; Hole 78, Core 9). A suitable mineral standard which resembles the poorly crystalline goethite occurring in deep marine sediments has not yet been obtained. Consequently a semi-quantitative estimate of the goethite content was not possible. Where the mineral was detected, a P was placed in the mineral tables.

Barite was frequently found in the Leg 9 sediments. Drilling mud was not used on this leg, and the barite is considered to be of natural origin.

The X-ray mineralogy results are discussed in the framework of the oceanic formations developed for the equatorial Pacific by Tracey *et al.* (Leg 8) and by Cook (Chapter 22, this volume).

RESULTS

Site 76

This site is located about 100 kilometers northeast of the Tuamotu coral-volcanic Archipelago in an area underlain by a thick sequence of apparently well-bedded sediments. A highly varied sequence of dusky brown volcanic zeolitic clay, carbonate ooze, and allochthonous carbonate debris beds were recovered. This sequence, which is Pliocene to Pleistocene in age, is divided into five units. Drilling was terminated at about 30 meters in a brown silicified foraminiferal (?) limestone.

Unit one is predominantly a massive, dark brown zeolitic clay with a few interbedded allodapics[1] debris beds. A high percentage of amorphous iron-manganese colloids probably gives the sediment its dark brown color and also masks the crystalline minerals. Calcite, quartz, and phillipsite are the only minerals detected in the composited sample of the bulk fraction (Figure 1). Two individual samples, however, contain montmorillonite, mica, apatite and clinoptilolite in addition to calcite, quartz and phillipsite (Figures 1 and 2; Table 1).

[1]Meischner (1964) proposed the term allodapic for shoal-water organic and inorganic carbonate sands which were transported (allochthonous) to a contemporaneous deeper water environment before they were lithified.

TABLE 1
Results of X-Ray Diffraction Analysis from Site 76

Table 1a. Hole 76, Bulk

Core	Depth	Sample Depth (m. below sea floor)	Diff.	Amorph.	Calc.	Quar.	Mica	Clin.	Phil.
1	0-9.1	0.12-8.23	79.7	68.3	62.7	–		–	37.3
		1.58	87.5	80.5	–	3.5	14.7	2.2	79.6
		7.78	86.7	79.2	13.0	2.7	–	1.5	82.8

Table 1a. Hole 76, 2-20μ

Core	Depth	Sample Depth (m. below sea floor)	Lithostratigraphy Formation	Lithostratigraphy Unit	Amorph.	Clin.	Phil.
1	0-9.1	0.12-8.23	Undetermined	1	80	P	M
		1.58			66	P	M
		7.78			58	P	M

Table 1a. Hole 76, $< 2\mu$

Core	Depth	Sample Depth (m. below sea floor)	Diff.	Amorph.	Quar.	Mica	Mont.	Phil.	Apat.
1	0-9.1	0.12-823	98.6	97.8	5.3	–	–	70.0	24.7
		1.58	93.6	90.0	3.8	16.1	38.5	35.8	5.8
		7.78	94.2	90.0	3.1	–	50.9	29.5	16.5

Table 1b. Hole 76A, Bulk

Core	Depth	Sample Depth (m. below sea floor)	Diff.	Amorph.	Calc.	Quar.	Phil.
1	9.1-18.2	9.21	69.0	51.6	77.1	–	22.9
		9.63-12.10	65.3	45.8	87.0	–	13.0
		17.56	63.9	43.6	100.0	–	–
2	18.2-29.3	18.84-21.27	69.3	52.0	87.0	–	13.0
		21.89-27.02	65.0	45.3	100.0	–	–
		26.69	83.3	73.8	41.9	2.1	56.0

TABLE 1 – *Continued*

Table 1b. Hole 76A, 2-20μ

Core	Depth	Sample Depth (m. below sea floor)	Lithostratigraphy Formation	Unit	Amorph.	Side.	Clin.	Phil.	Apat.
1	9.1-18.2	9.21	Undetermined		76			M	
		9.63-12.10		2	74	P	P	M	T
		17.56		3	95			M	
2	18.2-27.3	18.84-21.27		4	61			M	
		21.89-27.02		5	85			M	
		26.69			64		P	M	

Table 1b. Hole 76A, < 2μ

Core	Depth	Sample Depth (m. below sea floor)	Diff.	Amorph.	Quar.	Kaol.	Mica	Mont.	Phil.	Apat.	Goet.
1	9.1-18.2	9.63-12.10	93.5	89.8	3.3	–	–	48.8	35.4	12.5	P
		17.56	99.3	98.9	–	–	–	100.0	–	–	–
2	18.2-27.3	18.84-21.27	94.2	90.0	4.2	–	–	34.1	46.2	15.5	P
		21.89-27.02	95.1	92.3	4.3	2.6	26.8	17.5	40.6	8.4	–
		26.69	92.8	88.8	3.2	2.4	–	64.6	20.6	9.3	P

TABLE 2
Results of X-Ray Diffraction Analysis from Site 76

Table 2a. Hole 77, Bulk

Core	Depth	Sample Depth (m. below sea floor)	Diff.	Amorph.	Calc.
1	0-9.1	0.04	67.7	49.5	100.0

Table 2a. Hole 77, 2-20μ

Core	Depth	Sample Depth (m. below sea floor)	Lithostratigraphy Formation	Unit	Amorph.
1	0-9.1	0.04	Clipperton	Cyclic	100

Table 2a. Hole 77, < 2μ

Core	Depth	Sample Depth (m. below sea floor)	Diff.	Amorph.	Quar.	K-Fe.	Plag.	Mica	Chlor.	Mont.
1	0-9.1	0.04	99.4	99.1	14.5	20.0	8.0	25.6	16.3	15.5

Table 2b. Hole 77A, Bulk

Core	Depth	Sample Depth (m. below sea floor)	Diff.	Amorph.	Calc.
1	0-9.1	0.08-8.22	68.3	50.5	100.0

Table 2b. Hole 77A, 2-20μ

Core	Depth	Sample Depth (m. below sea floor)	Lithostratigraphy Formation	Unit	Amorph.	Bari.
1	0-9.1	0.08-8.22	Clipperton	Cyclic	96	M

Table 2b. Hole 77A, < 2μ

Core	Depth	Sample Depth (m. below sea floor)	Diff.	Amorph.	Quar.	K-Fe.	Plag.	Kaol.	Mont.	Bari.
1	0-9.1	0.08-8.22	99.3	98.9	11.2	11.7	10.7	17.0	31.6	17.8

Table 2c. Hole 77B, Bulk

Core	Depth	Sample Depth (m. below sea floor)	Diff.	Amorph.	Calc.	Quar.	Plag.	Mica	Mont.	Clin.	Bari.
1	9.1-18.2	9.35	67.2	48.8	100.0	–	–	–	–	–	–
		9.88-17.42	66.4	47.5	100.0	–	–	–	–	–	–
2	18.2-27.3	18.41-19.24	69.5	52.3	100.0	–	–	–	–	–	–
		19.80-26.53	67.4	49.1	100.0	–	–	–	–	–	–
3	27.3-36.6	27.33-28.11	67.7	49.5	100.0	–	–	–	–	–	–
		28.85-34.12	66.8	48.1	100.0	–	–	–	–	–	–
4	36.6-45.6	36.65-44.92	69.1	51.7	100.0	–	–	–	–	–	–
5	45.6-5.84	45.70-46.34	71.3	55.2	100.0	–	–	–	–	–	–
		47.20-53.92	72.7	57.3	100.0	–	–	–	–	–	–
6	54.8-64.0	54.85-63.12	69.5	52.3	100.0	–	–	–	–	–	–
7	64.0-73.1	64.05-72.30	64.6	44.7	100.0	–	–	–	–	–	–
8	73.1-82.2	76.15-81.42	65.5	46.1	100.0	–	–	–	–	–	–
9	82.2-91.5	83.75-90.52	63.3	42.7	100.0	–	–	–	–	–	–
10	91.5-100.6	93.05-99.82	62.6	41.6	100.0	–	–	–	–	–	–
12	109.6-118.8	109.64-117.92	63.2	42.5	100.0	–	–	–	–	–	–
13	118.8-128.0	120.35-127.12	64.8	45.0	100.0	–	–	–	–	–	–
14	128.0-137.1	129.55-136.32	67.1	48.6	100.0	–	–	–	–	–	–
15	137.1-146.2	138.67-145.42	62.2	40.9	100.0	–	–	–	–	–	–
16	146.2-155.5	147.75-151.52	67.8	49.7	100.0	–	–	–	–	–	–
		153.75-154.52	65.3	45.8	100.0	–	–	–	–	–	–
17	155.5-161.6	155.55-161.50	64.8	45.0	100.0	–	–	–	–	–	–
18	161.6-170.6	163.15-169.62	69.8	52.8	100.0	–	–	–	–	–	–

TABLE 2 – *Continued*

Table 2c. Hole 77B, Bulk – *Continued*

Core	Depth	Sample Depth (m. below sea floor)	Diff.	Amorph.	Calc.	Quar.	Plag.	Mica	Mont.	Clin.	Bari.
19	170.6-179.9	170.65-171.52	66.1	47.0	100.0	–	–	–	–	–	–
		172.32-178.92	64.6	44.7	100.0	–	–	–	–	–	–
20	179.7-189.0	181.25-188.12	61.4	39.7	100.0	–	–	–	–	–	–
21	189.0-198.1	189.05-195.82	61.1	39.2	100.0	–	–	–	–	–	–
22	198.1-207.2	199.65-206.42	62.2	40.9	100.0	–	–	–	–	–	–
23	207.2-216.3	208.75-215.52	60.6	38.4	100.0	–	–	–	–	–	–
24	216.3-225.6	217.85-218.62	60.6	38.4	100.0	–	–	–	–	–	–
		222.37-224.62	61.4	39.7	100.0	–	–	–	–	–	–
25	225.6-234.6	227.15-233.92	62.0	40.6	100.0	–	–	–	–	–	–
26	234.6-243.8	236.25-242.92	62.0	40.6	100.0	–	–	–	–	–	–
27	243.8-253.0	243.85-252.12	65.6	46.2	100.0	–	–	–	–	–	–
28	253.0-262.1	254.55-261.32	65.2	45.6	100.0	–	–	–	–	–	–
29	262.1-271.2	263.65-270.42	62.2	40.9	100.0	–	–	–	–	–	–
30	271.2-280.3	272.75-279.52	61.1	39.2	100.0	–	–	–	–	–	–
31	280.3-289.6	281.94-288.62	60.3	38.0	100.0	–	–	–	–	–	–
32	298.6-298.6	291.15-297.92	60.7	38.6	100.0	–	–	–	–	–	–
33	298.6-307.8	300.20-306.92	60.7	38.6	100.0	–	–	–	–	–	–
34	307.8-317.0	309.36	60.9	38.9	100.0	–	–	–	–	–	–
		310.10-315.37	60.2	37.8	100.0	–	–	–	–	–	–
36	326.1-335.2	327.65-329.17	60.8	38.8	100.0	–	–	–	–	–	–
37	335.2-344.3	336.75-341.27	60.9	38.9	100.0	–	–	–	–	–	–
		342.76	60.0	37.5	100.0	–	–	–	–	–	–

Table 2c. Hole 77B, Bulk – *Continued*

Core	Depth	Sample Depth (m. below sea floor)	Diff.	Amorph.	Calc.	Quar.	Plag.	Mica	Mont.	Clin.	Bari.
38	344.3-353.6	346.02	60.7	38.6	100.0	–	–	–	–	–	–
39	353.6-362.6	355.34-361.17	59.1	36.1	100.0	–	–	–	–	–	–
40	362.6-371.8	364.15-367.17	59.6	36.9	100.0	–	–	–	–	–	–
41	371.8-381.0	373.35-379.37	59.2	36.2	100.0	–	–	–	–	–	–
42	381.0-390.1	382.60-388.57	58.8	35.6	100.0	–	–	–	–	–	–
43	390.1-399.2	391.65-397.67	59.1	36.1	100.0	–	–	–	–	–	–
44	399.2-408.3	400.65-406.72	58.7	35.5	100.0	–	–	–	–	–	–
45	408.3-417.6	409.86	59.8	37.2	100.0	–	–	–	–	–	–
		414.35-415.87	60.0	37.5	100.0	–	–	–	–	–	–
46	476.6-426.6	419.15-425.17	58.7	35.5	100.0	–	–	–	–	–	–
47	426.6-435.8	428.15-431.17	64.5	44.5	100.0	–	–	–	–	–	–
48	435.8-445.0	437.70-443.39	64.0	43.8	100.0	–	–	–	–	–	–
49	445.0-454.1	446.60-454.00	61.3	39.5	100.0	–	–	–	–	–	–
50	454.1-463.2	456.08	60.5	38.3	100.0	–	–	–	–	–	–
51	463.2-470.8	468.25-469.77	61.3	39.5	100.0	–	–	–	–	–	–
52	470.8-476.3	471.60	79.7	68.3	100.0	–	–	–	–	–	–
		472.36	90.6	85.3	7.1	4.6	27.8	16.0	20.9	8.3	15.3
53	476.3-481.0	476.93	83.7	74.5	90.7	–	–	–	9.3	–	–

TABLE 2 – *Continued*

Table 2c. Hole 77B, 2-20μ

Core	Depth	Sample Depth (m. below sea floor)	Lithostratigraphy Formation	Lithostratigraphy Unit	Amorph.	Side.	Cris.	Clin.	Bari.	Apat.	Magn.
1	9.1-18.2	9.35	Clipperton	Cyclic	100				M		
		9.88-17.42	Clipperton	Cyclic	96				M		
2	18.2-27.3	18.42-19.24	Clipperton	Cyclic	97				M		
		19.80-26.53	Clipperton	Cyclic	96				M		
3	27.3-36.6	27.33-28.11	Clipperton	Cyclic	98				M		
		28.85-34.12	Clipperton	Cyclic	95				M		
4	36.6-45.6	36.65-44.92	Clipperton	Cyclic	95				M		
5	45.6-54.8	45.70-46.34	Clipperton		97	P			M	T	
		47.20-53.92	Clipperton		97				M		
6	54.8-64.0	54.85-63.12	Clipperton		97				M		
7	64.0-73.1	64.05-72.30	Clipperton		99				M		
8	73.1-82.2	76.15-81.42	Clipperton		98	P			M		
9	82.2-91.5	83.75-90.52	Clipperton		97				M		
10	91.5-100.6	93.05-99.82	Clipperton		97				M		
12	109.6-118.8	109.64-117.92	Clipperton		99				M		
13	118.8-128.0	120.35-127.12	Clipperton	Varicolored	100	P			M		
14	128.0-137.1	129.55-136.32	Clipperton		98				M		
15	137.1-146.2	138.67-145.42	Clipperton		94				M		
16	146.2-155.5	147.75-151.52	Clipperton		96				M		
		153.75-154.52	Clipperton		100						
17	155.5-161.6	155.55-161.50	Clipperton		98				M		

Table 2c. Hole 77B, 2-20μ – *Continued*

Core	Depth	Sample Depth (m. below sea floor)	Lithostratigraphy Formation	Unit	Amorph.	Side.	Cris.	Clin.	Bari.	Apat.	Magn.
18	161.6-170.6	163.15-169.62	Clipperton		95				M		
19	170.6-179.7	170.65-171.52	Clipperton		97				M		
		172-32-178.92	Marquesas	Grey	100						
20	179.7-189.0	181.25-188.12	Marquesas	Grey	99				M		
21	189.0-198.1	189.05-195.82	Marquesas	Grey	99				M		
22	198.1-207.2	199.65-206.42	Marquesas	Grey	98				M		
23	207.2-216.3	208.75-215.52	Marquesas	Grey	97				M		
24	216.3-225.6	217.85-218.62	Marquesas	Grey	97				M		
	216.4-225.6	222.37-224.62	Marquesas	Grey	97				M		
25	225.6-234.6	227.15-233.92	Marquesas	Grey	92				M		
26	234.6-243.8	236.25-242.92	Marquesas	Grey	98				M		
27	243.8-253.0	243.85-252.12	Marquesas	Grey	97				M		
28	253.0-262.1	254.55-261.32	Marquesas	Brown	89				M		
30	271.2-280.3	272.75-279.52	Marquesas	Brown	88				M		P
31	280.3-289.6	281.94-288.62	Marquesas	Grey	88				M		
32	289.6-298.6	291.15-297.92	Marquesas	Grey	84				M		
33	298.6-307.8	300.20-306.92	Marquesas	Grey	90				M		P
34	307.8-317.0	309.36	Marquesas	Grey	97				M		
		310.10-315.37	Marquesas	Grey	92				M		
36	326.1-335.2	327.65-329.17	Marquesas	Grey	96				M		
37	335.2-344.3	336.75-341.27	Marquesas	Grey	92				M		
38	344.3-353.6	346.02	Marquesas	Grey	98				M		

TABLE 2 – *Continued*

Table 2c. Hole 77B, 2-20μ – *Continued*

Core	Depth	Sample Depth (m. below sea floor)	Lithostratigraphy Formation	Lithostratigraphy Unit	Amorph.	Side.	Cris.	Clin.	Bari.	Apat.	Magn.
39	353.6-362.6	355.34-361.17			88				M		
40	362.6-371.8	364.15-367.17			87				M		
41	371.8-381.0	373.35-379.37			88				M		
42	381.0-390.1	382.60-388.57		Grey	93				M		
43	390.1-399.2	391.65-397.67			89				M		
44	399.2-408.3	400.65-406.72			93				M		
45	408.3-417.6	409.86		Brown	99						
		414.35-415.87		Brown	96		M		P		
46	417.6-426.6	419.15-425.17	Marquesas		92				M		
47	426.6-435.8	428.15-431.17			100				M		
48	435.8-445.0	437.70-443.39		Grey	98				M		
49	445.0-454.1	446.60-454.00			91				M		
50	454.1-463.2	456.08			92				M		
51	463.2-470.8	468.25-469.77			91				M		
52	470.8-476.3	471.60			97						
	470.8-476.3	472.36						P	M		
53	476.3-481.0	476.93	Line Islands				M				

Table 2c. Hole 77B, <2μ

Core	Depth	Sample Depth (m. below sea floor)	Diff.	Amorph.	Side.	Quar.	K-Fe.	Plag.	Kaol.	Mica	Mont.	Bari.
1	9.1-18.2	9.35	97.1	95.5	–	9.0	7.8	7.8	10.1	42.5	18.4	4.5
		9.88-17.42	96.7	94.8	–	9.3	3.0	6.8	9.7	32.5	31.8	7.0
2	18.2-27.3	18.41-19.24	96.0	93.8	–	10.1	2.8	9.3	9.0	28.4	30.8	9.6
		19.80-26.53	96.5	94.5	–	11.8	5.6	9.4	12.8	28.8	22.8	8.8
3	27.3-36.6	27.33-28.11	97.0	95.3	–	6.7	8.7	8.7	–	–	64.4	11.4
		28.85-34.12	95.3	92.7	–	3.4	–	4.8	7.5	23.2	51.5	9.6

Table 2c. Hole 77B, $<2\mu$ – *Continued*

Core	Depth	Sample Below (m. below sea floor)	Diff.	Amorph.	Side.	Quar.	K-Fe.	Plag.	Kaol.	Mica	Mont.	Bari.
4	36.6-45.6	36.65-44.92	100.0	100.0	–	–	–	–	–	–	–	–
5	45.6-54.8	45.70-46.34	98.0	96.9	–	14.4	5.5	10.1	–	–	59.1	10.8
		47.20-53.92	94.9	92.0	–	5.8	–	6.5	–	–	68.7	19.0
6	54.8-64.0	54.85-63.12	99.6	99.4	–	2.3	6.1	6.1	–	–	69.6	15.9
7	64.0-73.1	64.05-72.30	99.4	99.1	–	1.7	–	8.5	15.8	39.8	17.3	16.9
8	73.1-82.2	76.15-81.42	100.0	100.0	–	–	–	–	–	–	–	–
9	82.2-91.5	83.75-90.52	100.0	100.0	–	–	–	–	–	–	–	–
10	91.5-100.6	93.05-99.82	99.8	99.7	–	5.4	–	–	–	–	66.3	28.3
12	109.6-118.8	109.64-117.92	100.0	100.0	–	–	–	–	–	–	–	–
13	118.8-128.0	120.35-127.12	100.0	100.0	–	–	–	–	–	–	–	–
14	128.0-137.1	129.55-136.32	99.1	98.6	–	7.7	–	–	–	–	66.1	26.2
16	146.2-155.5	147.75-151.52	99.8	99.7	–	42.0	–	–	–	–	–	58.0
		153.75-154.52	99.8	99.7	–	37.1	–	–	–	–	–	62.9
17	155.5-161.6	155.55-161.50	99.5	99.2	–	–	–	–	–	–	–	100.0
18	161.6-170.6	163.15-169.62	98.7	98.0	–	1.9	–	–	–	–	69.4	28.8
19	170.6-179.7	170.65-171.52	99.7	99.5	–	–	–	–	–	–	–	100.0
20	179.7-189.0	181.25-188.12	99.7	99.5	–	23.6	–	–	–	–	–	76.4
21	189.0-198.1	189.05-195.82	99.7	99.5	–	–	–	–	–	–	–	100.0
22	198.1-207.2	199.65-206.42	98.9	98.3	–	7.6	–	–	–	–	71.4	21.0
23	207.2-216.3	208.75-215.52	98.9	98.3	–	20.8	–	–	–	–	–	79.2
24	216.3-225.6	217.85-218.62	99.6	99.4	–	–	–	–	–	–	58.9	41.1
		222.37-224.62	98.3	97.3	–	6.8	–	–	–	–	71.7	21.5
25	225.6-234.6	227.15-233.92	97.6	96.2	–	3.6	–	–	–	–	40.5	55.9
26	234.6-243.8	236.25-242.92	98.3	97.3	–	3.6	–	–	–	–	40.5	55.9
28	253.0-262.1	254.55-261.32	92.6	88.4	–	5.5	–	–	–	–	82.7	11.8
29	262.1-271.2	263.65-270.42	95.0	92.2	–	–	–	–	–	–	93.2	6.8

TABLE 2 – *Continued*

Table 2c. Hole 77B, <2μ – *Continued*

Core	Depth	Sample Depth (m. below sea floor)	Diff.	Amorph.	Side.	Quar.	K-Fe.	Plag.	Kaol.	Mica	Mont.	Bari.
30	271.2-280.3	272.75-279.52	90.1	84.5	–	5.8	–	–	–	–	73.6	20.6
31	280.3-289.6	281.94-288.62	90.0	84.4	–	3.2	–	–	–	–	89.2	7.5
33	298.6-307.8	300.20-306.92	90.3	84.8	–	3.2	–	–	–	–	81.7	15.1
34	307.8-317.0	310.10-315.37	88.8	82.5	–	3.5	–	–	–	–	86.8	9.7
37	335.2-344.3	336.75-341.27	88.9	82.7	–	2.8	–	1.2	–	8.7	84.9	1.6
38	344.3-353.6	346.02	99.3	98.9	–	9.7	8.9	12.4	–	58.2	–	10.8
39	353.6-362.6	355.34-361.17	94.1	90.8	–	15.9	–	7.0	4.1	54.5	–	18.5
40	362.6-371.8	364.15-367.17	97.6	96.2	–	9.5	5.9	9.0	7.1	57.2	–	10.6
41	371.8-381.0	373.35-379.37	97.5	96.1	–	9.2	7.9	10.1	7.5	53.1	–	12.2
42	381.0-390.1	382.60-388.57	99.8	99.7	–	6.4	6.4	8.9	–	69.5	–	8.8
43	390.1-399.2	391.65-397.67	99.6	99.4	–	5.5	6.6	10.6	–	65.6	–	11.6
44	399.2-408.3	400.65-406.72	99.7	99.5	–	6.1	6.7	10.0	10.2	36.5	23.8	6.8
45	408.3-417.6	409.86	100.0	100.0	–	–	–	–	–	–	–	–
		414.35-415.87	99.8	99.7	–	100.0	–	–	–	–	–	–
46	417.6-426.6	419.15-425.17	99.9	99.8	–	100.0	–	–	–	–	–	–
47	426.6-435.8	428.15-431.17	98.4	97.5	–	17.4	–	–	18.3	–	64.3	–
48	435.8-445.0	437.70-443.39	97.9	96.7	10.5	7.2	12.4	9.0	–	–	56.0	4.9
49	445.0-454.1	446.60-454.00	94.5	91.4	11.3	6.1	–	–	–	59.4	23.2	–
50	454.1-463.2	456.08	98.0	96.9	5.4	7.0	6.4	5.6	6.3	17.6	51.6	–
51	463.2-470.8	468.25-469.77	100.0	100.0	–	–	–	–	–	–	–	–
52	470.8-476.3	471.60	98.5	97.7	–	–	–	–	–	–	100.0	–
		472.36	91.0	85.9	–	15.8	–	37.8	–	–	13.5	32.9
53	476.3-481.0	476.93	91.4	86.6	–	–	–	–	–	–	97.9	–

TABLE 3
Results of X-Ray Diffraction Analysis from Site 78

Hole 78, Bulk

Core	Depth	Sample Depth (m. below sea floor)	Diff.	Amorph.	Calc.
1	0-9.1	1.55-7.57	55.9	31.1	100.0
2	9.1-18.2	10.65-16.67	59.4	36.6	100.0
3	18.2-27.4	19.76	53.0	26.6	100.0
		23.01	52.1	25.2	100.0
		25.84	57.1	33.0	100.0
4	27.4-36.6	28.95-34.97	60.4	38.1	100.0
5	36.6-45.7	39.00-44.17	56.3	31.7	100.0
6	45.7-54.9	47.26	57.0	32.8	100.0
		50.25-53.27	52.7	26.1	100.0
7	54.9-64.0	55.45-60.97	49.5	21.1	100.0
8	64.0-73.1	64.68	55.5	30.5	100.0
9	73.1-82.3	80.66	51.7	24.5	100.0
10	82.3-91.4	82.35-89.87	49.4	20.9	100.0
11	91.4-100.6	92.95-98.97	48.8	20.0	100.0
12	100.6-109.9	105.15-108.17	49.4	20.9	100.0
13	109.7-118.9	111.20-117.27	51.4	24.1	100.0
14	118.9-128.0	122.45-125.47	52.8	26.2	100.0
15	128.0-137.1	132.55-135.57	51.6	24.4	100.0
16	137.1-146.3	141.65-146.10	52.8	26.2	100.0
17	146.3-155.4	147.85-150.87	51.1	23.6	100.0
18	155.4-164.6	163.11	51.2	23.8	100.0
19	164.6-173.7	169.15-172.19	50.0	21.9	100.0
20	173.7-182.9	175.25-181.29	50.0	21.9	100.0
21	182.9-192.2	184.43-190.47	50.6	22.8	100.0
22	192.2-201.2	199.87	48.2	19.1	100.0
23	201.2-210.3	205.75-208.77	48.2	19.1	100.0

TABLE 3 – *Continued*

Hole 78, Bulk – *Continued*

Core	Depth	Sample Depth (m. below sea floor)	Diff.	Amorph.	Calc.
24	210.3-219.4	211.94	50.1	22.0	100.0
25	219.4-228.6	223.95-226.97	48.0	18.8	100.0
27	237.7-246.9	242.47-245.27	47.2	17.5	100.0
28	246.9-256.0	251.45-254.69	48.2	19.1	100.0
29	256.0-265.1	265.56	46.7	16.7	100.0
30	265.1-274.3	272.74	46.9	17.0	100.0
31	274.3-283.5	281.83	48.9	20.2	100.0
32	283.5-292.6	291.06	50.1	22.0	100.0
35	310.9-320.0	319.01	55.9	31.1	100.0

Hole 78, 2-20μ

			Lithostratigraphy							
Core	Depth	Sample Depth (m. below sea floor)	Formation	Unit	Amorph.	Cris.	Clin.	Bari.	Magn.	Goet.
1	0-9.1	1.55-7.57			85			M		
2	9.1-18.2	10.65-16.67			88			M		
3	18.2-27.4	19.76			90		M	P		
		23.01			94			M		
		25.84			89			M		
4	27.4-36.6	28.95-34.97			89		P	M		
5	36.6-45.7	39.00-44.17			87			M		
6	45.7-54.9	47.26			92			M		
		50.25-53.27			93			M		
7	54.9-64.0	55.45-60.97			96			M		
8	64.0-73.1	64.68			92			M		
10	82.3-91.4	82.35-89.87			92			M		
11	91.4-100.6	92.95-98.97			90			M		
12	100.6-109.7	105.15-108.17			90			M		

TABLE 3 – *Continued*

Hole 78, 2-20μ – *Continued*

Core	Depth	Sample Depth (m. below sea floor)	Lithostratigraphy Formation	Lithostratigraphy Unit	Amorph.	Cris.	Clin.	Bari.	Magn.	Goet.
13	109.7-118.9	111.20-117.27			94			M		
14	118.9-128.0	122.45-125.47			92		P	M		
15	128.0-137.1	132.55-135.57			90			M		
16	137.1-146.3	141.65-146.10			89			M		
17	146.3-155.4	147.85-150.87			93			M		
18	155.4-164.6	163.11			94			M		
19	164.6-173.7	169.15-172.17			90			M		
20	173.7-182.9	175.25-181.29			91			M		
21	182.9-192.2	184.43-190.47			94			M	P	
22	192.2-201.2	199.87			99					
23	201.2-210.3	205.75-208.77			89			M		
24	210.3-219.4	211.94			89			M		
25	219.4-228.6	223.95-226.97			99			M		
27	237.7-246.9	242.47-245.27			97	M				
28	246.9-256.0	251.45-254.69			94			M		
29	256.0-265.1	263.56			96	P		M		
30	265.1-274.3	272.74			98	P		M		
31	274.3-283.5	281.83			98	M				
32	283.5-292.6	291.06			94	P		M		
35	310.9-320.0	319.01	Line Islands		94			P		

TABLE 3 – *Continued*

Hole 78, <2μ

Core	Depth	Sample Depth (m. below sea floor)	Diff.	Amorph.	Quar.	Cris.	K-Fe.	Plag.	Kaol.	Mica	Mont.	Bari.	Goet.
1	0-9.1	1.55-7.57	92.7	88.6	6.0	–	–	13.3	9.3	22.4	43.7	5.3	–
2	9.1-18.2	10.65-10.67	90.7	85.5	8.1	–	–	22.5	6.5	7.2	43.6	12.1	–
3	18.2-27.4	19.76	97.8	96.6	3.3	25.8	–	–	–	–	70.9	–	–
		23.01	94.5	91.4	4.8	4.6	–	10.2	6.6	32.6	36.3	4.9	–
		25.84	91.0	85.9	3.6	–	–	8.4	–	–	85.9	2.1	–
4	27.4-36.6	28.95-34.97	93.9	90.5	4.0	–	–	7.8	3.4	18.9	61.4	4.5	–
5	36.6-45.7	39.00-44.17	90.6	85.3	2.2	–	–	5.1	2.2	11.6	75.3	3.7	–
6	45.7-54.9	47.26	90.6	85.3	1.2	–	–	4.3	2.8	11.8	76.7	3.2	–
		50.25-53.27	88.5	82.0	1.9	–	–	9.6	–	–	76.4	12.1	–
7	54.9-64.0	55.45-60.97	90.0	84.4		–	–	1.2	–	–	95.5	2.9	–
8	64.0-73.1	64.68	90.7	85.5	1.9	–	–	3.0	1.9	–	91.2	2.0	–
9	73.1-82.3	80.66	90.8	85.6	–	–	–	–	–	–	100.0	–	P
10	82.3-91.4	82.35-89.87	89.2	83.1	1.6	–	3.6	2.9	–	–	86.8	5.1	–
11	91.4-100.6	92.95-98.97	84.9	76.4	–	–	–	–	–	–	98.0	1.3	–
12	100.6-109.7	105.15-108.17	87.4	80.3	–	–	–	1.2	–	–	94.9	3.1	–
13	109.7-118.9	111.20-117.27	88.0	81.2	–	–	–	4.7	–	–	84.3	10.7	–
14	118.9-128.0	122.45-125.47	88.6	82.2	–	–	–	1.2	–	–	96.0	2.0	–
15	128.0-137.1	132.55-135.57	88.3	81.7	2.1	–	–	6.2	3.5	20.0	56.5	11.7	–
16	137.1-146.3	141.65-146.10	87.6	80.6	–	–	–	2.1	–	–	95.1	2.6	–
17	146.3-155.4	147.85-150.87	90.6	85.3	2.3	–	7.0	6.3	–	–	68.7	15.7	–
18	155.4-164.6	163.11	92.3	88.0	1.2	–	–	3.0	2.0	–	90.2	3.5	–
19	164.6-173.7	169.15-172.17	89.5	83.6	1.3	–	–	–	–	–	95.9	2.8	–
20	173.7-182.9	175.25-181.29	89.5	83.6	5.8	–	–	6.5	2.6	–	72.0	13.2	–
21	182.9-192.2	184.43-190.47	91.3	86.4	1.3	–	2.7	6.1	–	–	80.6	9.2	–
22	192.2-201.2	199.87	93.6	90.0	2.0	–	–	2.3	–	–	95.7	–	–
23	201.2-210.3	205.75-208.77	90.9	85.8	–	–	2.6	4.4	–	–	86.2	6.7	–

TABLE 3 – *Continued*

Hole 78, < 2μ – *Continued*

Core	Depth	Sample Depth (m. below sea floor)	Diff.	Amorph.	Quar.	Cris.	K-Fe.	Plag.	Kaol.	Mica	Mont.	Bari.	Goet.
24	210.3-219.4	211.94	90.6	85.3	1.1	–	–	4.6	–	–	86.4	7.8	–
25	219.4-228.6	223.95-226.97	91.6	86.9	1.1	–	–	2.8	–	15.2	76.2	4.6	–
27	237.7-246.9	242.47-245.27	93.5	89.8	–	–	1.6	4.1	2.6	27.0	58.7	5.0	–
28	246.9-256.0	251.45-254.69	91.7	87.0	1.1	–	–	2.3	–	12.4	80.7	3.5	–
29	256.0-265.1	263.56	91.9	87.3	–	–	–	2.4	2.6	12.0	78.1	5.0	–
30	265.1-274.3	272.74	93.7	90.2	–	–	–	–	–	–	97.3	2.2	–
31	274.3-283.5	281.83	93.2	89.4	1.5	–	–	8.5	–	–	90.0	–	–
32	283.5-292.6	291.06	89.7	83.9	2.0	–	–	–	–	–	96.2	1.8	–
35	310.9-320.0	319.01	86.9	79.5	1.0	–	–	–	–	–	99.0	–	–

TABLE 4
Results of X-Ray Diffraction Analysis from Site 79

Table 4a. Hole 79, Bulk

Core	Depth	Sample Depth (m. below sea floor)	Diff.	Amorph.	Calc.
1	0-9.1	1.54-7.57	65.5	46.1	100.0
2	60.3-69.5	60.35-66.37	63.0	42.2	100.0
		67.86	55.6	30.6	100.0
3	126.8-135.9	126.85-134.37	58.8	35.6	100.0
4	193.5-202.7	193.55-199.57	58.5	35.2	100.0
5	260.3-269.4	263.35-267.87	52.7	26.1	100.0
6	326.7-335.9	327.60-332.77	65.0	45.3	100.0
7	335.9-345.0	336.04-342.72	59.1	36.1	100.0
8	395.0-350.1	345.05-351.00	60.8	38.8	100.0
9	350.1-355.7	350.15-353.17	51.3	23.9	100.0
10	355.7-364.2	357.25-359.27	51.7	24.5	100.0
11	364.2-373.4	365.75-371.77	50.1	22.0	100.0
12	373.4-380.4*	373.50-376.47	48.9	20.2	100.0
		377.95-380.97	51.6	24.4	100.0
13	380.4-389.5*	382.60-387.97	51.0	23.4	100.0
14	389.5-398.7	389.55-397.07	51.7	24.5	100.0
15	398.7-406.0	400.26	49.5	21.1	100.0
16	406.0-413.6	409.06	49.3	20.8	100.0

Table 4a. Hole 79, 2-20μ

Core	Depth	Sample Depth (m. below sea floor)	Lithostratigraphy Formation	Lithostratigraphy Unit	Amorph.	Dolo.	Bari.
1	0-9.1	1.54-7.57		Cyclic	98		M
2	60.3-69.5	60.35-66.37			95		M
		67.86			99		

*Depth changed on plot in order to accommodate samples received.

Table 4a. Hole 79, 2-20μ – *Continued*

Core	Depth	Sample Depth (m. below sea floor)	Lithostratigraphy Formation	Unit	Amorph.	Dolo.	Bari.
3	126.8-135.9	126.85-134.37			94		M
4	193.5-202.7	193.55-199.57			97		M
5	260.3-269.4	263.35-267.87			90		M
6	326.7-335.9	327.60-332.77			96		M
7	335.9-345.0	336.04-342.72			89		M
8	345.0-350.1	345.05-351.00			92		M
9	350.1-355.7	350.15-353.17			88		M
10	355.7-364.2	357.25-359.27			84		M
11	364.2-373.4	365.75-371.77			90		M
12	373.4-380.4*	373.50-376.47			89		M
		377.95-380.97			88		M
13	380.4-389.5*	382.60-387.97			89	P	M
14	389.5-398.7	389.55-397.07			82		M
15	398.7-406.0	400.26			82		M
16	406.0-413.6	409.06			88		M

Table 4a. Hole 79, <2μ

Core	Depth	Sample Depth (m. below sea floor)	Diff.	Amorph.	Quar.	Plag.	Kaol.	Mica	Mont.	Bari.
1	0-9.1	1.54-7.57	95.9	93.6	10.0	8.7	9.6	23.8	30.9	17.0
2	60.3-69.5	60.35-66.37	100.0	100.0	–	–	–	–	–	–
		67.86	100.0	100.0	–	–	–	–	–	–
3	126.8-135.9	126.85-134.37	99.6	99.4	–	–	–	–	100.0	–
4	193.5-202.7	193.55-199.57	99.4	99.1	13.7	–	–	–	86.3	–
5	260.3-269.4	263.35-267.87	98.9	98.3	2.6	–	–	–	84.1	13.3

*Depth changed on plot in order to accommodate samples received.

TABLE 4 – *Continued*

Table 4a. Hole 79, <2μ – *Continued*

Core	Depth	Sample Depth (m. below sea floor)	Diff.	Amorph.	Quar.	Plag.	Kaol.	Mica	Mont.	Bari.
6	326.7-335.9	327.60-332.77	96.3	94.2	–	–	–	–	96.2	3.8
7	335.9-345.0	336.04-342.72	90.5	85.2	–	–	–	–	94.9	5.1
8	345.0-350.1	345.05-351.00	87.6	80.6	–	–	–	–	96.0	4.0
9	350.1-355.7	350.15-353.17	89.2	83.1	–	–	–	–	96.0	4.0
10	355.7-364.2	357.25-359.27	90.4	85.0	–	–	–	–	96.9	3.1
11	364.2-373.4	365.75-371.77	89.7	83.9	–	–	–	–	94.9	5.1
12	373.4-380.4*	373.50-376.47	88.1	81.4	–	–	–	–	95.6	4.4
		377.95-380.97	87.2	80.0	–	–	–	–	98.3	1.7
13	380.4-389.5*	382.60-387.97	87.4	80.3	–	–	–	–	96.5	3.5
14	389.5-398.7	389.55-397.07	88.1	81.4	–	–	–	–	96.0	4.0
15	398.7-406.0	400.26	94.9	92.0	–	–	–	–	100.0	–
16	406.0-413.6	409.06	91.4	86.6	–	–	1.4	–	97.6	–

Table 4b. Hole 79A, Bulk

Core	Depth	Sample Depth (m. below sea floor)	Diff.	Amorph.	Calc.	Quar.	Plag.	Bari.
1	9.1-18.3	9.56	84.3	75.5	86.9	1.6	5.0	6.5
		10.65-16.17	80.4	69.4	91.1	–	2.6	5.7
2	69.5-78.6	69.55-77.07	66.3	47.3	100.0	–	–	–
3	145.1-154.2	145.15-152.67	70.1	53.3	100.0	–	–	–
4	278.6-287.7	286.16	56.1	31.4	100.0	–	–	–

Table 4b. Hole 79A, 2-20μ

Core	Depth	Sample Depth (m. below sea floor)	Lithostratigraphy Formation	Unit	Amorph.	Bari.
1	9.1-18.3	9.56		Cyclic	97	P
		10.65-16.17		Cyclic	95	M
2	69.5-78.6	69.55-77.07			95	M
3	145.1-154.2	145.15-152.67			96	M
4	278.6-287.7	286.16			97	M

Table 4b. Hole 79A, $< 2\mu$

Core	Depth	Sample Depth (m. below sea floor)	Diff.	Amorph.	Quar.	K-Fe.	Plag.	Mica	Mont.	Phil.	Bari.
1	9.1-18.3	9.56	96.5	94.5	4.6	–	–	18.6	45.3	26.3	5.2
		10.65-16.17	99.2	98.8	16.4	–	13.5	–	66.4	–	3.7
2	69.5-78.6	69.55-77.07	99.6	99.4	6.1	6.8	–	–	80.8	–	6.3
3	145.1-154.2	145.15-152.67	98.0	96.9	2.2	5.0	–	–	88.6	–	4.3
4	278.6-287.7	286.16	99.1	98.6	–	–	–	–	100.0	–	–

TABLE 5
Results of X-Ray Diffraction Analysis from Site 80

Table 5a. Hole 80, Bulk

Core	Depth	Sample Depth (m. below sea floor)	Diff.	Amorph.	Calc.
1	0-9.1	0.05-7.57	50.1	22.0	100.0
2	61-70.1	61.05-68.57	59.9	37.3	100.0
3	127.5-136.6	127.55-135.07	52.0	25.0	100.0
4	165.7-175.0	167.25-171.77	47.8	18.4	100.0
5	193.3-202.4	193.53-196.37	56.7	32.3	100.0

Table 5a. Hole 80, 2-20μ

Core	Depth	Sample Depth (m. below sea floor)	Lithostratigraphy Formation	Unit	Amorph.	Clin.	Bari.
1	0-9.1	0.05-7.57	Clipperton		96		M
2	61.0-70.1	61.05-68.57	Clipperton		97		M
3	127.5-136.6	127.55-135.07	Marquesas	Brown	91		M
4	166.7-175.0	167.25-171.77	Marquesas	Brown	87		M
5	193.3-202.4	193.53-196.37	Line Island		95	P	M

Table 5a. Hole 80, < 2μ

Core	Depth	Sample Depth (m. below sea floor)	Diff.	Amorph.	Side.	Quar.	K-Fe.	Plag.	Kaol.	Mont.	Bari.
1	0-9.1	0.05-7.57	100.0	100.0	–	–	–	–	–	–	–
2	61-70.1	61.05-68.57	99.0	98.4	–	6.6	–	7.4	–	75.1	11.0
3	127.5-136.6	127.55-135.07	97.4	95.9	–	2.0	4.3	4.9	–	80.1	8.6
4	165.7-175.0	167.25-171.77	84.8	76.2	–	1.9	3.3	3.6	4.0	84.9	2.3
5	193.3-202.4	193.53-196.37	90.8	85.6	2.2	1.6	–	–	–	96.1	–

Table 5b. Hole 80A, Bulk

Core	Depth	Sample Depth (m. below sea floor)	Diff.	Amorph.	Calc.
2	42.7-51.8	42.75-47.27	62.7	41.7	100.0
3	86.6-95.7	86.65-94.17	58.4	35.0	100.0
4	109.1-118.2	109.15-116.67	51.0	23.4	100.0
5	155.8-164.9	156.11-163.37	51.3	23.9	100.0

Table 5b. Hole 80A, 2-20μ

Core	Depth	Sample Depth (m. below sea floor)	Lithostratigraphy Formation	Unit	Amorph.	Bari.
2	42.7-51.8	42.75-47.27			99	M
3	86.6-95.7	86.65-94.17			97	M
4	109.1-118.3	109.15-116.67			90	M
5	155.8-164.9	156.11-163.37			91	M

Table 5b. Hole 80A, < 2μ

Core	Depth	Sample Depth (m. below sea floor)	Diff.	Amorph.	Quar.	K-Fe.	Plag.	Kaol.	Mont.	Bari.
2	42.7-51.8	42.75-47.27	99.8	99.7	100.0	–	–	–	–	–
3	86.6-95.7	86.65-94.17	100.0	100.0	–	–	–	–	–	–
4	109.1-118.3	109.15-116.67	88.9	82.7	4.1	–	–	–	92.6	3.4
5	155.8-164.9	156.11-163.37	89.8	84.1	2.5	.2.0	2.0	2.6	88.4	2.6

TABLE 6
Results of X-Ray Diffraction Analysis from Site 81

Hole 81, Bulk

Core	Depth	Sample Depth (m. below sea floor)	Diff.	Amorph.	Calc.	Kaol.	Mont.
1	0-9.1	0.05-1.59	50.2	22.2	100.0		–
		3.05-7.57	52.7	26.1	100.0	–	–
2	319.7-323.3*	321.25-325.77	58.1	34.5	100.0	–	–
3	376.3-383.1*	377.85-383.87	53.7	27.7	100.0	–	–
4	389.1-395.6	389.30-395.17	52.3	25.5	100.0	–	–
5	395.6-404.7	398.66	58.5	35.2	91.6	–	8.4
6	404.7-408.3	407.91	58.1	34.5	81.7	1.5	16.8

Hole 81, 2-20μ

Core	Depth	Sample Depth (m. Below sea floor)	Lithostratigraphy Formation	Unit	Amorph.	Bari.	Apat.	Magn.
1	0-9.1	0.05-159	Clipperton	Cyclic	97	M		T
		3.05-7.57	Clipperton	Varicolored	93	P		
2	319.7-323.3*	321.25-325.77	San Blas		95	M		
3	376.3-383.1*	377.85-383.87	San Blas		98	M		
4	389.1-395.6	389.30-395.17	Line Islands		89	M		
5	395.6-404.7	398.66	Line Islands		82	M		
6	404.7-408.3	407.91	Line Islands		77	M		

*Depth changed on plot in order to accommodate samples received.

TABLE 6 – *Continued*

Hole 81, < 2μ													
Core	Depth	Sample Depth (m. below sea floor)	Diff.	Amorph.	Side.	Quar.	K-Fe.	Plag.	Kaol.	Mont.	Bari.	Gypsum	Unknown
1	0-9.1	0.05-1.59	98.7	98.0	–	36.5	–	–	–	1.4	62.0	–	X
		3.05-7.57	96.3	94.2	3.2	4.2	5.1	–	6.6	72.2	8.8	–	–
2	319.7-323.3*	321.25-325.79	98.1	97.0	–	–	–	–	–	89.6	9.8	–	–
3	376.3-383.1*	377.85-383.87	93.3	89.5	3.0	–	–	4.8	–	85.2	6.6	–	–
4	389.1-395.6	389.30-395.17	87.9	81.1	–	–	–	–	–	95.9	3.1	–	–
5	395.6-404.7	398.66	89.1	83.0	–	–	–	–	–	100.0	–	–	–
6	404.7-408.3	407.91	84.3	75.5	–	–	–	–	2.7	91.9	5.4	?	–

*Depth changed on plots in order to accommodate samples received.

TABLE 7
Results of X-Ray Diffraction Analysis from Site 82

Table 7a. Hole 82, Bulk

Core	Depth	Sample Depth (m. below sea floor)	Diff.	Amorph.	Calc.
1	0-9.1	0.05-3.82	55.6	30.6	100.0
		4.57-7.57	55.4	30.3	100.0
2	68.8-78.0	68.85-76.37	55.8	30.9	100.0
3	135.3-144.5	135.35-142.87	61.1	39.2	100.0
4	191.3-200.5	191.35-198.87	59.3	36.4	100.0
5	200.5-209.6	201.56	53.3	27.0	100.0
6	209.6-218.8	212.66	60.4	38.1	100.0
		214.15-217.17	60.3	38.0	100.0

Table 7a. Hole 82, 2-20μ

Core	Depth	Sample Depth (m. below sea floor)	Lithostratigraphy		Amorph.	Pyri.	Bari.
			Formation	Unit			
1	0-9.1	0.05-3.82	Clipperton	Cyclic	98		M
		4.57-7.57			93		M
2	68.8-78.0	68.85-76.37			90		M
3	135.3-144.5	135.35-142.87			96	P	M
4	191.3-200.5	191.35-198.87			99		P
5	200.5-209.6	201.56			99		P
6	209.6-218.8	212.66	Line Islands		99		P
		214.15-217.17	Line Islands		97		M

Table 7a. Hole 82, < 2μ

Core	Depth	Sample Depth (m. below sea floor)	Diff.	Amorph.	Side.	Quar.	K-Fe.	Plag.	Kaol.	Mica	Mont.	Bari.	Gypsum and/or Unknown
1	0-9.1	0.05-3.82	97.5	96.1	–	2.7	4.2	6.2	5.0	21.1	54.9	6.0	–
		4.57-7.57	94.3	91.1	–	5.5	–	–	–	–	94.5	–	–
2	68.8-78.0	68.85-76.37	94.3	91.1	6.7	–	–	11.8	–	–	70.3	11.2	G. & unk.
3	135.3-144.5	135.35-142.87	98.5	97.7	–	4.3	–	–	–	–	70.1	25.6	–
4	191.3-200.5	191.35-198.87	99.5	99.2	–	–	–	–	–	–	87.2	12.8	–
5	200.5-209.6	201.56	97.0	95.3	–	1.7	–	–	–	–	90.6	7.7	–
6	209.6-218.8	212.66	98.2	97.2	–	–	–	–	–	–	100.0	–	
		214.15-217.17	91.7	87.0	–	–	–	–	–	–	97.3	–	Fe or Mn oxide ? Unk.

Table 7b. Hole 82A, Bulk

Core	Depth	Sample Depth (m. below sea floor)	Diff.	Amorph.	Calc.
1	18.3-27.5	19.85-25.87	55.1	29.8	100.0
2	36.5-45.6	36.55-44.07	58.0	34.4	100.0
3	101.7-111.0	101.80-107.77	52.1	25.2	100.0

Table 7b. Hole 82A, 2-20μ

Core	Depth	Sample Depth (m. below sea floor)	Lithostratigraphy Formation	Lithostratigraphy Unit	Amorph.	Bari.
1	18.3-27.5	19.85-25.87	San Blas		92	M
2	36.5-45.6	36.55-44.07	San Blas		94	M
3	101.7-111.0	101.80-107.77	San Blas		98	M

TABLE 7 – *Continued*

Table 7b. Hole 82A, $<2\mu$

Core	Depth	Sample Depth (m. below sea floor)	Diff.	Amorph.	Quar.	K-Fe.	Plag.	Mont.	Bari.
1	18.3-27.5	19.85-25.87	90.6	85.3	3.6	1.3	2.0	91.3	1.8
2	36.5-45.6	36.55-44.07	92.0	87.5	4.6	3.5	3.5	83.3	5.1
3	101.7-111.0	101.80-107.77	92.4	88.1	1.8	–	–	97.0	1.2

TABLE 8
Results of X-Ray Diffraction Analysis from Site 83

Table 8a. Hole 83, Bulk

Core	Depth	Sample Depth (m. below sea floor)	Diff.	Amorph.	Calc.	Quar.	Plag.	Mont.	Bari.
1	0-5.1	1.55-4.57	68.7	51.1	96.9	1.4	1.8	–	–
2	5.1-14.3	5.15-11.17	63.6	43.1	97.1	–	2.2	–	–
		12.66	79.4	67.7	77.8	1.0	4.5	12.0	4.9
3	14.3-23.4	14.80-17.37	76.3	63.0	81.8	1.0	4.7	8.4	4.1
4	68.8-78.0	71.86	73.0	57.8	87.3	1.1	2.5	5.8	3.3
5	136.2-145.3	137.77-143.77	67.2	48.8	100.0	–	–	–	–
6	202.3-211.5	203.85-209.87	61.2	39.4	100.0	–	–	–	–
7	221.8-231.0	222.47-227.87	70.1	53.3	100.0	–	–	–	–
		228.86	66.7	48.0	100.0	–	–	–	–

Table 8a. Hole 83, 2-20μ

Core	Depth	Sample Depth (m. below sea floor)	Lithostratigraphy Formation	Lithostratigraphy Unit	Amorph.	Pyri.	Bari.	Magn.
1	0-5.1	1.55-4.57			90		M	T
2	5.1-14.3	5.15-11.17	Clipperton		93		P	
		12.66			87		M	
3	14.3-23.4	14.80-17.37			90		M	
4	68.8-78.0	71.86			91		P	
5	136.2-145.3	137.77-143.77			93	P	M	
6	202.3-211.5	203.85-209.87			97	P	M	
7	221.8-231.0	222.47-227.87			95		M	
		228.86			97		M	

TABLE 8 – *Continued*

Table 8a. Hole 83, <2μ

Core	Depth	Sample Depth (m. below sea floor)	Diff.	Amorph.	Quar.	Plag.	Kaol.	Mont.	Bari.
1	0-5.1	1.55-4.57	97.0	95.3	10.8	11.8	14.5	52.7	10.3
2	5.1-14.3	5.15-11.17	94.2	90.9	13.8	7.9	10.4	67.9	–
		12.66	89.6	83.8	4.7	3.8	–	91.5	–
3	14.3-23.4	14.80-17.37	92.1	87.7	5.4	5.9	–	84.2	4.5
4	68.8-78.0	71.86	89.5	83.6	4.6	2.7	4.5	88.1	–
5	136.2-145.3	137.77-143.77	92.8	88.8	2.6	3.4	–	92.5	1.6
6	202.3-211.5	203.85-209.87	91.6	86.9	1.8	–	–	92.3	5.9
7	221.8-231.0	222.47-227.87	93.8	90.3	1.7	–	–	92.7	5.6
		228.86	93.2	89.4	–	–	–	100.0	–

Table 8b. Hole 83A, Bulk

Core	Depth	Sample Depth (m. below sea floor)	Diff.	Amorph.	Calc.	Dolo.	Quar.	Plag.	Mont.	Bari.
1	13.1-22.1	14.66	71.9	56.1	91.3	–	–	–	4.7	4.0
		17.66	66.8	48.1	100.0	–	–	–	–	–
2	22.1-31.4	23.65-29.67	68.6	50.9	100.0	–	–	–	–	–
3	31.4-40.5	31.45-38.97	74.3	59.8	79.0	10.0	–	–	8.1	3.0
4	40.5-49.6	45.05-48.07	70.4	53.8	96.9	–	1.3	1.8	–	–
5	49.6-58.8	51.30-57.17	71.3	55.2	97.5	–	1.4	1.2	–	–
6	58.8-67.9	60.35-66.37	67.3	48.9	99.0	–	1.0	–	–	–
7	67.9-77.1	72.45-75.47	82.0	71.9	80.2	–	2.0	4.6	8.2	5.0
8	77.1-86.1	78.80-84.67	73.7	58.9	89.0	–	–	2.6	4.6	3.3
9	86.1-92.4	87.65-93.67	66.8	48.1	99.0	–	1.0	–	–	–
10	95.4-104.5	96.95-102.97	62.4	41.2	99.5	–	–	–	–	–
11	104.5-113.6	106.05-112.07	69.5	52.3	99.5	–	–	–	–	–
12	113.6-122.8	115.15-121.17	82.0	71.9	77.3	–	–	–	19.8	2.9

Table 8b. Hole 83A, Bulk – *Continued*

Core	Depth	Sample Depth (m. below sea floor)	Diff.	Amorph.	Calc.	Dolo.	Quar.	Plag.	Mont.	Bari.
13	122.8-131.9	124.35-130.37	67.0	48.4	100.0	–	–	–	–	–
14	158.1-167.3	159.65-165.67	66.1	47.0	100.0	–	–	–	–	–
15	179.5-188.6	181.05-187.07	70.0	53.1	100.0	–	–	–	–	–
16	211.1-220.3	212.65-218.67	61.2	39.4	100.0	–	–	–	–	–

Table 8b. Hole 83A, 2-20μ

Core	Depth	Sample Depth (m. below sea floor)	Lithostratigraphy Formation	Lithostratigraphy Unit	Amorph.	Dolo.	Pyri.	Bari.
1	13.1-22.1	14.66			91			M
		17.66			89			M
2	22.1-31.4	23.65-29.67			84			M
3	31.4-40.5	31.45-38.97			83			M
4	40.5-49.6	45.05-48.07			86			M
5	49.6-58.8	51.30-57.17			86			M
6	58.8-67.9	60.35-66.37			91		P	M
7	67.9-77.1	72.45-75.47			87			M
8	77.1-86.1	78.80-84.67			86			M
9	86.1-95.4	87.65-93.67			87		P	M
10	95.4-104.5	96.95-102.97			96		M	P
11	104.5-113.6	106.05-112.07			97			M
12	113.6-122.8	115.15-121.17			91		M	P
13	122.8-131.9	124.35-130.37			95	P		M
14	158.1-167.3	159.65-165.67			94		P	M
15	179.5-188.6	181.05-187.07			95			M
16	211.1-220.3	212.65-218.67			88		P	M

TABLE 8 – *Continued*

Table 8b. Hole 83A, $<2\mu$

Core	Depth	Sample Depth (m. below sea floor)	Diff.	Amorph.	Quar.	K-Fe.	Plag.	Kaol.	Mont.	Bari.	Gyps.
1	13.1-22.1	14.66	92.1	87.7	10.9	–	–	–	89.1	–	–
		17.66	90.6	85.3	8.9	–	–	–	91.1	–	–
2	22.1-31.4	23.65-29.67	92.8	88.8	6.3	–	–	–	93.7	–	–
3	31.4-40.5	31.45-38.97	91.6	86.9	9.9	–	–	–	90.1	–	–
4	40.5-49.6	45.05-48.07	90.4	85.0	8.4	–	–	–	91.6	–	–
5	49.6-58.8	51.30-57.17	94.1	90.8	6.9	–	7.1	–	84.0	2.0	–
6	58.8-67.9	60.35-66.37	92.2	87.8	7.7	–	11.0	–	65.4	16.0	–
7	67.9-77.1	72.45-75.47	89.3	83.3	4.3	–	4.7	–	88.2	2.8	–
8	77.1-86.1	78.80-84.67	91.1	86.1	6.3	–	10.8	–	74.2	8.7	–
9	86.1-95.4	87.65-93.67	93.2	89.4	6.6	–	8.2	8.0	72.8	4.4	–
10	95.4-104.5	96.95-102.97	92.7	88.6	6.0	8.6	15.1	–	46.0	24.3	–
11	104.5-113.6	106.05-112.07	95.2	92.5	6.2	–	9.8	9.6	65.8	8.6	–
12	113.6-122.8	115.15-121.17	93.2	89.4	–	–	6.4	5.3	76.2	12.1	P
13	122.8-131.9	124.35-130.37	94.5	91.4	1.4	–	–	–	98.6	–	–
14	158.1-167.3	159.65-165.67	92.1	87.7	–	–	–	–	100.0	–	–
15	179.5-188.6	181.05-187.07	90.3	84.8	–	–	–	–	100.0	–	–

TABLE 9
Results of X-Ray Diffraction Analysis from Site 84

Hole 84, Bulk

Core	Depth	Sample Depth (m. below sea floor)	Diff.	Amorph.	Calc.	Quar.	K-Fe.	Plag.	Kaol.	Mica	Chlor.	Mont.	Clin.	Pyrite
1	0-9.2	0.05-7.57	86.6	79.1	23.9	24.1	–	20.0	–	–	13.1	11.9	3.1	3.9
2	9.2-18.3	10.75-16.77	87.7	80.8	37.5	22.7	–	14.0	–	–	12.0	9.6	–	4.2
3	18.3-27.4	19.85-25.87	86.9	79.5	40.4	14.1	–	11.0	–	–	5.2	24.8	3.0	2.5
4	27.4-36.6	28.95-34.97	86.5	78.9	32.2	15.9	6.9	10.2	–	–	11.6	18.1	1.0	4.0
5	36.6-45.7	38.16	90.6	85.3	32.1	18.0	–	13.8	9.0	–	–	23.0	–	4.0
		41.15-44.17	82.4	72.5	67.8	8.0	–	6.8	–	–	–	13.9	–	3.4
6	45.7-54.9	47.25-50.27	81.6	71.2	67.0	8.4	5.8	5.8	3.8	–	–	6.9	–	2.5
7	54.9-64.0	56.45-62.47	87.6	80.6	27.2	11.9	–	35.2	6.1	–	–	14.0	1.8	3.8
8	64.0-73.2	65.56	85.1	76.7	56.4	9.5	–	6.5	5.3	–	–	20.2	–	2.1
		68.55-71.57	86.8	79.4	52.0	12.4	–	9.0	6.8	–	–	16.0	–	3.9
9	73.2-82.3	74.75-80.77	86.1	78.3	21.2	13.5	–	10.9	4.9	5.1	–	38.9	1.4	4.1
10	82.3-91.4	83.85- 86.87	85.7	77.7	29.9	12.9	–	7.7	5.0	–	–	41.4	–	3.0
		89.86	78.5	66.4	59.2	6.6	–	4.2	3.3	4.7	–	21.2	–	–
11	91.4-100.6	92.95-98.97	77.3	64.5	62.7	6.3	–	4.5	2.4	4.9	–	19.3	–	–
12	100.6-109.7	102.15-108.17	81.1	70.5	55.3	8.6	–	6.4	4.2	–	–	25.5	–	–
13	109.7-118.9	111.25-117.27	75.3	61.4	73.1	5.0	–	4.2	2.7	–	–	15.0	–	–
14	118.9-128.0	120.45-126.47	78.2	65.9	70.7	6.2	–	4.1	2.6	5.6	–	10.9	–	–
16	137.2-146.3	138.75-144.77	65.8	46.6	93.7	4.1	–	1.0	1.2	–	–	–	–	–
17	146.3-155.5	147.866	67.4	49.1	95.3	2.7	–	–	–	–	–	–	–	–
18	155.5-164.6	157.15-160.07	65.7	46.4	97.1	2.0	–	–	–	–	–	–	–	–
19	164.6-173.7	169.15-172.17	68.0	50.0	89.5	1.8	–	–	–	–	–	7.7	–	–
20	173.7-182.9	175.26	69.8	52.8	94.2	2.4	–	1.7	1.1	–	–	–	–	–
21	182.9-192.0	189.41	63.2	42.5	94.0	1.0	–	–	–	–	–	4.5	–	–
22	192.0-201.2	193.71	78.8	66.9	83.9	5.5	–	3.2	2.4	–	–	–	–	4.9
		199.56	63.1	42.3	97.5	1.5	–	–	–	–	–	–	–	–
23	201.2-210.3	205.76	68.7	51.1	96.5	2.2	–	1.2	–	–	–	–	–	–

TABLE 9 – *Continued*

Hole 84, Bulk – *Continued*

Core	Depth	Sample Depth (m. below sea floor)	Diff.	Amorph.	Calc.	Quar.	K-Fe.	Plag.	Kaol.	Mica	Chlor.	Mont.	Clin.	Pyrite
24	210.3-219.5	211.85-214.87	64.1	43.9	97.5	1.0	–	1.5	–	–	–	–	–	–
25	219.5-228.6	221.06	66.2	47.2	99.0	1.0	–	–	–	–	–	–	–	–
26	228.6-237.8	233.16	60.4	38.1	99.6	–	–	–	–	–	–	–	–	–
		234.16	55.8	30.9	99.6	–	–	–	–	–	–	–	–	–
27	237.8-246.9	239.35-245.37	60.8	38.8	99.5	–	–	–	–	–	–	–	–	–

Hole 84, 2-20μ

Core	Depth	Sample Depth (m. below sea floor)	Lithostratigraphy Formation	Unit	Amorph.	Dolo.	Clin.	Pyri.	Bari.
1	0-9.2	0.05-7.57			75		P	P	
2	9.2-18.3	10.75-16.77			74		P	P	
3	18.3-27.4	19.85-25.87			77		P	P	
4	27.4-36.6	28.95-34.97			79		P	P	
5	36.6-45.7	38.16			81		P	P	
		41.15-44.17			79		P	P	
6	45.7-54.9	47.25-50.27			91		P	P	
7	54.9-64.0	56.45-62.47			80		P	P	
8	64.0-73.2	65.56			79		P	P	
		68.55-71.57			80		P	P	
9	73.2-82.3	74.75-80.77			79		P	P	
10	82.3-91.4	83.85-86.87			80		P	P	P
		89.86			82		P	P	
11	91.4-100.6	92.95-98.97			81		P	P	P
12	100.6-109.7	102.15-108.17			81		P	P	P
13	109.7-118.9	111.25-117.27			84		P	P	P
14	118.9-128.0	120.45-126.47			82		P	P	P

TABLE 9 – *Continued*

Hole 84, 2-20μ – *Continued*

Core	Depth	Sample Depth (m. below sea floor)	Lithostratigraphy Formation	Unit	Amorph.	Dolo.	Clin.	Pyri.	Bari.
17	146.3-155.5	147.86			82		P	P	P
18	155.5-164.6	157.15-160.07			82		P	P	
19	164.6-173.7	169.15-172.17			84		P	P	
20	173.7-182.9	175.26			84		P	P	
21	182.9-192.0	189.41			89		P	P	P
22	192.0-201.2	193.71			82			P	P
		199.56			87		P	P	P
23	201.2-210.3	205.76			85			P	P
24	210.3-219.5	211.85-214.87			86			P	P
25	219.5-228.6	221.06			94		P	P	P
26	228.6-237.8	233.16			93			P	P
		234.16			92				P
27	237.8-246.9	239.35-245.37			91				P
28	246.9-250.9	246.90-259.90			98	T	P		M

Hole 84, <2μ

Core	Depth	Sample Depth (m. below sea floor)	Diff.	Amorph.	Side.	Quar.	K-Fe.	Plag.	Kaol.	Mica	Mont.	Clin.	Pyri.	Bari.
1	0-9.2	0.05-7.57	86.6	79.1	–	12.5	6.9	7.8	10.1	7.9	50.2	2.6	2.0	–
2	9.2-18.3	10.75-16.77	88.2	81.6	–	13.8	–	8.0	13.3	–	62.4	–	2.5	–
3	18.3-27.4	19.85-25.87	87.5	80.5	–	12.8	–	9.4	12.3	–	63.1	–	2.3	–
4	27.4-36.6	28.95-34.97	87.1	79.8	–	17.8	–	16.4	8.0	4.5	46.89	1.8	4.6	–
5	36.6-45.7	38.16	87.6	80.6	–	4.6	–	2.8	8.3	–	84.2	–	–	–
		41.15-44.17	88.2	81.6	–	6.5	–	2.7	7.1	–	80.9	–	2.8	–
6	45.7-54.9	47.25-50.27	87.2	80.0	–	6.0	–	3.2	6.0	–	81.8	1.0	2.0	–
7	54.9-64.0	56.45-62.47	85.9	78.0	–	13.3	–	7.4	10.0	–	65.6	–	3.7	–

TABLE 9 – *Continued*

Hole 84, <2μ – *Continued*

Core	Depth	Sample Depth (m. below sea floor)	Diff.	Amorph.	Side.	Quar.	K-Fe.	Plag.	Kaol.	Mica	Mont.	Clin.	Pyri.	Bari.
8	64.0-73.2	65.56	86.5	78.9	–	4.3	–	–	7.7	–	88.0	–	–	–
		68.55-71.57	90.4	85.0	–	13.0	–	9.9	12.1	–	58.3	–	4.7	2.0
9	73.2-82.3	74.75-80.77	86.6	79.1	–	7.9	–	4.3	6.5	–	81.2	–	–	–
10	82.3-91.4	83.85-86.87	89.5	83.6	–	10.8	–	7.4	8.7	–	70.8	2.2	–	–
		89.86	86.1	78.3	–	2.2	–	–	3.9	–	93.0	–	–	–
11	91.4-100.6	92.95-98.97	89.3	83.3	–	10.5	–	4.8	8.8	5.3	68.7	1.9	–	–
12	100.6-109.7	102.15-108.17	89.9	84.2	–	15.9	–	9.9	12.9	–	61.3	–	–	–
13	109.7-118.9	111.25-117.27	90.4	85.0	–	12.6	–	6.7	10.2	–	70.4	–	–	–
14	118.9-128.0	120.45-126.47	88.5	82.0	–	17.2	8.7	9.9	12.9	10.8	38.1	2.2	–	–
17	146.3-155.5	147.86	88.1	81.4	–	4.2	–	1.0	5.9	6.3	82.6	–	–	–
18	155.5-164.6	157.15-160.07	88.9	82.7	–	10.6	–	6.8	7.6	–	74.9	–	–	–
19	164.6-173.7	169.15-172.17	89.7	83.9	–	3.0	–	2.3	3.2	–	91.4	–	–	–
20	173.7-182.9	175.26	85.5	77.3	–	4.9	–	5.2	6.4	7.9	73.5	1.2	–	–
21	182.9-192.0	189.41	90.2	84.7	–	2.8	–	1.7	3.8	7.5	83.5	–	–	–
22	192.0-201.2	193.71	89.2	83.1	–	5.6	–	3.0	7.0	9.7	70.4	2.5	1.9	–
		199.56	89.8	84.1	–	5.4	–	2.6	5.1	9.3	77.7	–	–	–
23	201.2-210.3	205.76	91.2	86.2	–	7.9	–	5.5	7.1	–	77.8	–	1.7	–
24	210.3-219.5	211.85-214.87	90.7	85.5	–	6.2	–	5.0	5.2	9.8	71.1	–	–	2.6
25	219.5-228.6	221.06	95.2	92.5	3.0	5.0	–	2.9	5.5	–	82.7	–	–	–
26	228.6-237.8	233.16	93.0	89.1	–	3.8	–	12.2	5.5	16.3	62.2	–	–	–
		234.16	94.0	90.6	5.7	3.2	–	2.7	5.5	–	82.9	–	–	–
27	237.8-246.9	239.35-245.37	90.9	85.8	–	7.2	–	5.7	7.7	6.0	69.1	–	–	4.4

Unit two consists mainly of massive, brown, calcareous clays with lesser amounts of interbedded allodapics. Phillipsite occurs in great abundance in the 2 to 20 micron fraction (Table 1) and is evident in the bulk and <2 micron fractions (Figures 3 and 4). Montmorillonite is the only clay mineral detected. Some apatite and goethite were found in the <2 micron fraction.

Unit three was very disturbed and only one sample was submitted for X-ray analysis. This unit is a clay-rich calcareous ooze whose mixed faunal assemblages suggest it is probably of an allochthonous origin. The mineralogy of this unit is unusually simple. Only calcite appears in the bulk sample. The 2 to 20 micron fraction only contains phillipsite, and the <2 micron fraction only contains montmorillonite.

The mineralogy of unit four greatly resembles that of unit two (Figures 3 and 4; Table 1).

Unit five consists of carbonate ooze which contain clay-rich and clay-poor calcareous allodapics as well as brown, zeolitic clay capping these allodapic beds. By contrast with the overlying units the <2 micron fraction of unit five contains mica, less montmorillonite, goethite and apatite, and the only occurrence of kaolinite at Site 76. Brown, chalcedonic chert encountered at the bottom of this unit was not submitted for X-ray analysis.

Site 77

Site 77 was drilled in an area of thick sediments with the purpose of obtaining maximum penetration for lithostratigraphic studies. It is near Sites 71, 72 and 73 of Leg 8, and contains a similar sequence of lithostratigraphic units. The entire section is highly calcareous (Figures 5, 7 and 9).

The Clipperton Oceanic Formation at Site 77 is divided into an upper cyclic unit and lower varicolored unit. The cyclic unit (Late Pliocene and Pleistocene) consists of alternating beds of orange calcareous ooze and brown siliceous ooze. Barite is the major crystalline phase in the 2 to 20 micron fraction (Table 2). Montmorillonite, mica and kaolinite persist throughout the unit in the <2 micron fraction, as do plagioclase and quartz (Figures 8 and 10). K-feldspar appears in most samples. A rare occurrence of chlorite in equatorial sediments is observed at the top of Hole 77 in the <2 micron fraction (Figure 6). The mineralogy in the cyclic unit at Site 77 is very similar to the cyclic unit in Leg 8 Sites 71, 72 and 73, except that K-feldspar and chlorite are often not detected in Leg 8's cyclic unit. No obvious mineral accounts for the color variation in the cyclic unit of Site 77. The dusky brown, "red clay" material is possibly amorphous iron oxides.

The varicolored unit (Late Miocene to Late Pliocene), composed mostly of radiolarian-nannofossil ooze, is characterized by pastel shades of purple, green and yellow. The dominant mineral of the 2 to 20 micron fraction is again barite. Small amounts of siderite occur in the 2 to 20 micron fraction (Table 2). The <2 micron fraction from the upper 30 meters is very similar to the cyclic unit (Figure 10). In the <2 micron fraction barite and montmorillonite are the only minerals detected throughout the lower part of the unit except for small quantities of quartz (Figure 10). No mineralogical differences could be associated with the color changes. The mineralogy of the varicolored unit to the west in Leg 8, Sites 71, 72 and 73 is much more diversified than in the varicolored unit at Site 77. Whereas, Site 77 barite, montmorillonite and quartz are the only noncalcareous minerals, these minerals plus mica, kaolinite, K-feldspar, and plagioclase are common throughout the unit on the other sites.

The Marquesas Oceanic Formation (Lower Oligocene to Middle Miocene) is subdivided into five informal alternating gray and brown units (see Site 77 lithologic description). The formation is highly calcareous throughout.

In the bulk samples, only calcite is detectable (Figure 9). Barite forms the major crystalline component in the 2 to 20 micron fraction in all samples, except Core 45 of Hole 77B where cristobalite was found (Table 2). Only the <2 micron fraction shows some variation with depth (Figure 10), and frequently the mineralogical changes of this fraction coincide with the gray and brown unit boundaries (Figure 10).

The first gray unit contains abundant barite and montmorillonite and a little quartz. It bears a strong resemblance to the lower portion of the overlying varicolored unit.

The first brown unit contains only barite, montmorillonite and traces of quartz, as in the unit above, but its upper boundary marks a sharp rise in the montmorillonite-barite ratio (Figure 10). This particular mineral assemblage extends well into the underlying second gray unit (that is, to Core 37). Beyond that, an abrupt change in the mineralogy of the second gray unit occurs. There is an absence of montmorillonite and a corresponding appearance of mica, plagioclase, kaolinite and K-feldspar along with a slight increase of the quartz content (Figure 10). This mineral assemblage terminates at the lower boundary of the second gray unit.

The underlying second brown unit has an exceedingly high content of amorphous materials and only quartz was detected. The mineralogy of the lowest gray unit is highly varied (Figure 10) and contains siderite.

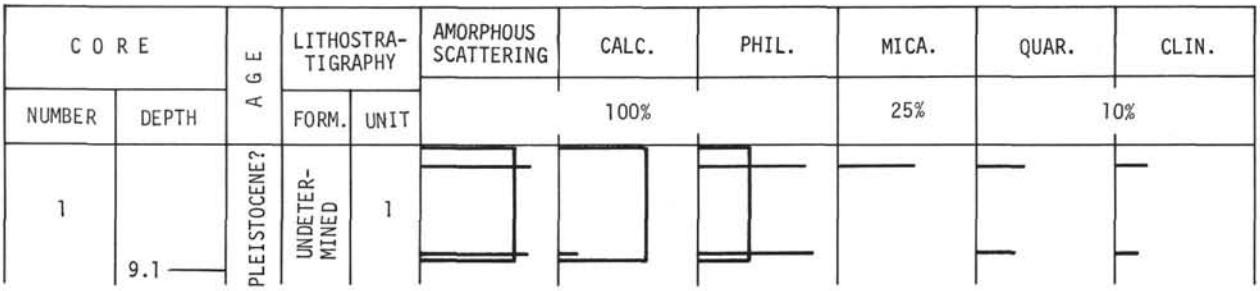

Figure 1. *Hole 76, bulk.*

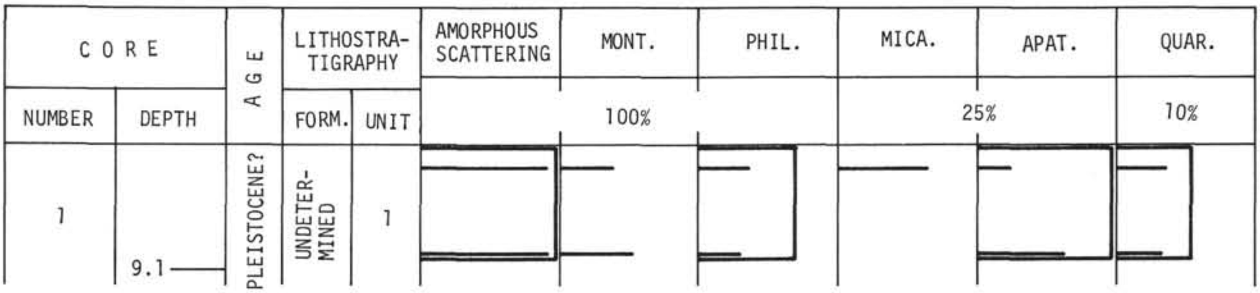

Figure 2. *Hole 76, < 2μ.*

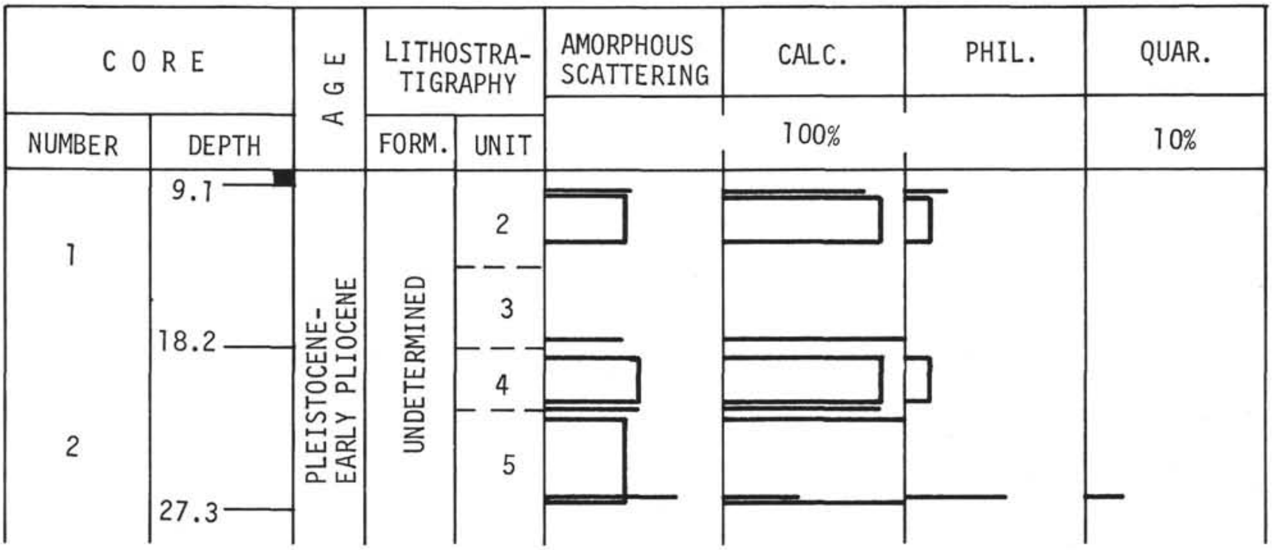

Figure 3. *Hole 76A, bulk.*

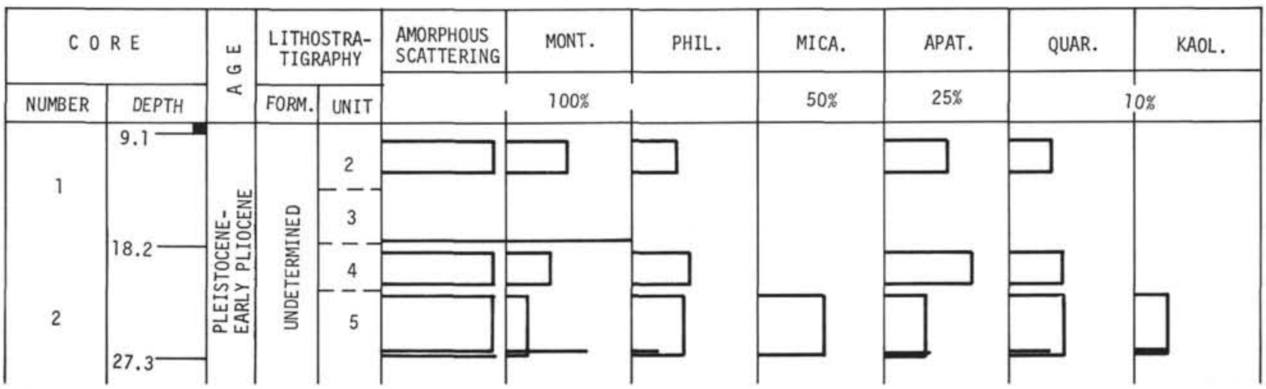

Figure 4. *76A, < 2μ.*

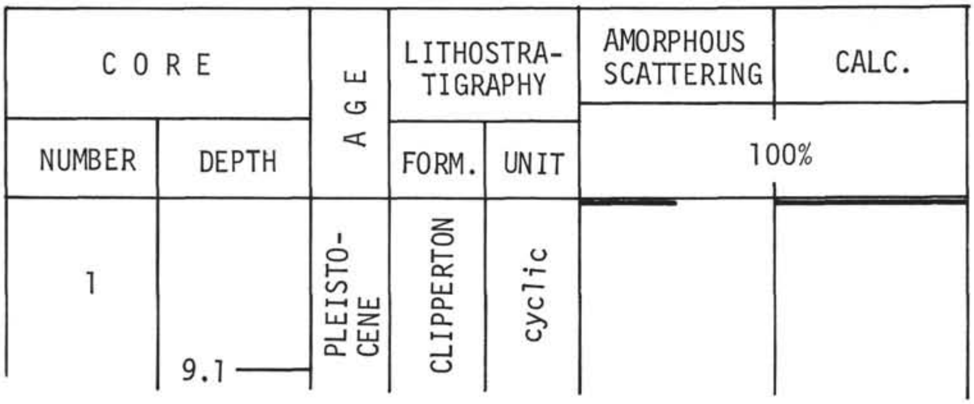

Figure 5. *Hole 77, bulk*

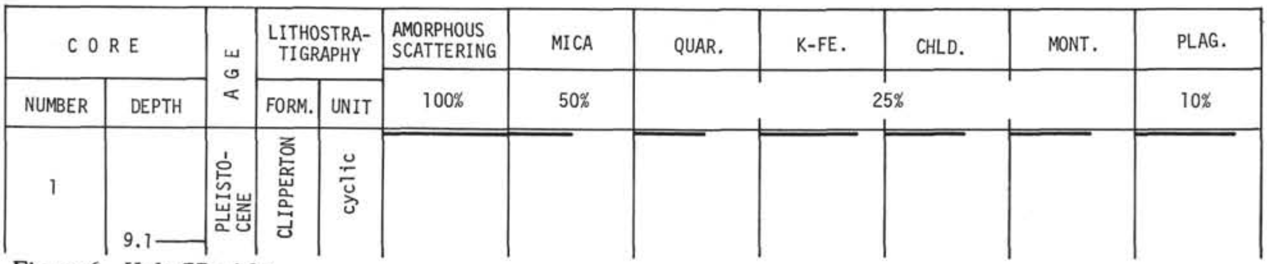

Figure 6. *Hole 77, <2μ.*

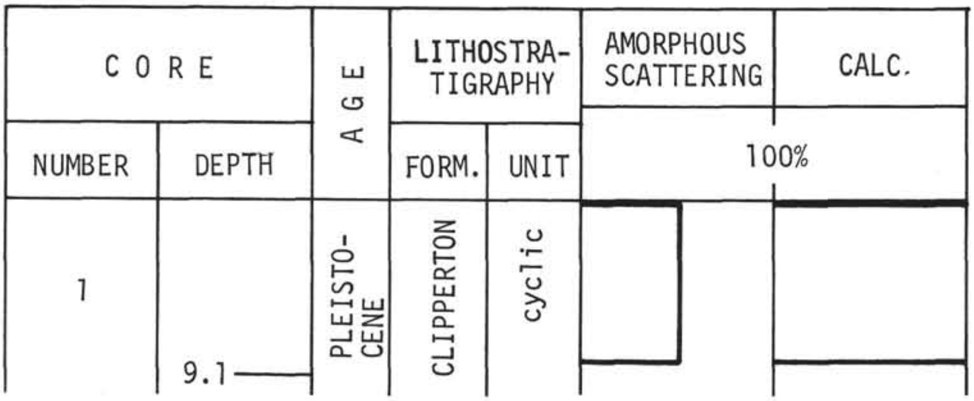

Figure 7. *Hole 77A, bulk.*

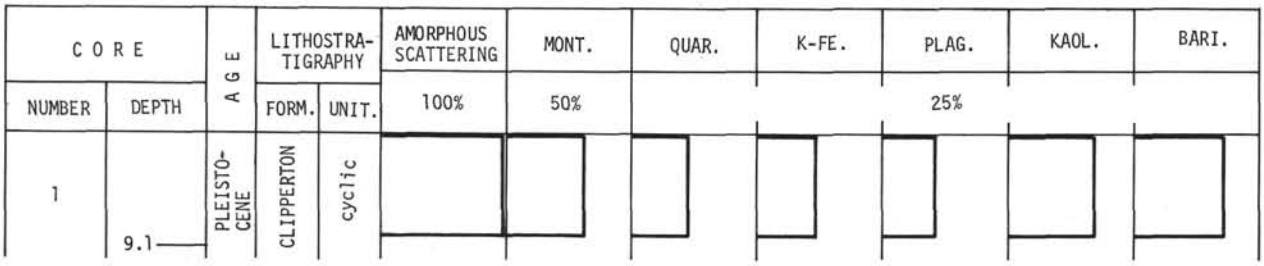

Figure 8. *Hole 77A, <2μ.*

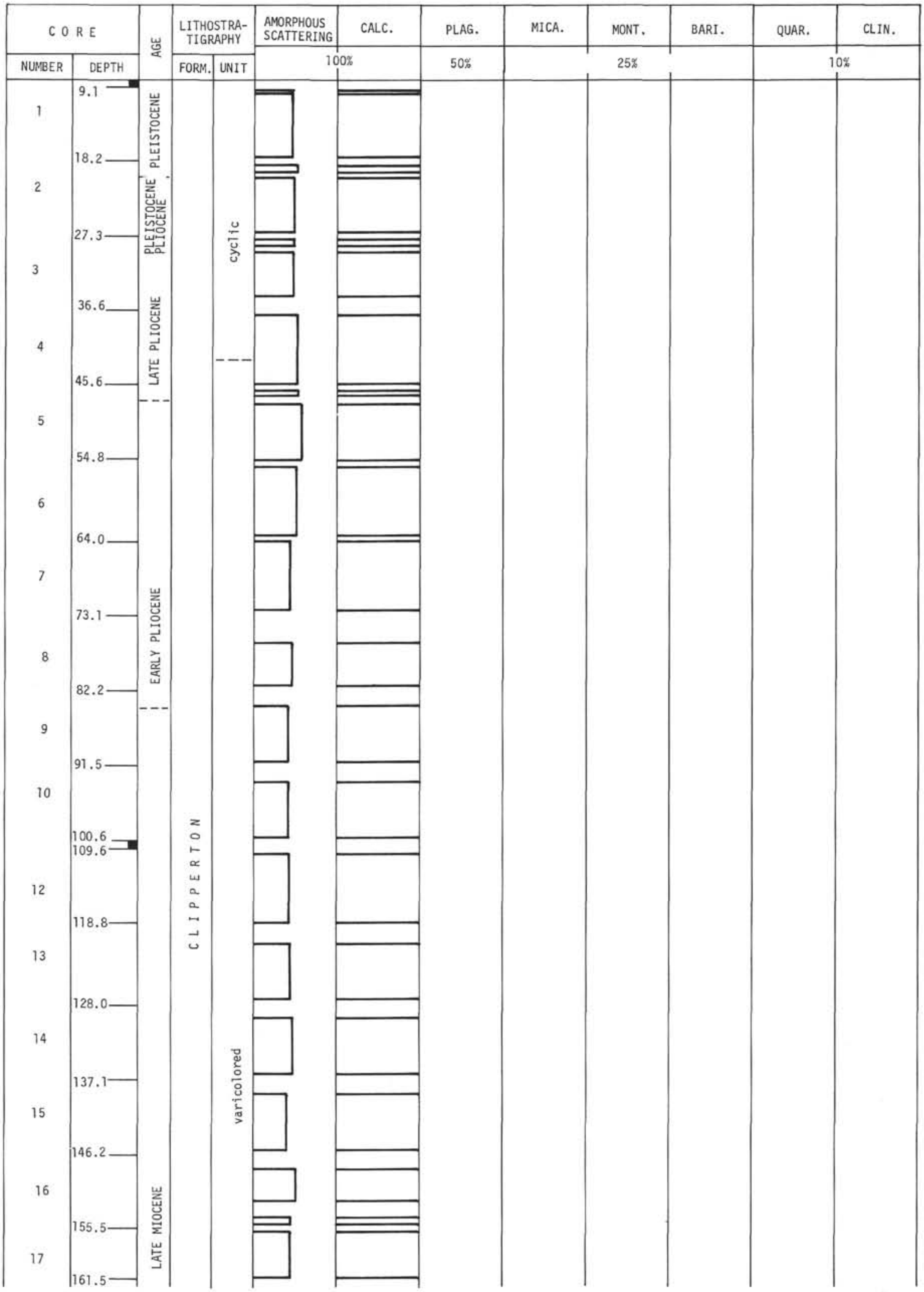

Figure 9. *Hole 77B, bulk.*

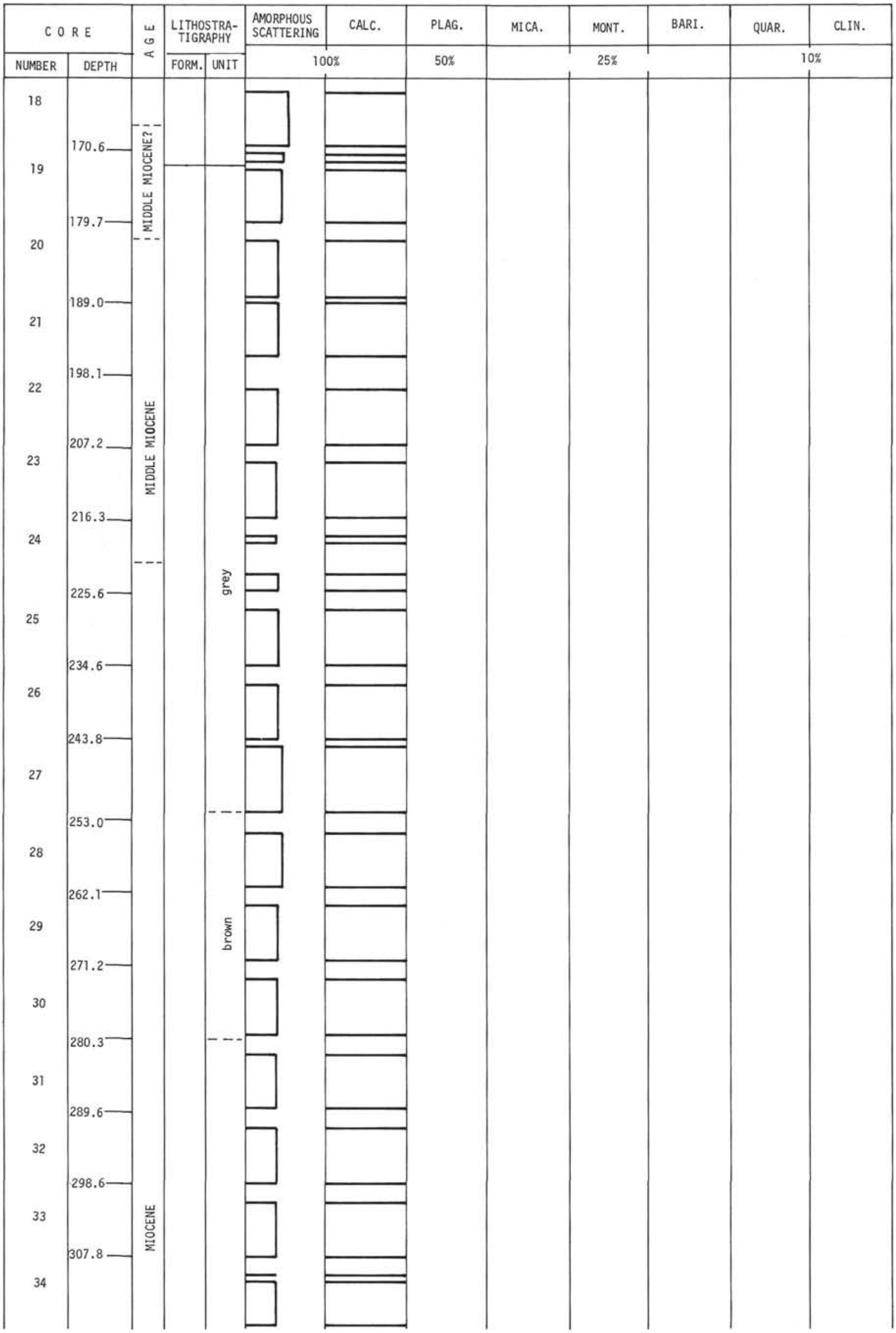

Figure 9. *Continued*

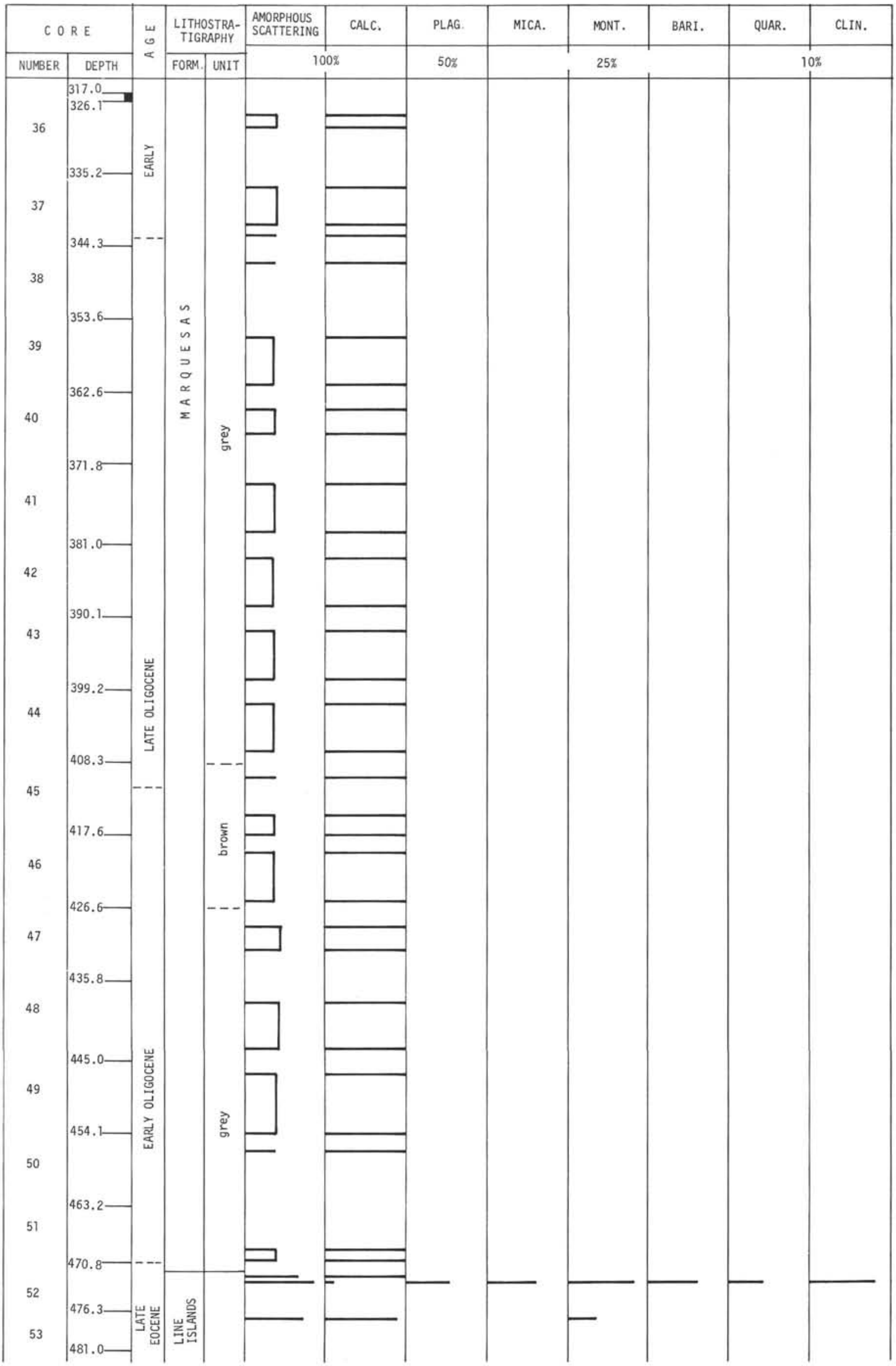

Figure 9. *Continued*

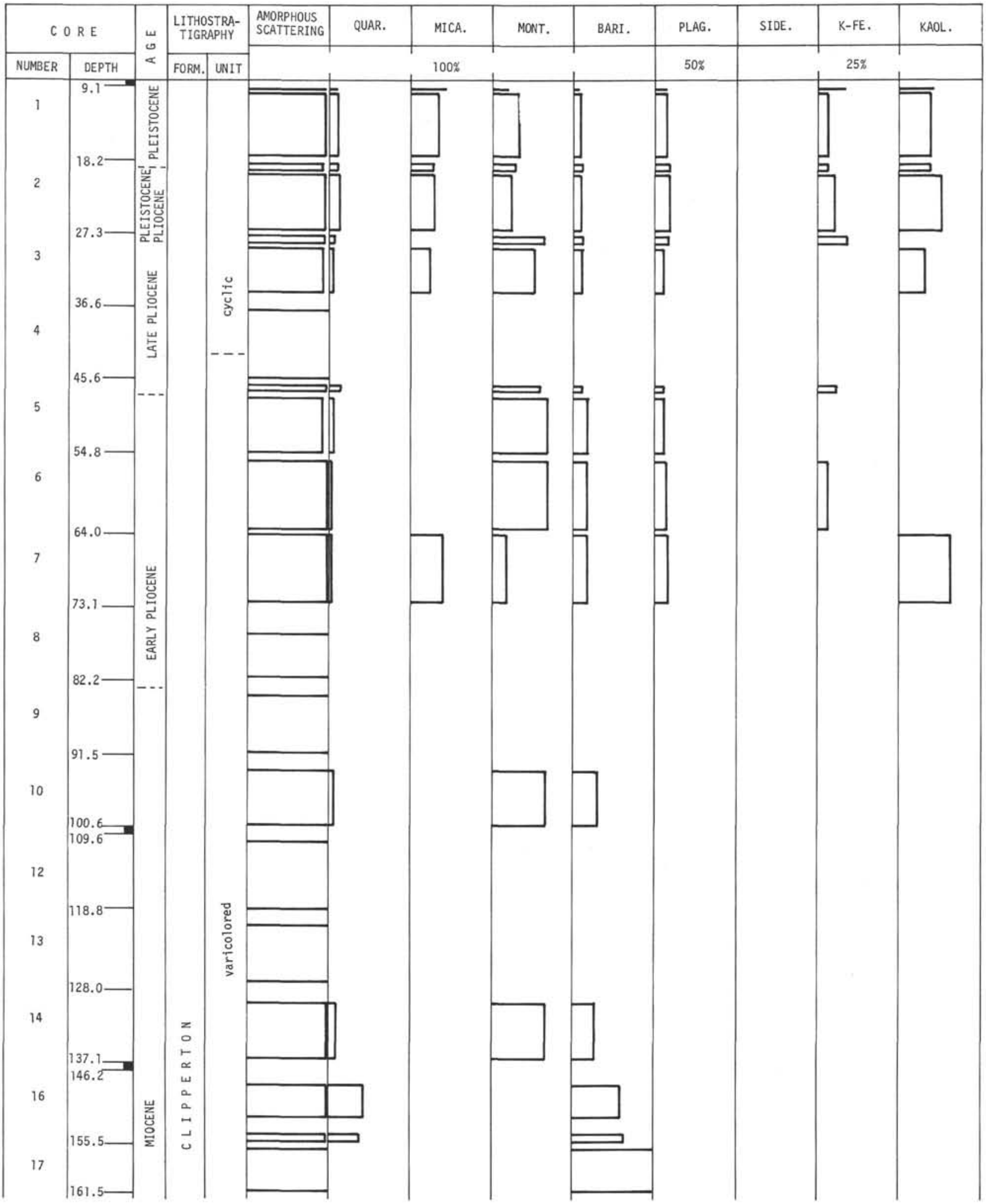

Figure 10. *Hole 77B, < 2μ.*

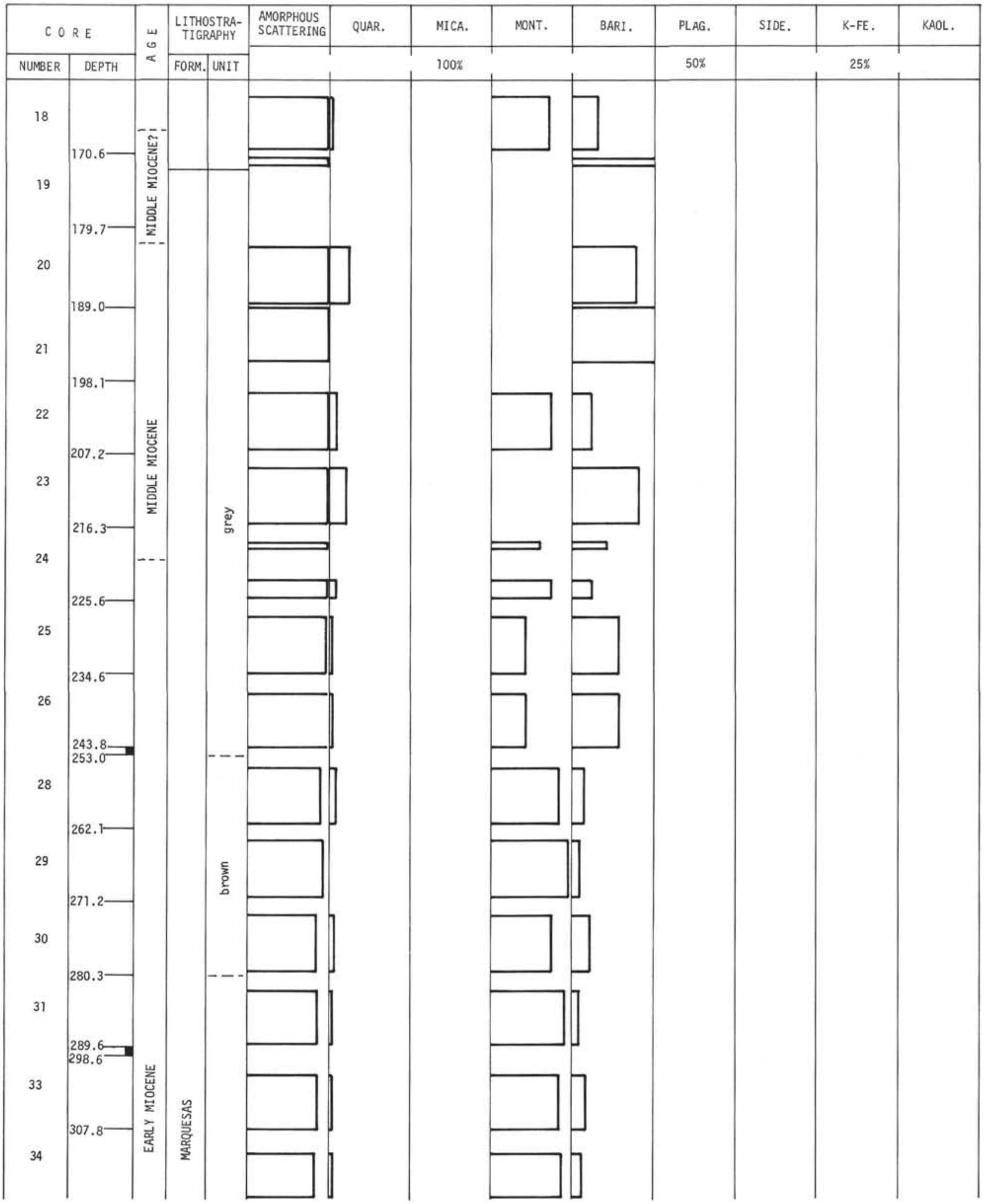

Figure 10. *Continued*

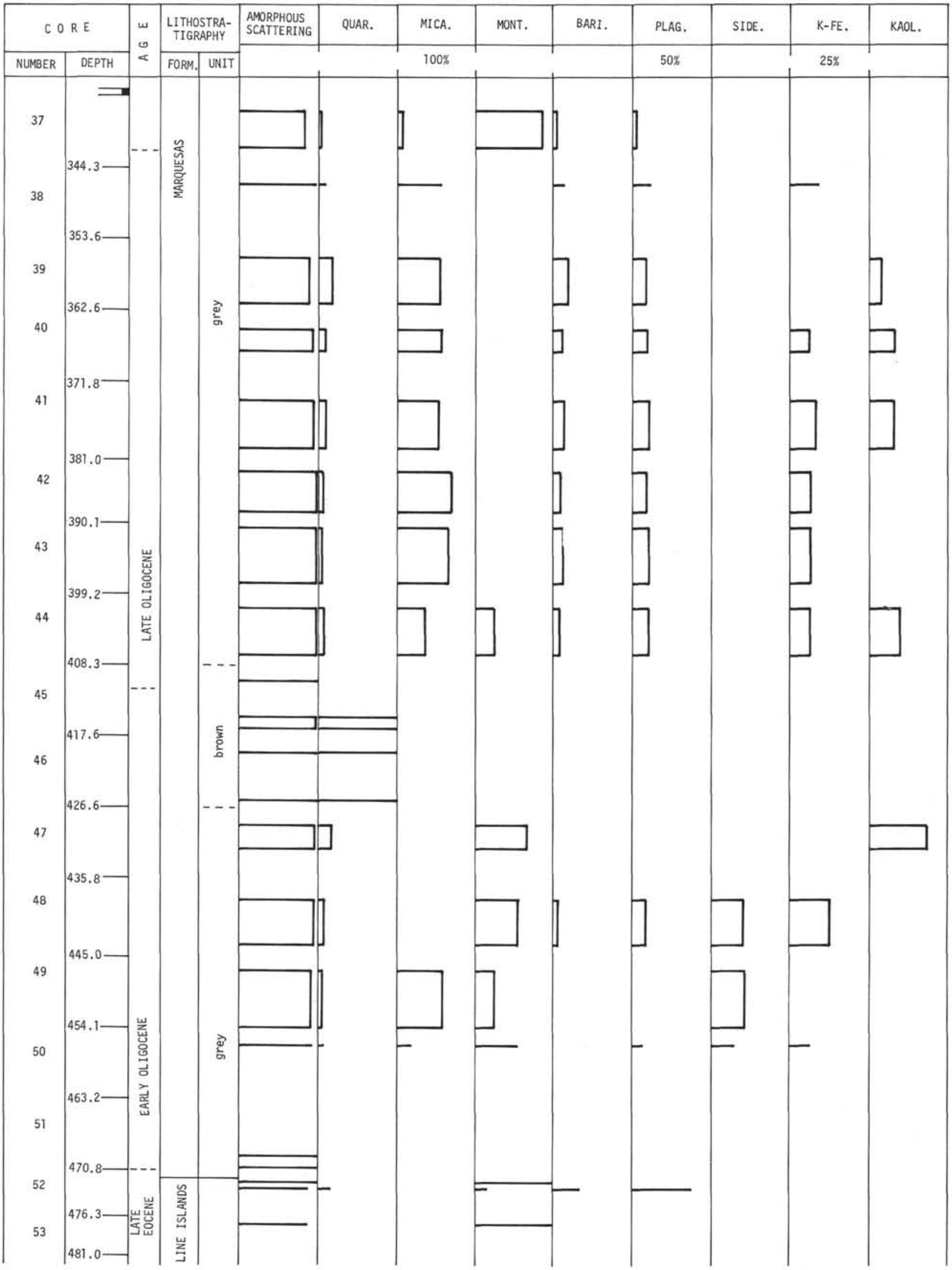

Figure 10. *Continued*

No corresponding fluctuations in the mineral assemblage in the <2 micron fraction of Site 77 are found in the Marquesas Oceanic Formation at Sites 71, 72, or 73.

The Late Eocene Line Islands Oceanic Formation overlies intrusive basalt and is in sharp contact with the Marquesas. The Line Islands exhibits laminations of varying shades of brown, but generally it grades downward from light brown to dusky brown, calcareous mudstones. Barite and clinoptilolite were detected in the bulk sample and constitute the major components of the 2 to 20 micron fraction (Figures 9 and 10). Montmorillonite is the dominant clay mineral but a trace of mica is seen in the bulk sample. Cristobalite occurs in the sediment at the basalt contact. Much of the dusky brown material is amorphous iron and manganese colloids (Cook, 1971, and Chapter 22, this volume).

Site 78

Site 78, which is the northernmost site of Leg 9, was drilled in an area of rugged bottom topography near the Clipperton Fracture Zone. Mineralogically and stratigraphically, Site 78 resembles Site 70 of Leg 8. The amorphous scattering percentage in the decalcified sediment is lower at this site than other Leg 8 and 9 sites near the equator which is probably due to the lower percentage of opaline biotic constituents.

Only the cyclic unit of the Clipperton Oceanic Formation is present at this site, and it consists of alternating pale orange calcareous ooze and dark brown siliceous ooze beds. Here the cyclic unit is Middle and Early Miocene. Barite forms the main crystalline phase of the 2 to 20 micron fraction. Clinoptilolite is present in several cores (Table 3). The very pale orange calcareous oozes have a fairly uniform mineral assemblage in the <2 micron fraction (Figure 12). Montmorillonite is the dominant clay mineral. Mica and kaolinite are also present but in lesser amounts. Plagioclase and quartz appear to co-vary (Figure 12). In contrast the interbedded dark brown siliceous oozes of the cyclic unit contain increased amounts of montmorillonite as well as some cristobalite and clinoptilolite; also, mica and kaolinite are absent from the siliceous oozes that were X-rayed. Barite is present in every sample.

The Marquesas Oceanic Formation (Early Oligocene to Early Miocene) is divided into three informal brown and gray units. This formation is a highly calcareous chalk ooze and only calcite was detected in the bulk samples (Figure 22). Barite occurs in nearly every sample of decalcified material (Table 3 and Figure 12). The mineralogy of the <2 micron fraction of the upper brown unit differs sharply from the overlying cyclic unit. Going from the cyclic unit into the upper brown unit of the Marquesas there is an abrupt disappearance of mica and kaolinite, an increase in the montmorillonite content, and plagioclase and quartz no longer covary. Goethite was detected in the <2 micron fraction of Core 9 (Table 3).

The succeeding gray unit largely resembles the first brown unit; however, in this gray unit there are scattered occurrences of clinoptilolite, magnetite and cristobalite in the 2 to 20 micron fraction (Table 3), and mica, kaolinite and K-feldspar in the <2 micron fraction (Figure 12). The lower brown unit is distinguished by having a very high montmorillonite content in the <2 micron fraction. Cristobalite occurs in large proportions in the 2 to 20 micron fraction (Table 3). The mineral assemblages of the <2 micron fraction of the Marquesas Oceanic Formation at Sites 70 and 78 show similarities in that they contain very little mica and kaolinite and both have high montmorillonite contents.

The Line Islands Formation is Early Oligocene and consists of a reddish brown, nannofossil chalk. A "baked" limestone was found in contact with basalt at the bottom of the hole. Only the chalk was submitted for X-ray analysis. The 2 to 20 micron fraction of this baked chalk contains some barite, and the <2 micron fraction is almost entirely composed of montmorillonite (Table 3, Figure 12).

Site 79

Here the Clipperton Oceanic Formation is Early Miocene to Pleistocene and consists of both the cyclic and varicolored units. In the cyclic unit barite is the major crystalline constituent of the 2 to 20 micron fraction (Table 4). Barite is also present in some bulk samples and all of the <2 micron samples (Figures 13, 15 and 16). Montmorillonite is the quantitatively important clay mineral. Mica and kaolinite are irregularly distributed. A dark, yellowish brown, radiolarian-rich ooze in Core 79A-1 contains the only occurrence of phillipsite at Site 79 in the <2 micron fraction (Figure 16).

The varicolored unit is highly calcareous (Figures 13 and 15), but the decalcified fractions have a high amorphous scattering percentage (Table 4). Montmorillonite occurs in consistently high concentrations in the <2 micron fraction. Barite and K-feldspar are randomly distributed.

The two units of the Clipperton Oceanic Formation differ markedly from one another: in the <2 micron fraction mica and kaolinite occur only in the cyclic unit, and the varicolored unit has a higher content of montmorillonite. In comparison with Sites 72, 73 and 78, the Clipperton at Site 79 resembles the other equatorial sites in their high calcium carbonate content and the dominance of barite in the 2 to 20 micron fraction.

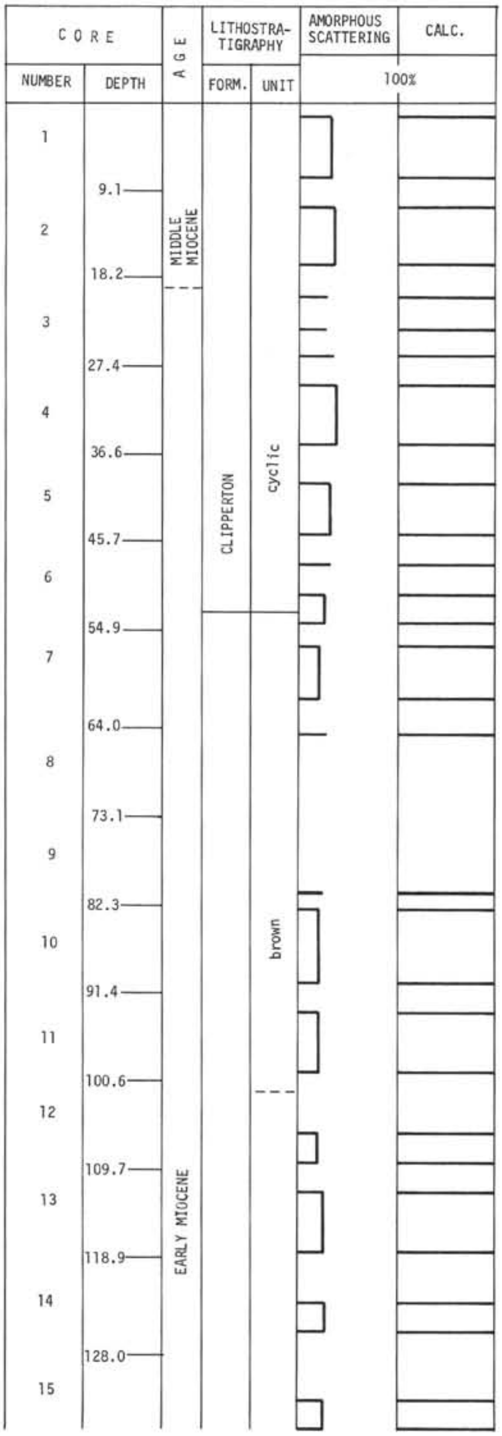

Figure 11. *Hole 78, bulk.*

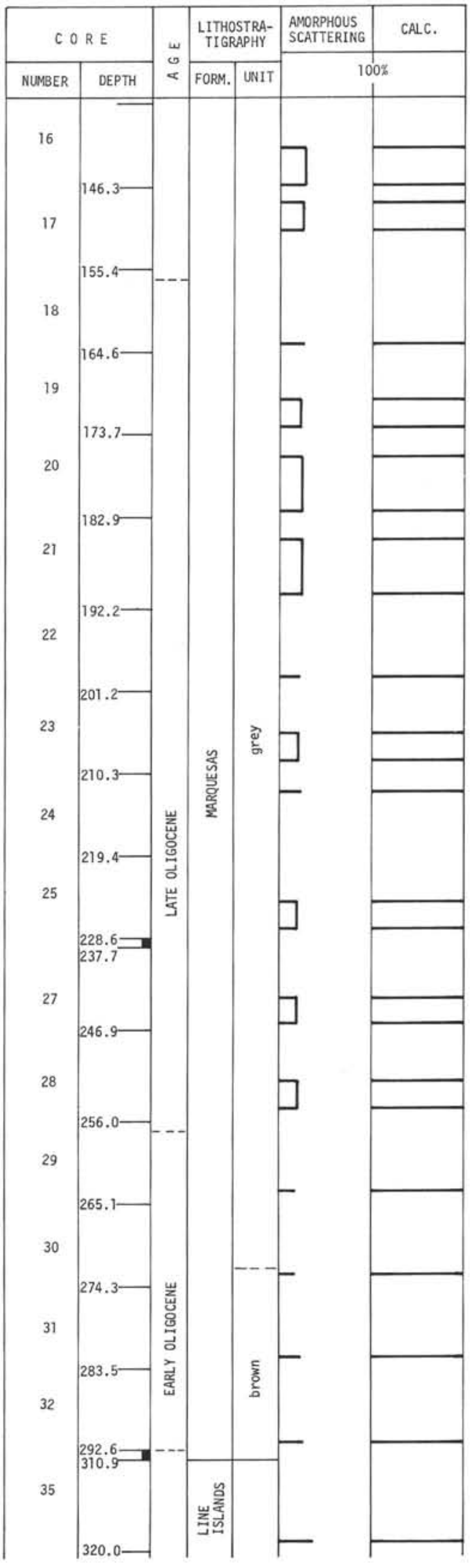

Figure 11. *Continued*

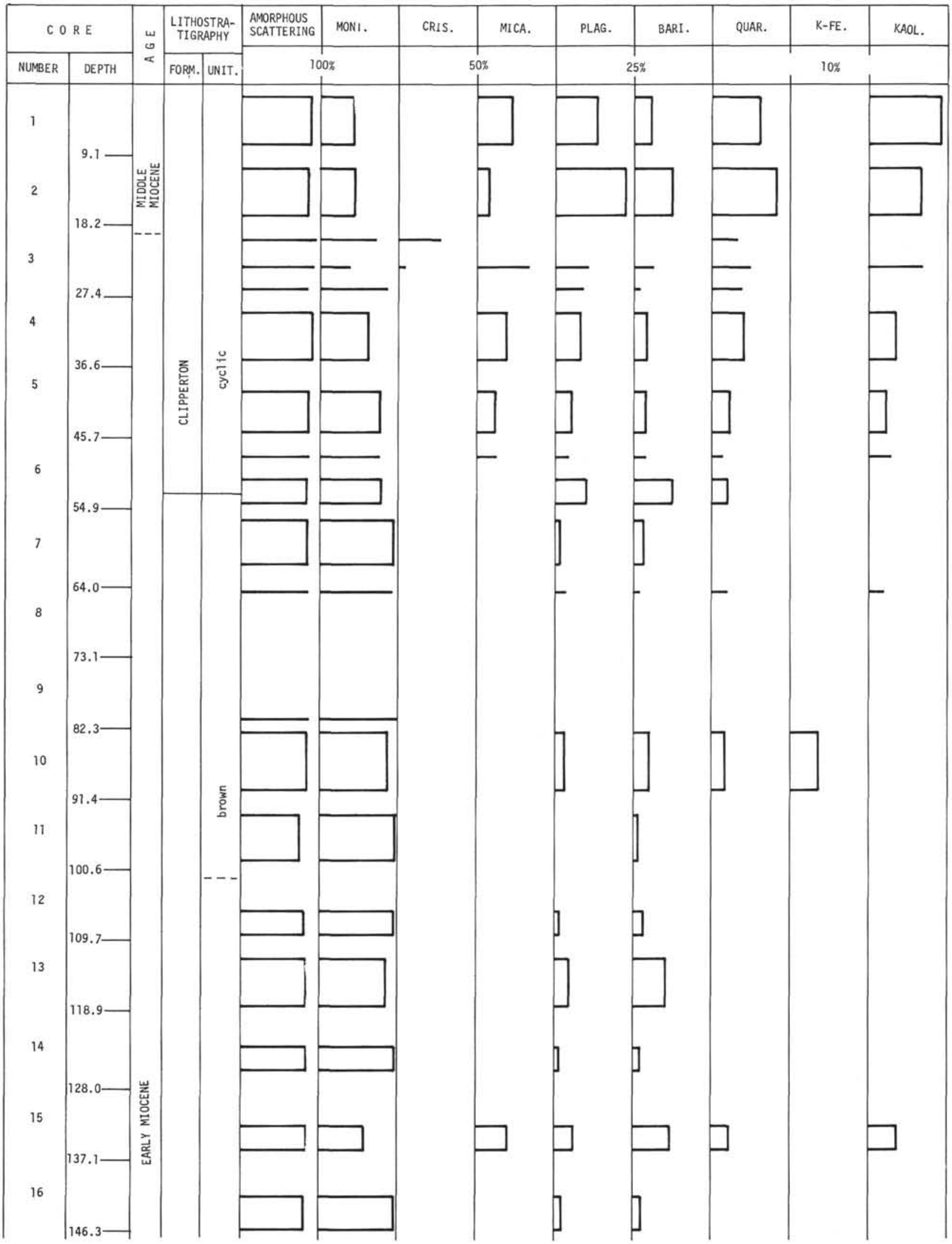

Figure 12. *Hole 78, $< 2\mu$.*

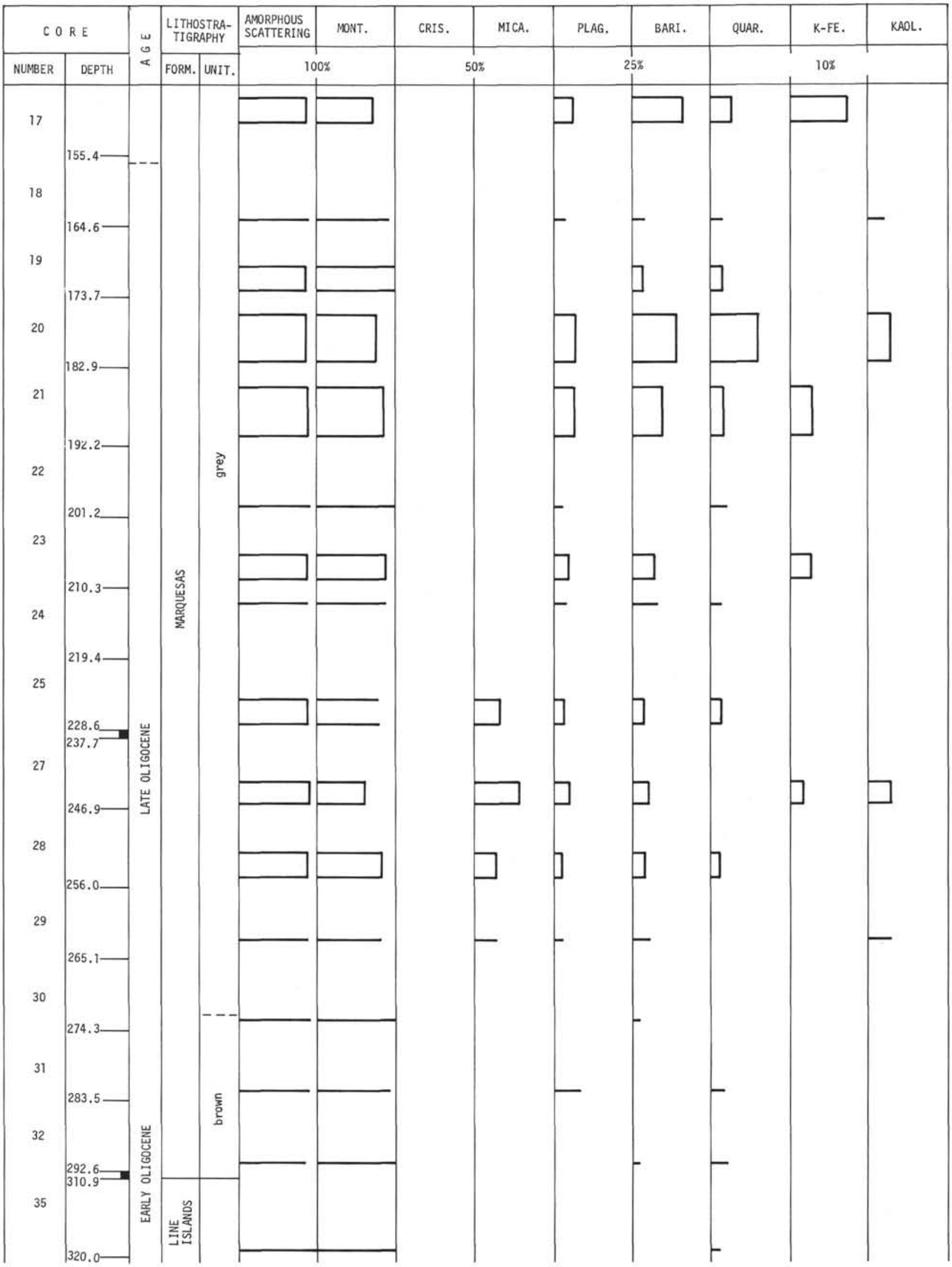

Figure 12. *Continued*

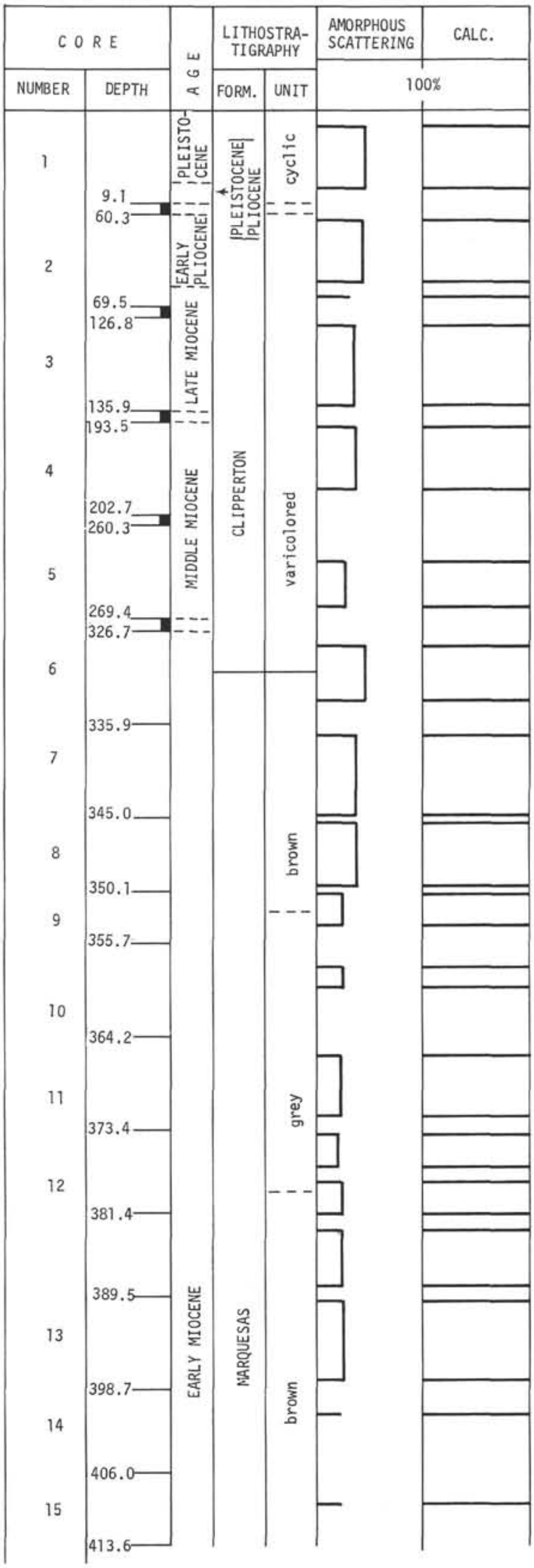

Figure 13. *Hole 79, bulk.*

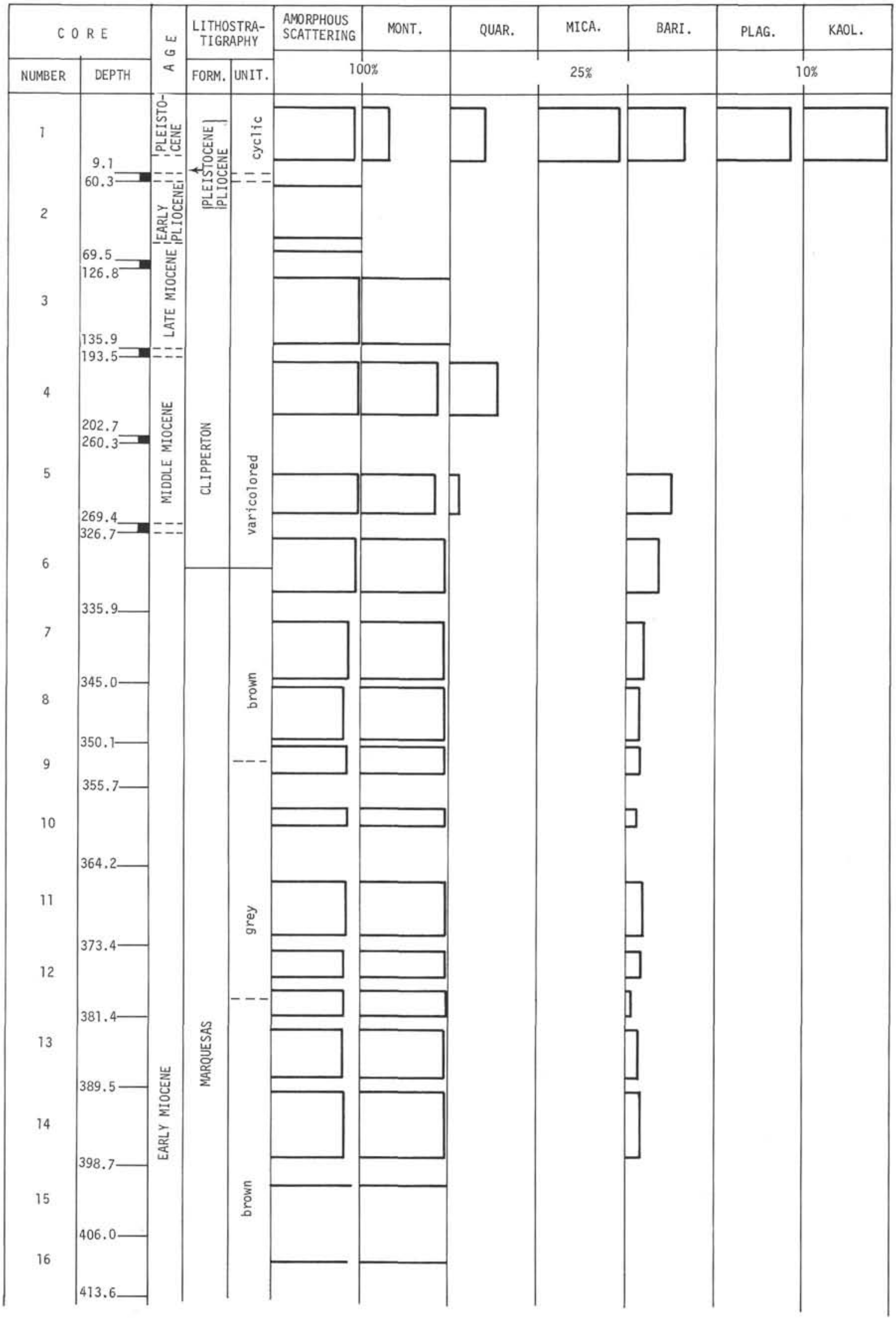

Figure 14. *Hole 79*, $< 2\mu$.

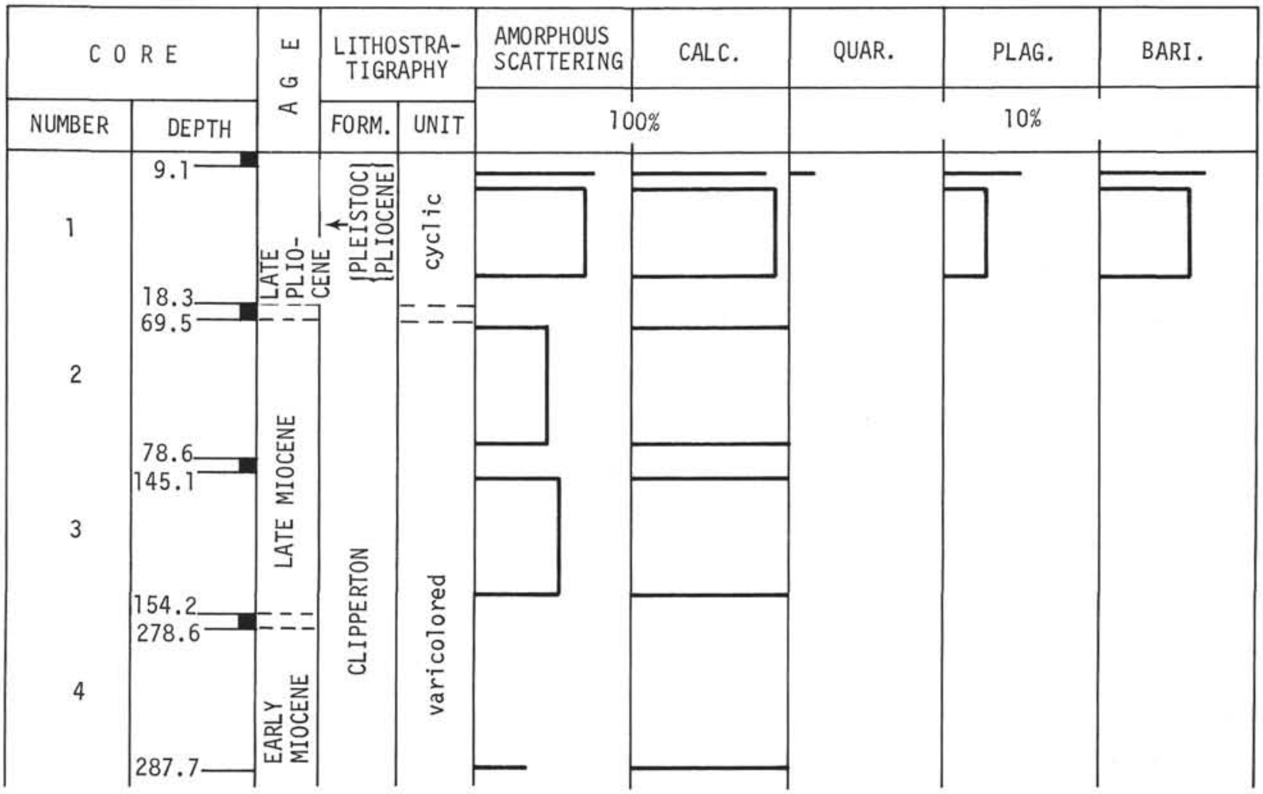

Figure 15. *Hole 79A, bulk*

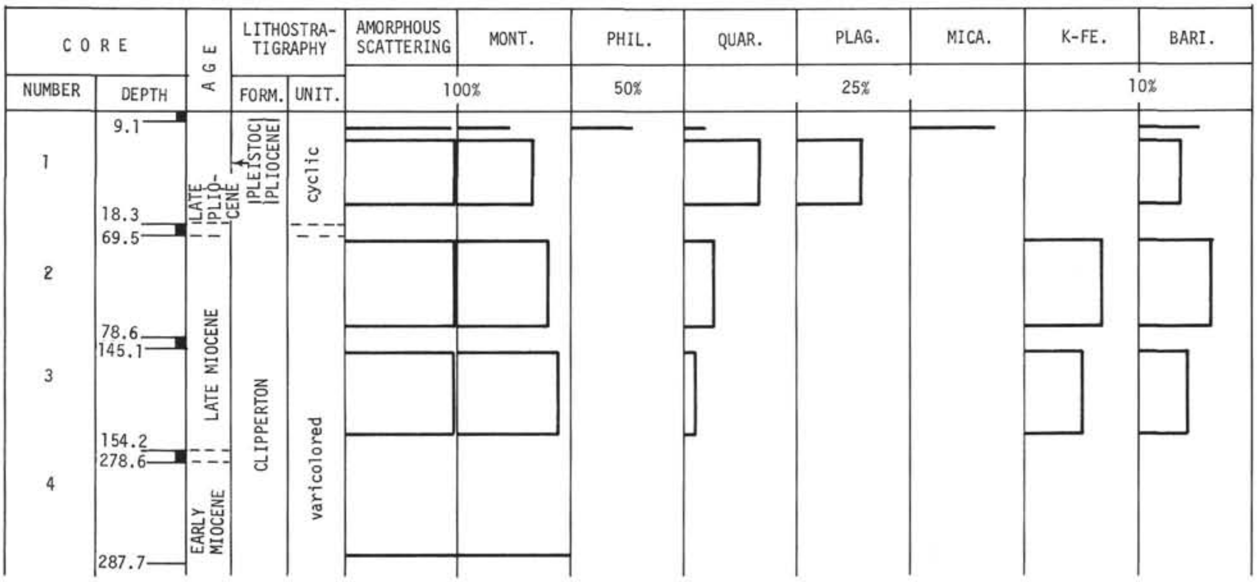

Figure 16. *79A, < 2μ.*

However, the mineralogy of the <2 micron fractions at each site is so highly variable that no simple comparison is possible.

The Marquesas Oceanic Formation (Early Miocene) is highly calcareous (Table 4). The formation was divided into three informal brown and gray units but no mineralogical differences could be discerned among them. Barite is the major mineral present in the 2 to 20 micron fraction throughout the formation. Dolomite is present in Core 13 of Hole 79 in a sequence of extremely well-indurated pale orange nannofossil chalks. The amorphous scattering is small in the decalcified fraction (Table 4). Montmorillonite, along with barite, make up the total of the crystalline phase in the <2 micron fraction (Figure 14). Samples of baked limestone in contact with basalt were not submitted for X-ray analysis.

Sediments of the Marquesas Oceanic Formation at Site 79 bear a strong resemblance to the Early Miocene sediments of Sites 77 and 78. Besides being highly calcareous and containing large quantities of barite, the <2 micron fractions at these sites contain high concentrations of montmorillonite and some barite. At Sites 77 and 79 these minerals occur virtually to the exclusion of other minerals. There appears to be no mineralogical similarity between the Marquesas at Site 79 and the Marquesas at Leg 8, Sites 72 and 73.

The Line Islands Oceanic Formation was not present at this site.

Site 80

Site 80 located 320 kilometers due south of Site 79, was chosen for the purposes of comparing the sedimentation and basement ages north and south of the equator. Here the Clipperton Oceanic Formation, which is Late Miocene through Pleistocene in age, consists of only the varicolored unit. It is a radiolarian-nannofossil ooze which is slightly more siliceous than the underlying Marquesas Oceanic Formation. Only calcite was detected in the bulk fraction and only barite was seen in the 2 to 20 micron fraction (Figures 17, 19 and Table 5). The <2 micron fraction is largely made up of siliceous ooze at the top of the formation, but samples lower in the formation contain large amounts of montmorillonite and lesser amounts of barite, quartz and plagioclase. The mineralogy of the <2 micron fraction from the bottom of the Clipperton Oceanic Formation resembles the underlying Marquesas Oceanic Formation. Other than the high content of calcite and barite, which is common to all the equatorial sediments, the varicolored units at Sites 79 and 80 bear very little resemblance to one another since their lithogeneous mineral assemblages are dissimilar. Furthermore, Sites 73 and 74 of Leg 8, which are located south of the equator, are also dissimilar.

The Marquesas Oceanic Formation is represented by cores consisting of very pale orange calcareous ooze and chalk. As at Site 70, the formation is Early Miocene and contains considerable amounts of barite in the 2 to 20 micron fraction (Table 5). The <2 micron fraction differs from Site 79 in that in addition to large quantities of montmorillonite and barite, some quartz, K-feldspar, plagioclase and kaolinite can be detected (Figures 13, 18 and 20). Sites 79 and 80 mark the easternmost sites where the Marquesas Oceanic Formation has been described.

The Early Miocene Line Islands Oceanic Formation is a thinly bedded, moderate brown, clay chalk which is in intrusive contact with basalt. A composite of three samples from the upper part of the formation shows only calcite in the bulk sample (Figure 17). Clinoptilolite and barite occur in the 2 to 20 micron fraction (Table 5), and the <2 micron fraction consists predominantly of montmorillonite with minor amounts of siderite and quartz (Figure 18).

Site 80

A thin cyclic unit and a portion of the varicolored unit of the Clipperton Oceanic Formation were cored at Site 81. The samples were of Pleistocene age. As at previous sites, the cyclic unit consists of brown, clayey, radiolarian-rich oozes interbedded with very pale orange, calcareous oozes. In both units calcite is the dominant mineral in the bulk sample and barite the main mineral in the 2 to 20 micron fraction (Figure 21 and Table 6). The <2 micron fraction of the cyclic unit contains a high proportion of amorphous material. Only barite, quartz and a trace of montmorillonite were detected. The <2 micron fraction of the varicolored unit, by contrast, contains a large concentration of montmorillonite and, in addition, small quantities of barite, quartz, siderite, K-feldspar and kaolinite. In this respect the varicolored unit resembles the cyclic unit at Site 79 which is also Pleistocene.

Site 81

Site 81 is the westernmost occurrence of the San Blas Oceanic Formation. Two cores were recovered of Middle Miocene age. The sediment is a blue and green radiolarian-nannofossil chalk and, as with most of the sediments in the area, calcite predominates in the bulk samples (Table 6). Barite is the most abundant crystalline phase in the 2 to 20 micron fraction, and the <2 micron fraction is rich in montmorillonite (Figures 21 and 22; Table 6).

The Line Islands Oceanic Formation is an Early Miocene, radiolarian-nannofossil chalk with manganese dendrites scattered throughout. The lower part of the formation consists of a pale orange, thinly bedded,

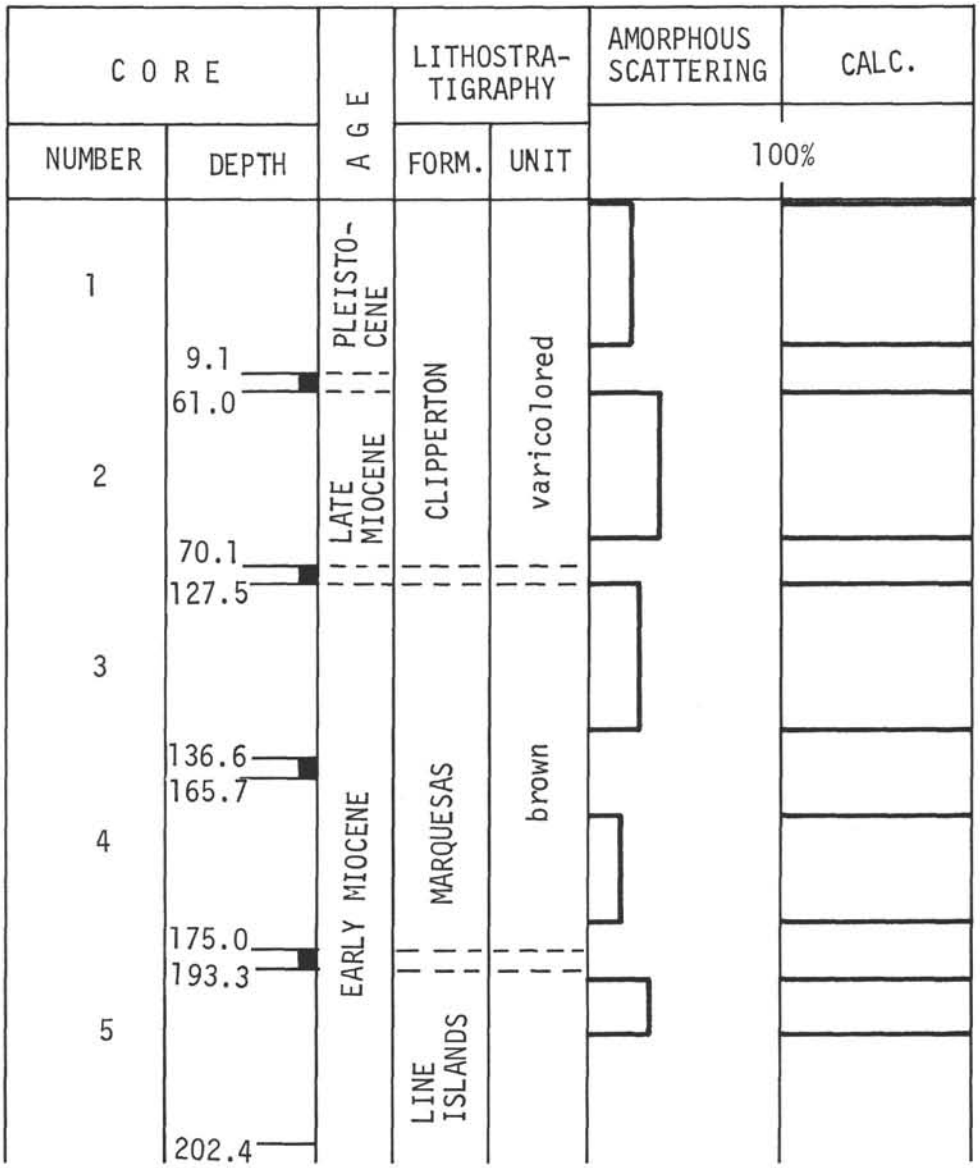

Figure 17. *Hole 80, bulk.*

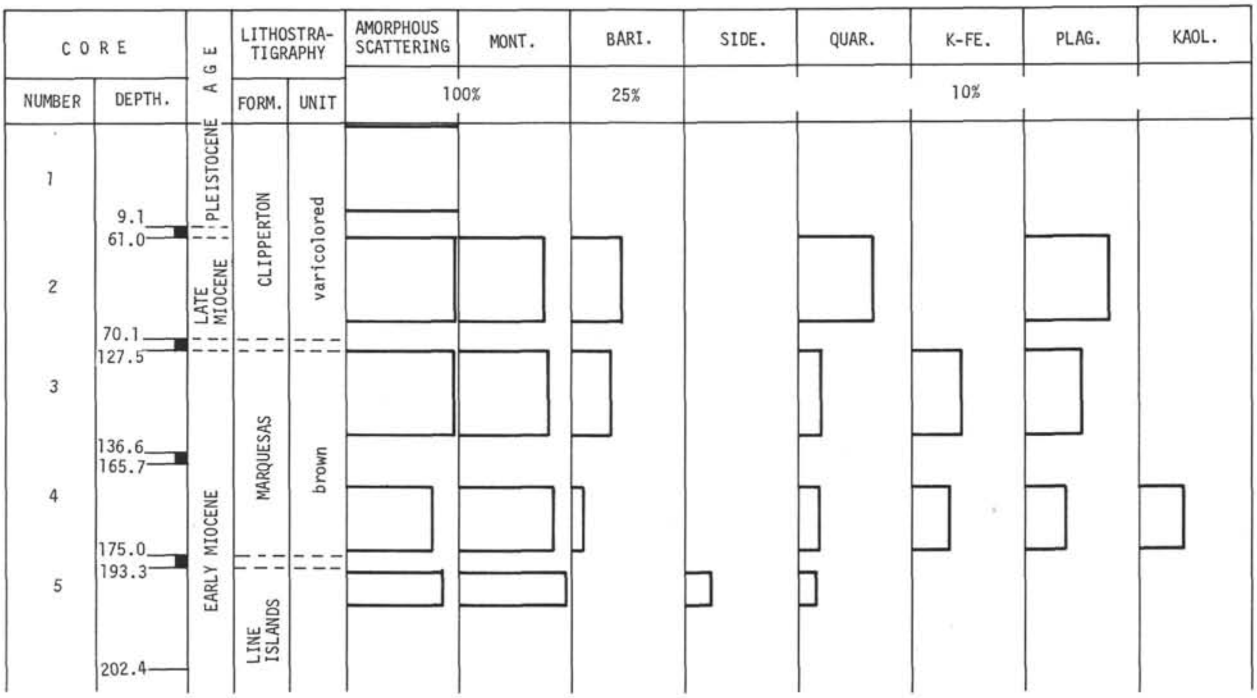

Figure 18. *Hole 80, < 2μ.*

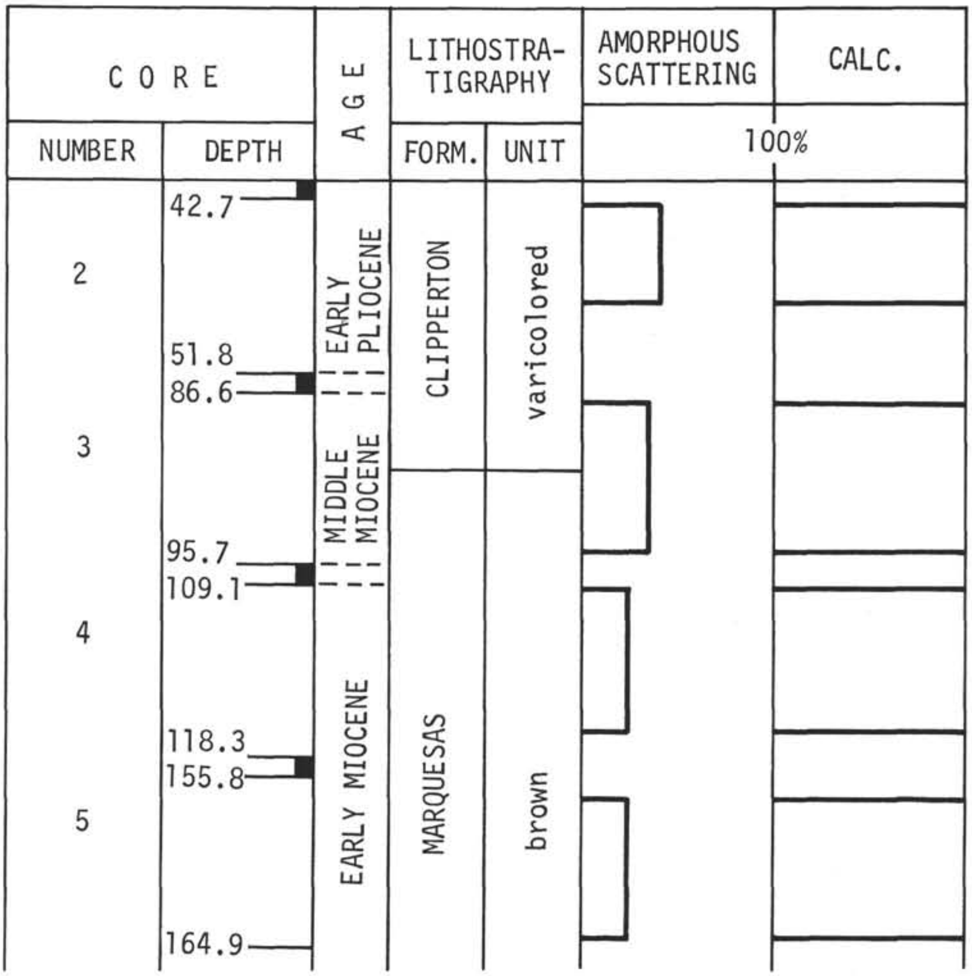

Figure 19. *Hole 80A, bulk.*

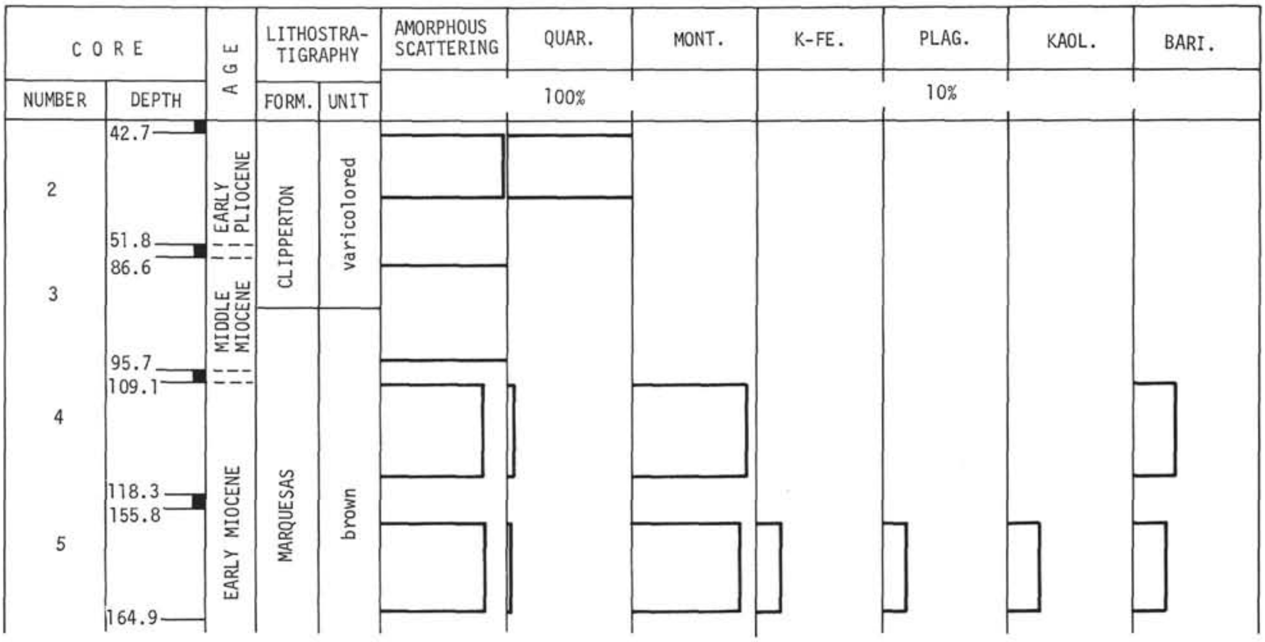

Figure 20. *Hole 80A, < 2μ.*

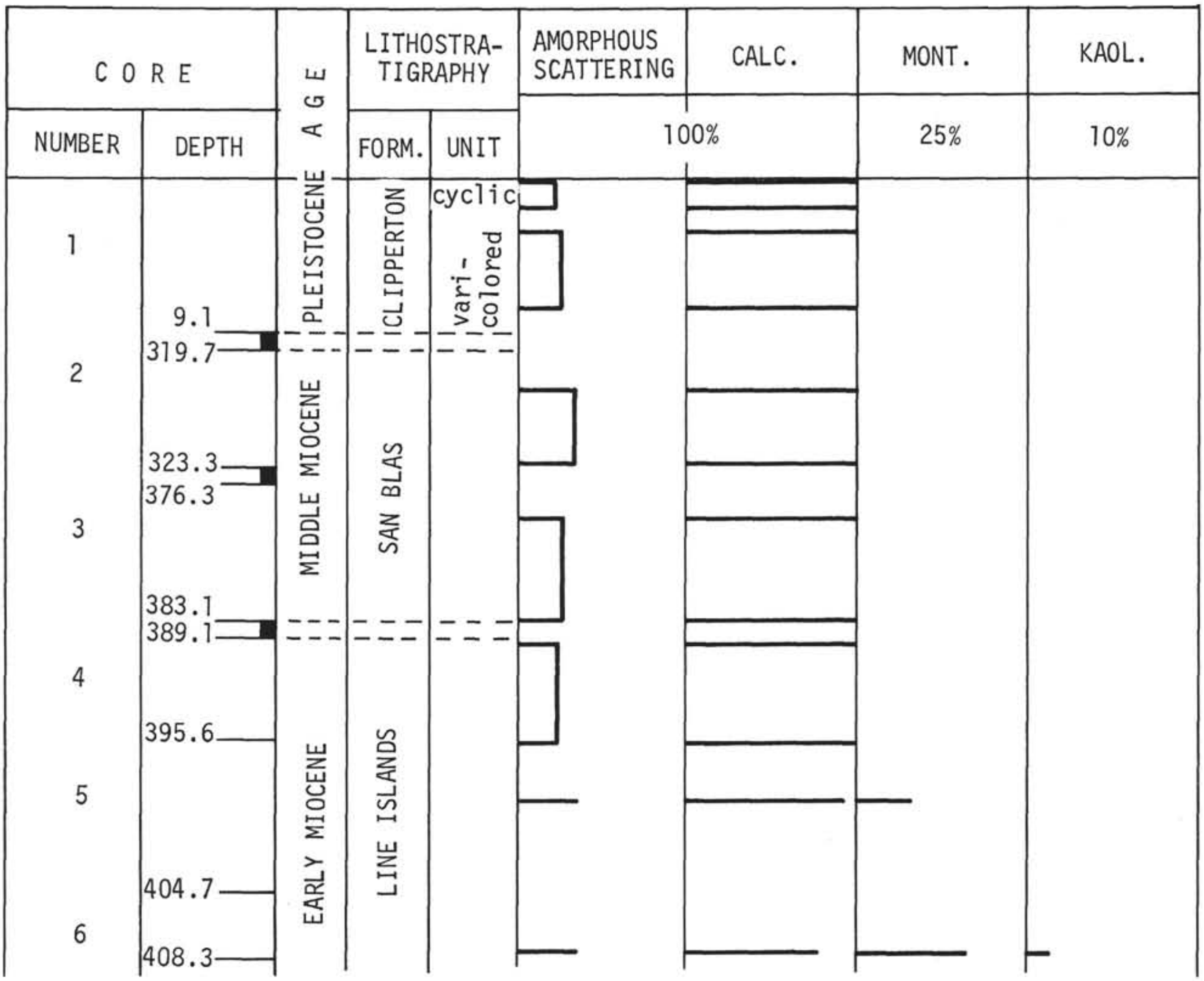

Figure 21. *Hole 81, bulk.*

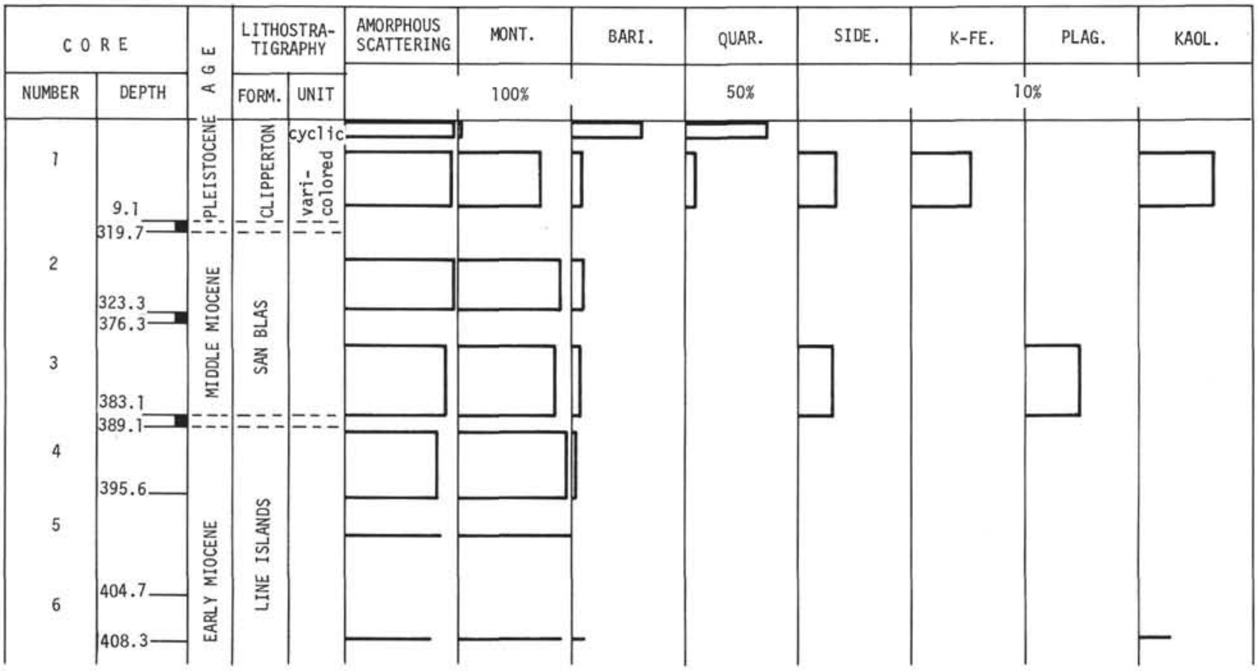

Figure 22. *Hole 81, < 2μ.*

brecciated, calcareous clay in intrusive contact with basalt. The formation is dominated by barite in the 2 to 20 micron fraction and by montmorillonite in the <2 micron fraction. Kaolinite is restricted to the lower part of the formation (Figures 21 and 22).

Site 82

Site 82 is located on the west flank of the East Pacific Rise at a point where, going westward, the sediment thickness abruptly increases. The Clipperton Oceanic Formation consists of only the cyclic unit and is entirely Pleistocene. Calcite and barite are the major crystalline phases of the bulk sample and 2 to 20 micron fractions, respectively (Figure 23 and Table 7). The <2 micron fraction consists mainly of montmorillonite. Some K-feldspar and kaolinite are found as in the Pleistocene sediments at Site 81. The only occurrence of mica at Site 82 is found in the <2 micron fraction of the cyclic unit (Figure 24).

The San Blas Oceanic Formation is a blue and green, radiolarian-nannofossil calcareous chalk ooze which ranges in age from Late Miocene to Pleistocene. The amorphous content is high in the 2 to 20 micron fractions (Table 7). Barite forms the major crystalline phase in the 2 to 20 micron fraction (Table 7), and montmorillonite is most abundant in the <2 micron fraction (Figures 24 and 26). The <2 micron fraction also contains a considerable proportion of lithogenous minerals as well as one occurrence of siderite in Core 2.

The Line Islands Oceanic Formation is a very pale orange, Late Miocene, siliceous chalk with manganese dendrites. Calcite is the only mineral seen in the bulk samples (Figures 23 and 25), barite is prevalent in the 2 to 20 micron fraction (Table 7), and montmorillonite is the only crystalline constituent detected in the <2 micron fraction.

Site 83

Site 83 was drilled on the east flank of the East Pacific Rise. The Clipperton Oceanic Formation consists of only the cyclic unit which is entirely Pleistocene as at Site 82. Calcite is the main mineral in the bulk samples (Figure 27), and barite predominates in the 2 to 20 micron fraction (Table 8). Montmorillonite is the dominant mineral in the <2 micron fraction, but small amounts of quartz, plagioclase, kaolinite and barite were detected. The mineral assemblages of the Clipperton's cyclic unit east and west of the East Pacific Rise are very similar.

The San Blas Oceanic Formation, Late Miocene to Pleistocene in age, is a green radiolarian-nannofossil ooze. It is subdivided into three informal units on the basis of color and bedding differences. In the bulk analyses (Figures 27 and 29) the entire formation is highly calcareous, but in the upper two dark green units, small quantities of montmorillonite, quartz, plagioclase, barite and dolomite can be detected. In the 2 to 20 micron fraction, barite occurs in every sample; pyrite appears randomly in about half of the samples.

In the <2 micron samples some broad mineralogical differences can be seen among the units of the San Blas, but sharp boundaries cannot be drawn (Figures 29 and 30). The top of unit one, which is the darkest green unit, resembles the cyclic unit (Figure 28). The remainder of the unit, however, contains a high percentage of montmorillonite accompanied by minor amounts of quartz. Unit two contains a reduced quantity of montmorillonite. The quartz content remains the same and detectable quantities of plagioclase, barite, K-feldspar and kaolinite are noted. The montmorillonite content increases abruptly with a corresponding reduction in the concentration of other minerals in unit three. Sediments from the bottom of unit three (Figure 23) show some quartz and barite in the <2 micron fraction resembling the underlying Line Islands Oceanic Formation in this respect.

The Line Islands Oceanic Formation is a brown, thinly bedded, intensely mottled, brecciated chalk in intrusive contact with basalt. The formation is Middle Miocene at this site. Calcite and barite make up the major crystalline phases of the bulk sample and the 2 to 20 micron fraction, respectively (Figure 27 and Table 8). In the <2 micron fraction, montmorillonite is the major mineral present with only quartz and barite occurring in trace amounts (Figure 28).

Site 84

The site is located in an area of low relief on the deep sea floor close to Panama. At Site 84 the San Blas Oceanic Formation, which is Late Miocene through Pleistocene, has been divided into five informal units, primarily on the basis of color and bedding (Chapters 10 and 22, this volume). Several mineralogical changes accompany the unit boundaries (Figures 31 and 32; Table 9).

The formation grades downward from dark greenish-black volcanic-radiolarian-nannofossil oozes in unit one to very light greenish-gray radiolarian-nannofossil chalks poor in volcanics in unit five. In general, the formation progressively becomes lighter green, poorer in volcanic constituents, and richer in biotic constituents with depth.

In the bulk analyses there is a progressive down-hole decrease in montmorillonite, plagioclase, kaolinite and quartz (Figure 31). Minerals which diminish with depth and are not detected in bulk analyses of the lower units include mica, chlorite, K-feldspar, clinoptilolite and

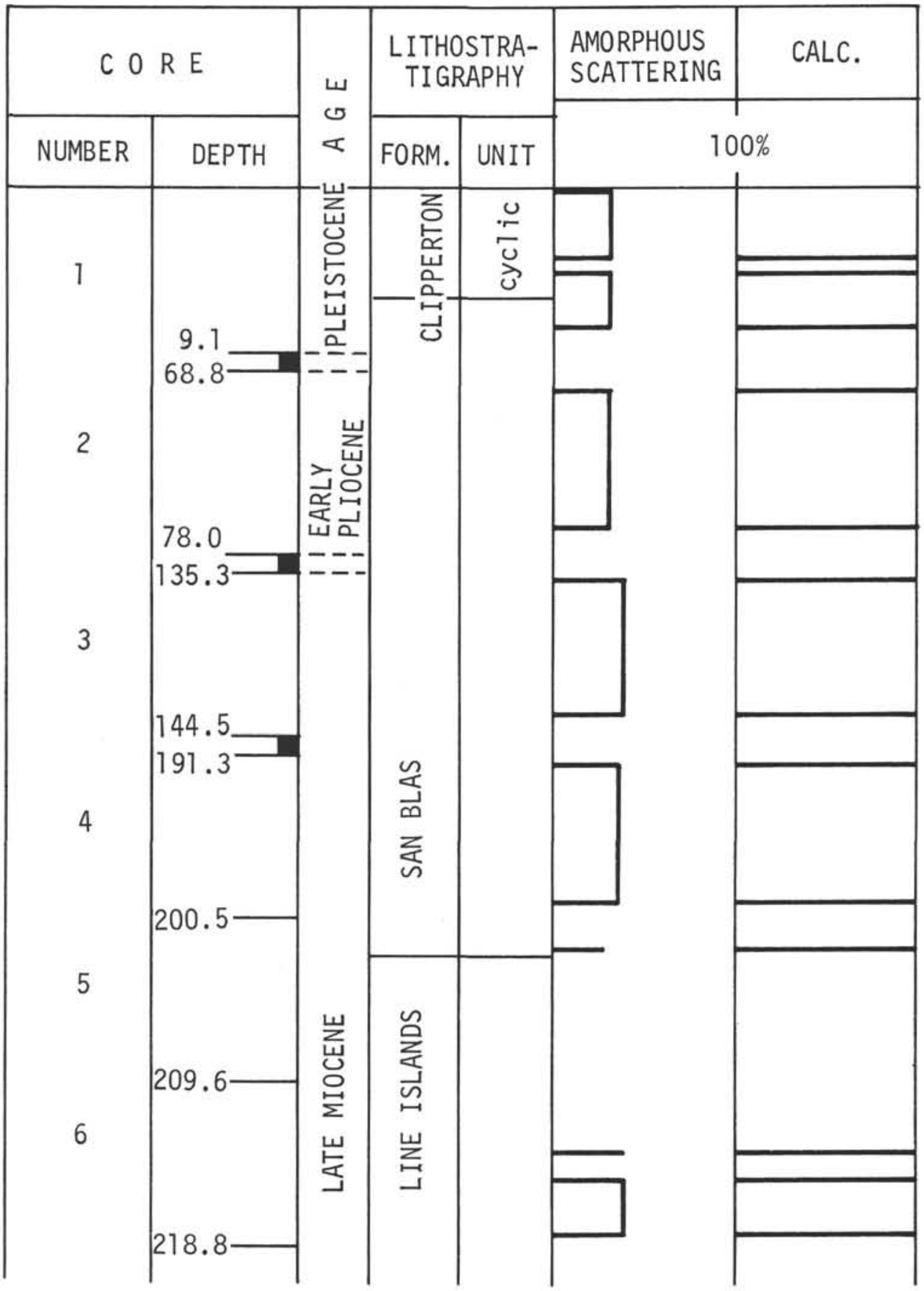

Figure 23. *Hole 82, bulk.*

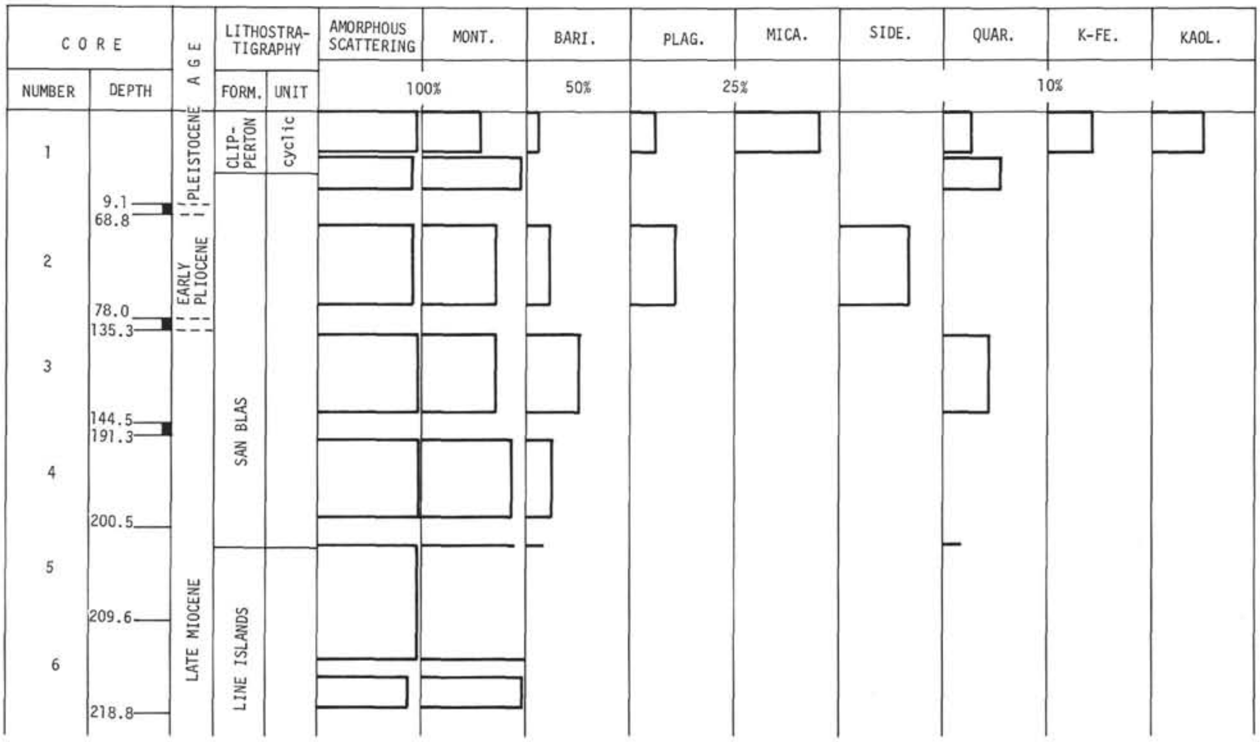

Figure 24. *Hole 82, < 2μ.*

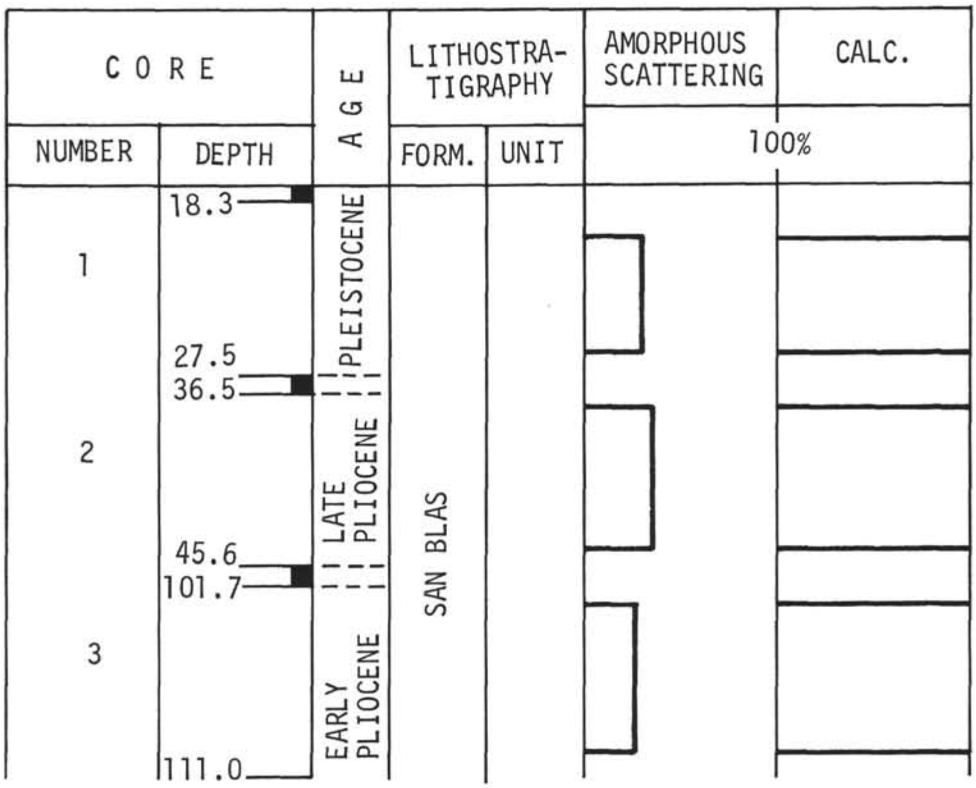

Figure 25. *Hole 82A, bulk.*

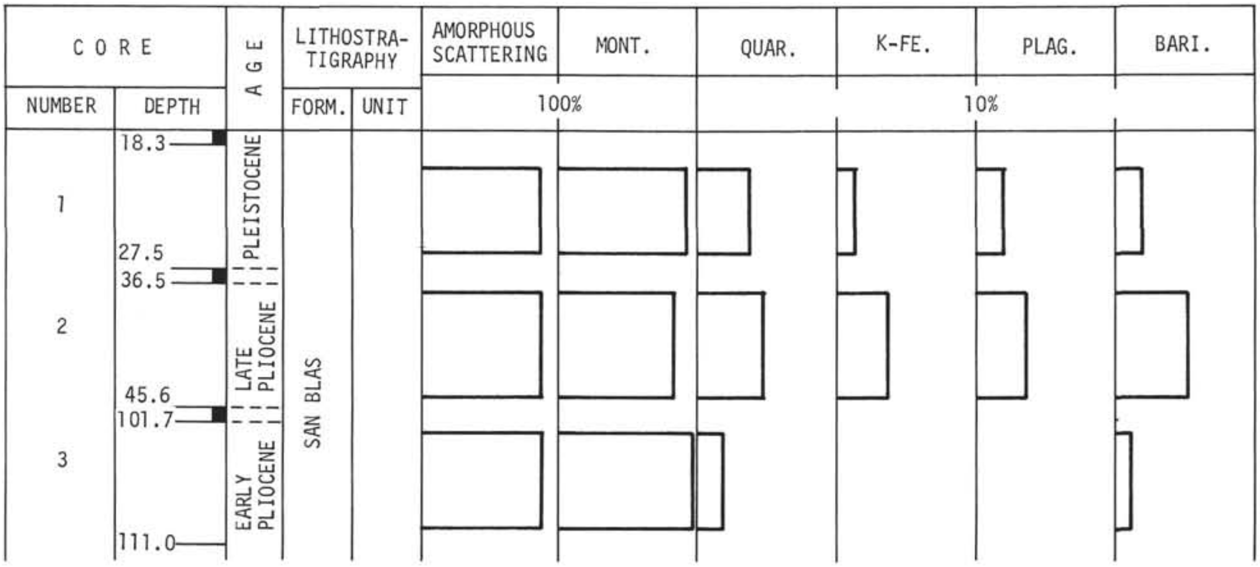

Figure 26. *Hole 82A, < 2μ.*

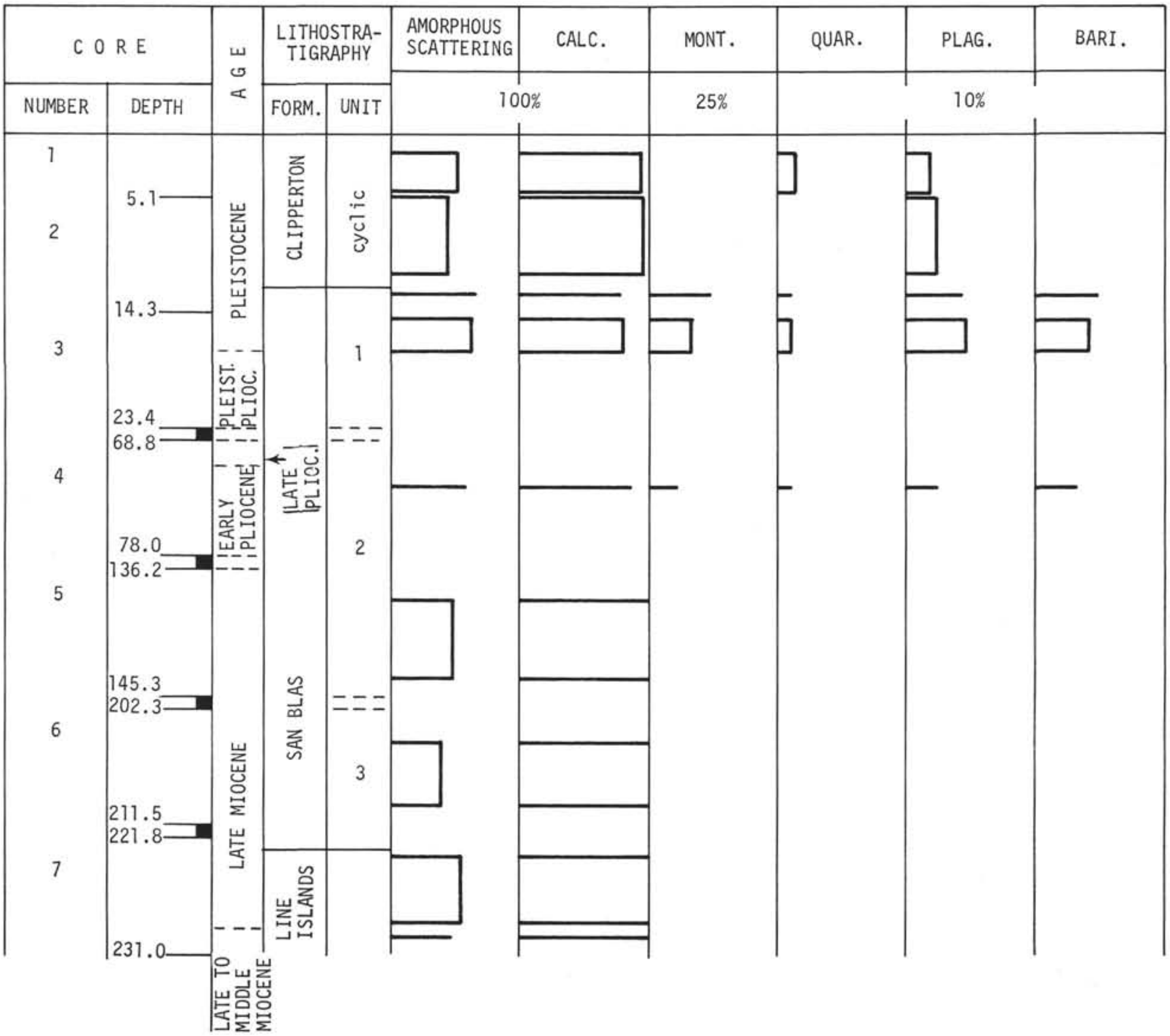

Figure 27. *Figure 83, bulk.*

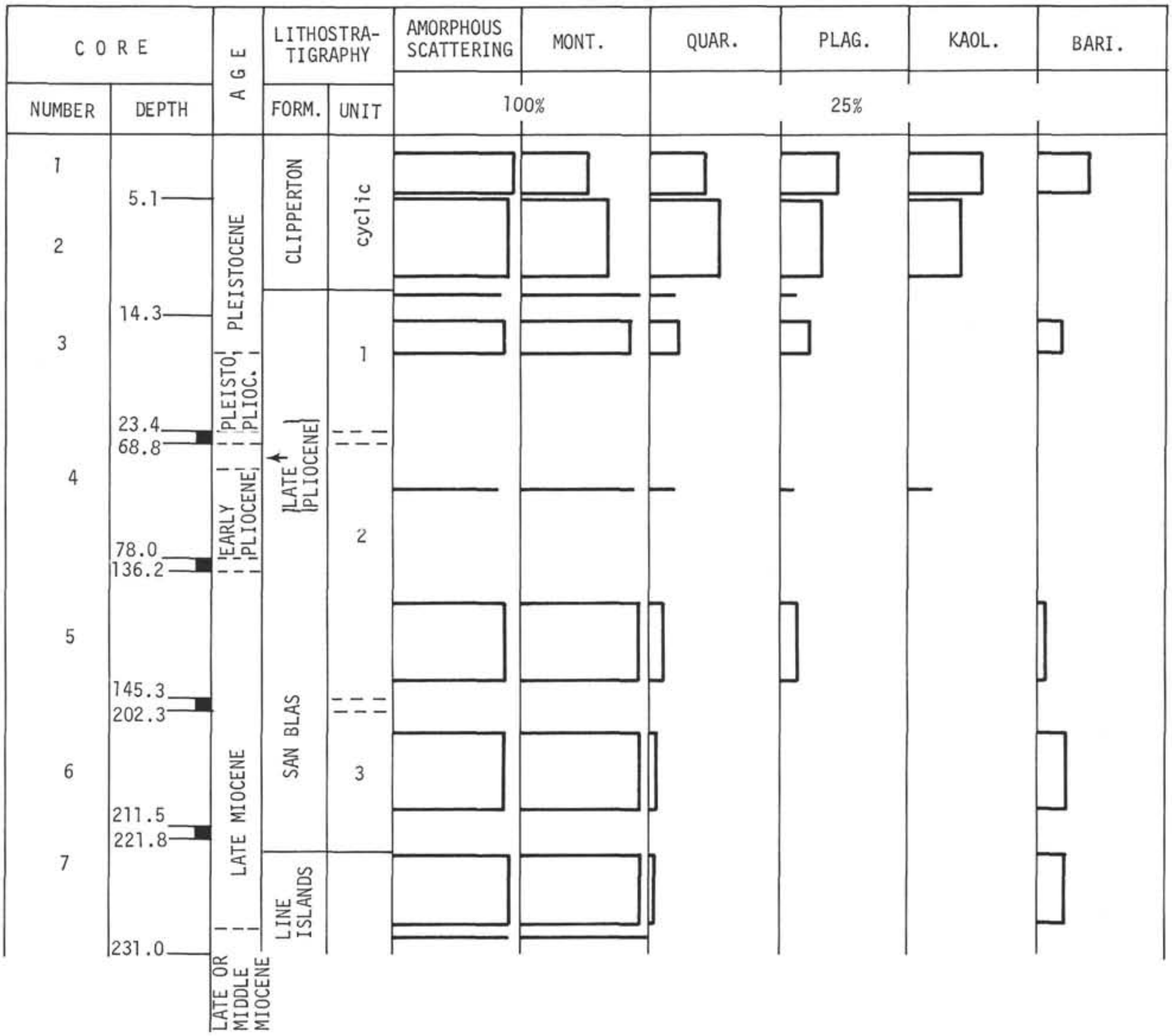

Figure 28. *Hole 83, < 2μ.*

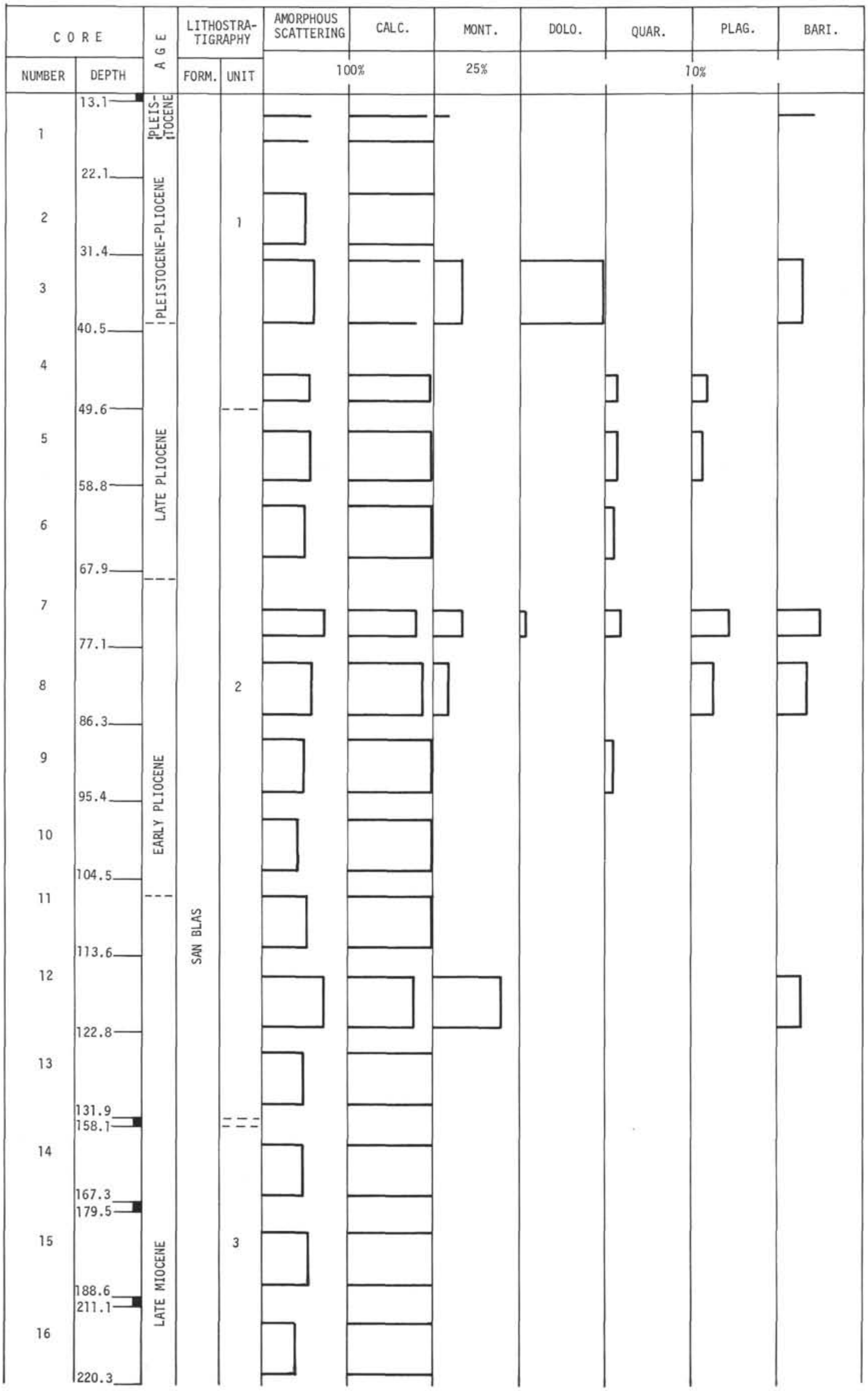

Figure 29. *Hole 83A, bulk.*

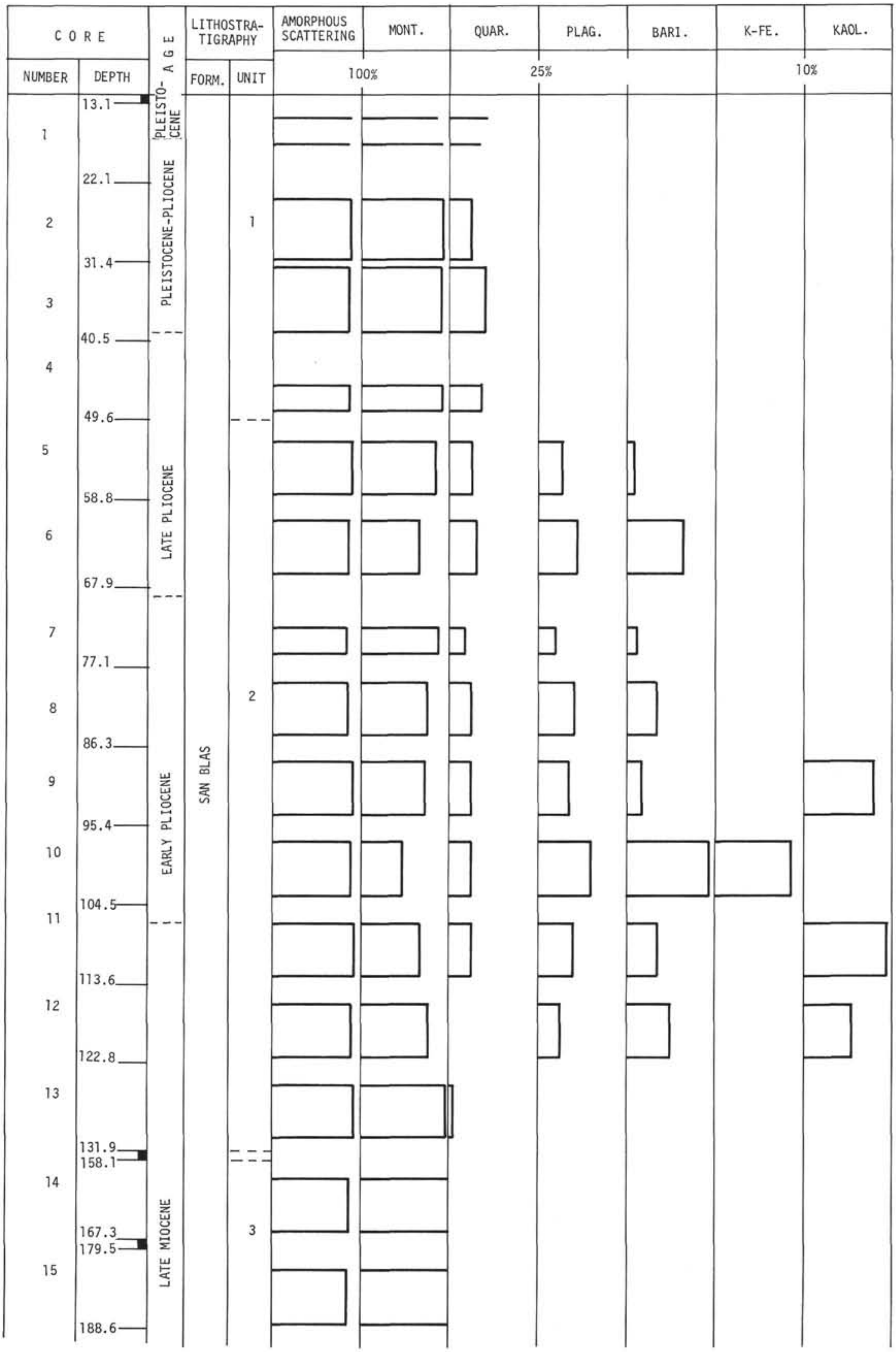

Figure 30. *Hole 83A, < 2μ.*

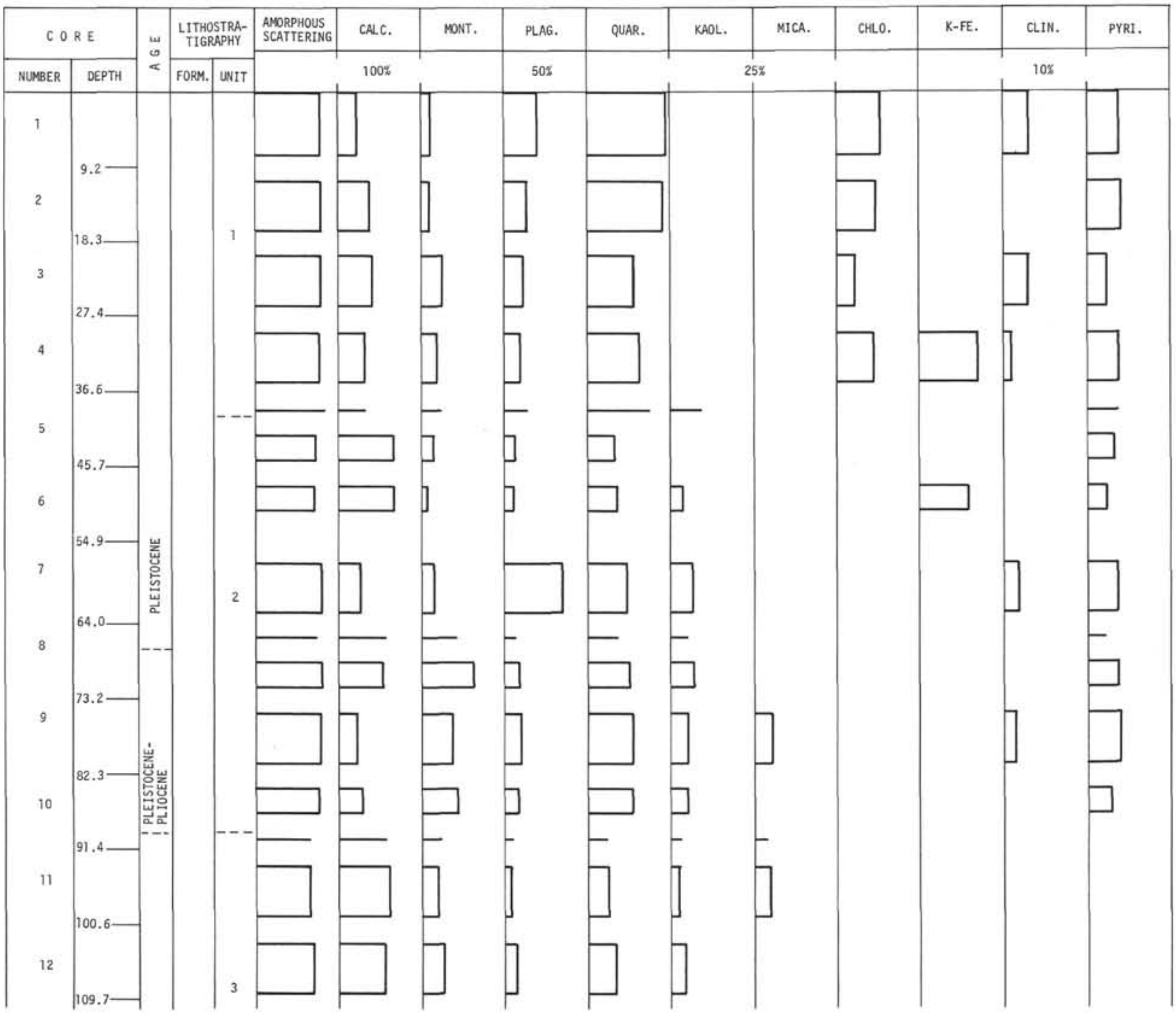

Figure 31. *Hole 84, bulk.*

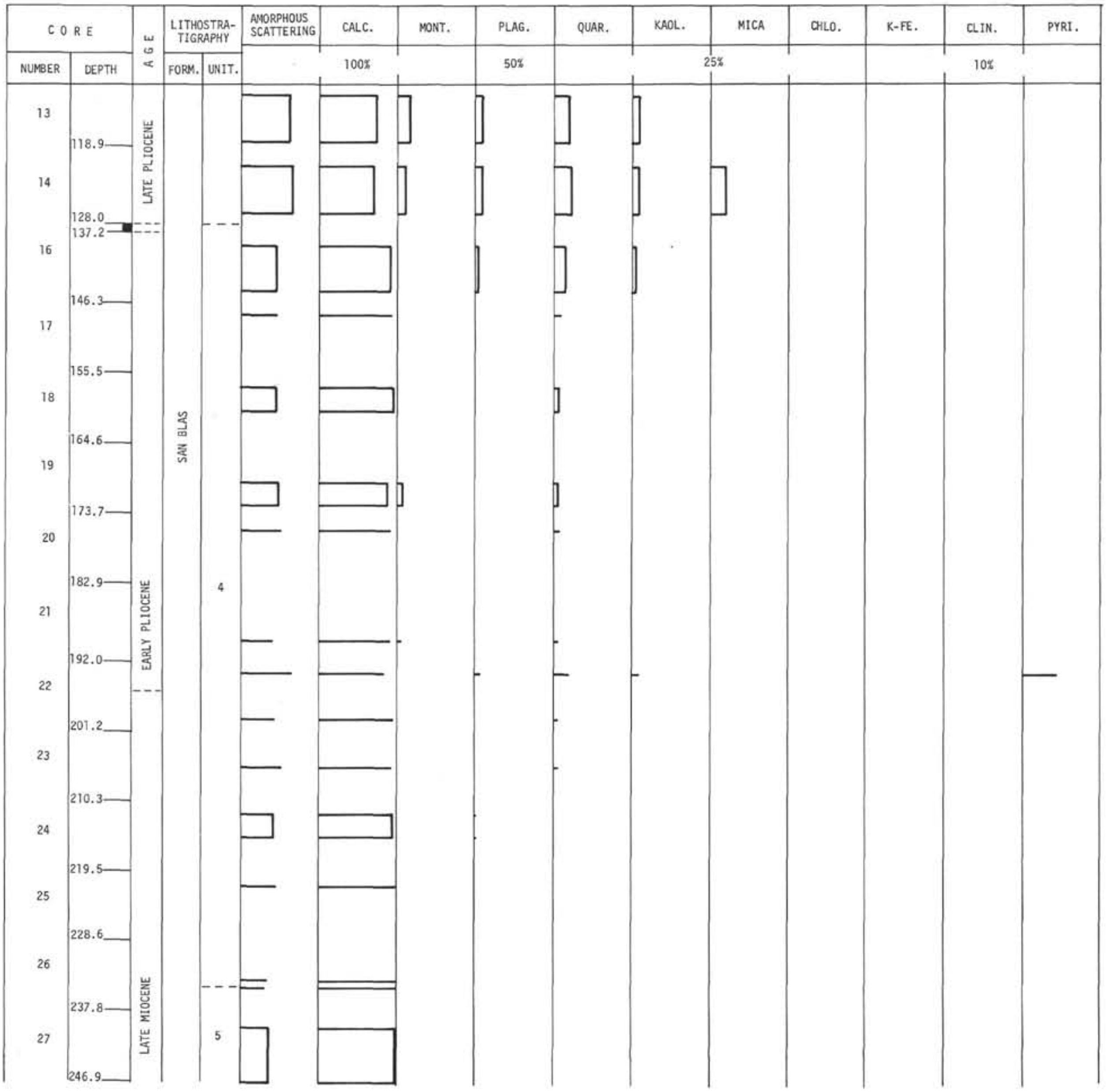

Figure 31. *Continued*

pyrite. This down-hole change is accompanied by a decrease in the observed volcanic constituents, such as shards, pumice fragments, oxyhornblende, euhedral laths of sanidine and plagioclase, as well as down-hole decrease in sedimentation rate.

In the 2 to 20 micron fraction, the amorphous scattering percentage increases with depth, which reflects an increasing radiolarian content. Pyrite is found throughout units one to three. Clinoptilolite occurs more frequently in the upper units, possibly in association with volcanic shards and pumice fragments. Conversely, the barite frequency increases with depth.

In the <2 micron fraction (Figure 32), montmorillonite occurs in large concentrations throughout the formation but not to the exclusion of other minerals as in many previous holes. It is noteworthy that the montmorillonite content in the <2 micron fraction shows no apparent increase in the pyroclastic-rich upper portions of the formation as it does in the bulk analyses (Figures 31 and 32). Kaolinite is present throughout the section; mica was detected only in a few scattered intervals. As in the bulk samples, pyrite in the <2 micron fraction is restricted to units one and two, and clinoptilolite occurs with greater frequency in the top half of the formation.

DISCUSSION AND CONCLUSIONS

Using the X-ray data of Legs 8 and 9, some interpretations of the mineral distribution of sediments from the eastern equatorial Pacific Ocean may be made. However, due to the large amount of X-ray data and the numerous variables involved (three sediment fractions of X-ray data, numerous minerals, diachronous formations, varying sedimentation rates, changing geographic location due to sea floor spreading, etc.), the following interpretations are subject to uncertainty and must be considered preliminary. More detailed petrography coupled with statistical analyses of the existing data are still needed.

The dusky brown, nannofossil-radiolarian-clay oozes of the Clipperton cyclic unit may have higher amorphous scattering percentages than the underlying stratigraphic units (Figures 9, 11, 13 and 15). This tendency was more obvious in Leg 8 sites (Cook and Zemmels, 1971). As in Leg 8, the amorphous material consists mainly of radiolarian tests, amorphous iron oxides and, to a lesser degree, brown palagonite. The cyclic unit in Leg 8, which was a north-south cruise across the equator, had lower amorphous scattering percentages near the equator than north or southward away from the equator. This latitudinal variation in the percentage of amorphous scattering in the cyclic unit of Leg 8 suggested that the sites closest to the equatorial high productivity belt have been diluted by calcareous biota. The cyclic unit in Leg 9 Sites 77, 79, 81, 82 and 83 which are near the equator have amorphous scattering percentages similar to Leg 8 Sites 71, 72 and 73 which are also near the equator. However, the Leg 9 Site 78, which is 8 degrees north of the equator, does not have extremely high amorphous scattering percentages; this is not consistent with a simple equatorial dilution hypothesis.

The brown coloration in the beds of the cyclic unit rich in "red clay" is probably due to several things—amorphous iron oxide, palagonite, kaolinite, and montmorillonite. Petrographic examination of these sediments during the Leg 9 cruise showed that much of the brown material consists of dark, reddish-brown particles about 2 to 5 microns in diameter with a mean refractive index which appears to be greater than 2.0. These particles are apparently X-ray amorphous. Also, some of the brown material, as in Site 79, was identified during the Leg 9 cruise as palagonite in various stages of devitrification. X-ray analyses show montmorillonite and phillipsite present in the cyclic unit at Site 79 (Figures 14 and 16). The phillipsite, and possibly the montmorillonite, represent devitrification products of this volcanic material.

The origin of the kaolinite in the cyclic unit is uncertain. Kaolinite is a characteristic constituent in the cyclic unit and its common general covariance with quartz and plagioclase at Sites 77 and 78 (Figures 10, 12) suggests an eolian origin (Rex and Goldberg, 1962). There was insufficient data to judge covariances at other Leg 9 sites.

Before the origin of the cyclic unit can be comprehensively resolved, a sampling program directed specifically toward its origin is needed. In addition, we must know the latitudinal positions of Leg 8 and 9 sites during the Miocene through Pleistocene in the framework of sea floor spreading. The "geologic fences," within which any hypotheses regarding the origin of the cyclic unit are briefly discussed by Cook, are found in Chapter 22, this volume.

The varicolored unit of the Clipperton Oceanic Formation is characterized by interbedded siliceous and calcareous oozes that display brilliant shades of purple and green. The purple color is probably due to some form of manganese. Petrographic examination of smear slides shows that this material coats the surfaces of radiolarians and occurs as silt-and sand-sized grains. No manganese minerals were detected in the X-ray analyses and the material may either be some form of amorphous manganese oxide or the concentrations were below our detectable threshold. Concentrated amounts of this material are currently being prepared for X-ray and chemical analyses.

At Leg 8 Sites 71, 72 and 73, the varicolored unit resembles the cyclic unit in its high content of quartz,

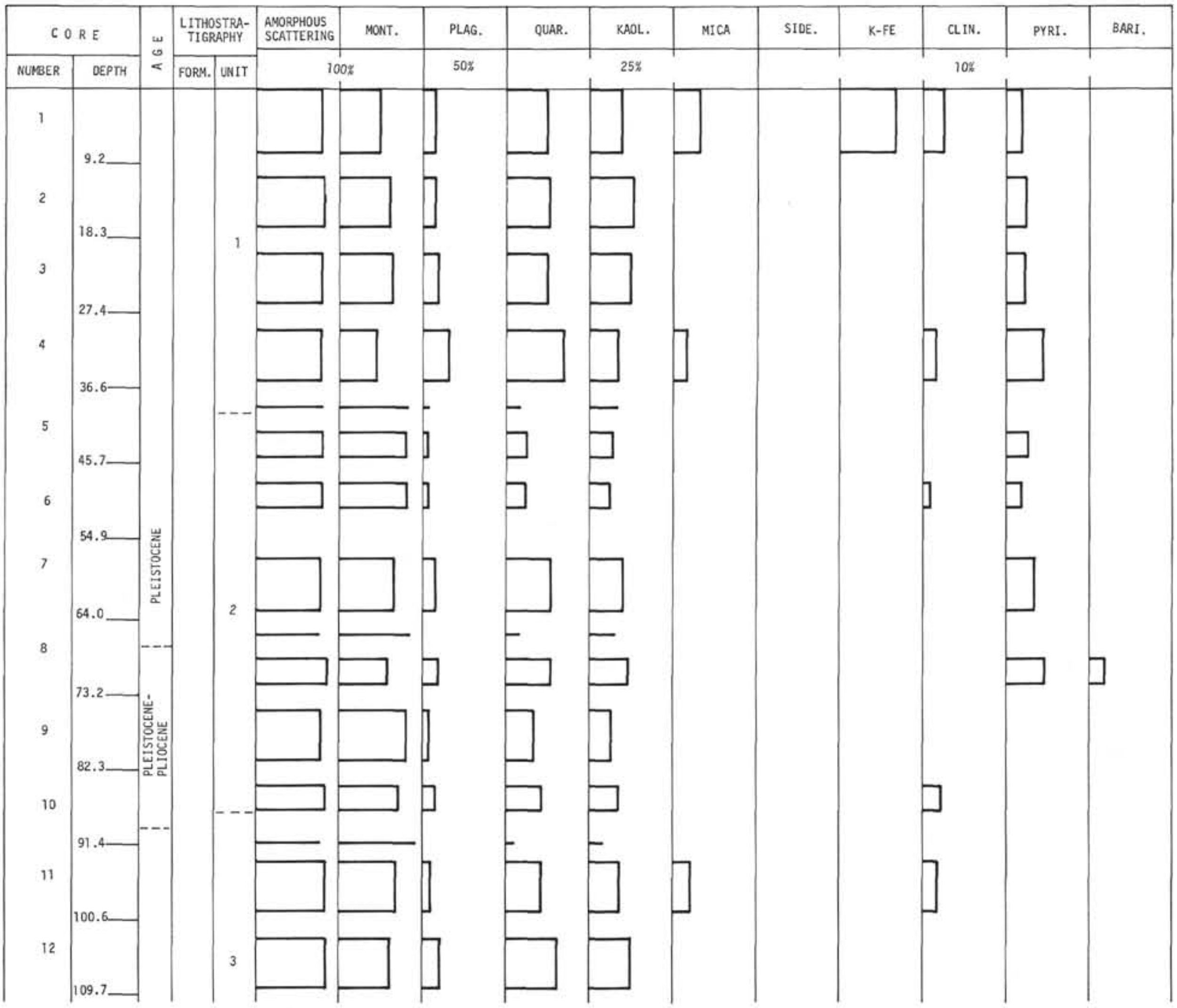

Figure 32. *Hole 84,* $<2\mu$.

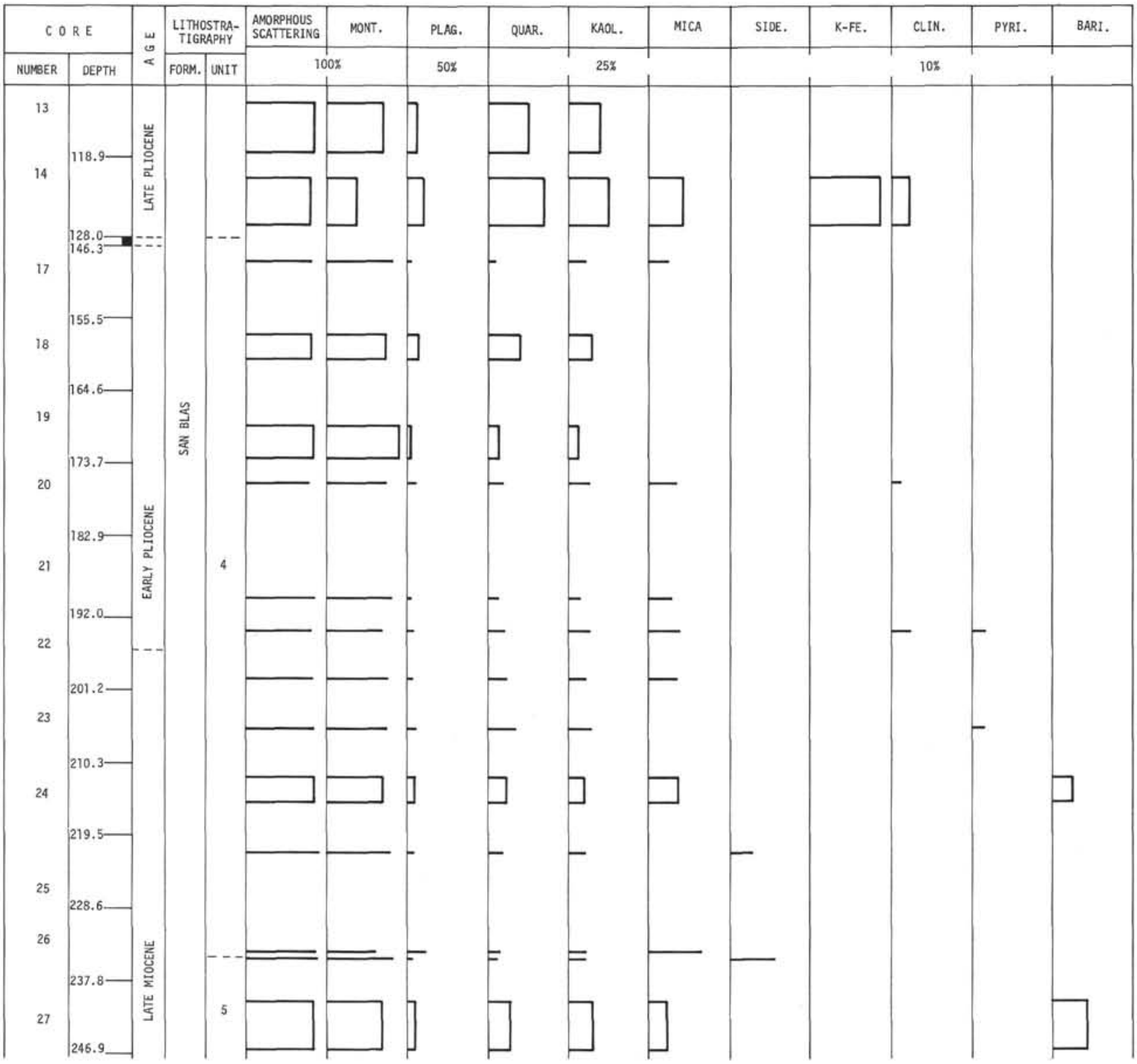

Figure 32. *Continued*

plagioclase, K-feldspar, and kaolinite. Eastward, however, this mineral suite is less abundant while the montmorillonite and amorphous content increase (Figures 14, 16, 20, Leg 8; Figures 10, 14, 18, 22, Leg 9). Petrographic examination of the sediments during Leg 9, indicates that volcanic shards and pumice fragments increase to the east. This vitroclastic material is in various stages of devitrification to a clay, and possibly accounts for the eastward increase in montmorillonite and at least some of the increase in amorphous materials.

The Marquesas Oceanic Formation has a very high calcium carbonate content. This is a characteristic feature of the Marquesas, as it is higher than the overlying Clipperton or underlying Line Islands. Generally, the decalcified <2 micron fraction of the Marquesas has a large content of quartz, plagioclase, mica and kaolinite except at Site 79 where it consists exclusively of montmorillonite and barite. The montmorillonite frequency increases eastward and exceeds the frequency of mica and kaolinite occurrence at Sites 70 and 77 through 80. As in the overlying Clipperton, petrographic examination of the sediments suggests that volcanic shards and pumice fragments increase eastward. Much of this volcanic material is devitrifying, at least in part, to montmorillonite. This may account for the eastward increase in montmorillonite.

Quartz and plagioclase co-vary fairly well at Leg 8 Sites 69 through 72 and 80, but not well at Leg 8 Sites 73 and 74 nor at Leg 9 Sites 77 and 78. The increase of volcanic constituents to the east may overshadow the eolian quartz and plagioclase in the Marquesas Oceanic Formation in Leg 9 sites.

The San Blas Oceanic Formation is restricted to the eastern sites of Leg 9 (81 through 84). It is easily distinguished from the other formations by its green colors (Cook, 1971a). This formation is further characterized by having abundant volcanic ash and euhedral crystals of sanidine, quartz, plagioclase, oxyhornblend, and pyroxenes. At Site 84 the sedimentation rate increases upward through the section. This upward increase in sedimentation rate is due to the increased eolian-derived pyroclastic materials which reached a peak in the Pleistocene. This increase in pyroclastic material upward is seen not only in thin section but is demonstrated in the bulk X-ray analyses (Figure 31). There is a direct correlation between the amount of volcanic glass and montmorillonite, kaolinite, plagioclase, quartz, and clinoptilolite (Figure 31). The green coloration is due to abundant green montmorillonite which appears to be the dominant authigenic mineral forming from the devitrification of the pyroclastic shards and pumice fragments. The clinoptilolite is also probably forming from the ash. Whether or not the kaolinite and chlorite found in the upper portions of the formation are authigenic is not known (Figures 31 and 32).

The widespread, diachronous Line Islands Oceanic Formation has been recognized at Leg 8 Sites 69 through 74 and at Leg 9 Sites 77, 78, 80 through 83. Its chief characteristics are its dusky brown to pale orange color and its stratigraphic position directly above basalt) (Plate 1, in pocket). The variable "red clay" content, which is responsible for its brown color, is mainly amorphous iron and manganese oxides (Cook, 1971b). The only iron minerals detected in this formation are geothite at Leg 8 Site 74 and siderite at Leg 9 Site 80 (Figure 18). The widespread occurrence of this facies further substantiates the suggestion by Bostrom and Peterson (1966, 1969) that during the formation of new basaltic basement at sea floor spreading centers exhalations of iron and manganese-rich solutions probably occur. This formation is further discussed by Cook (Chapter 22, this volume). The goethite and siderite are interpreted to be authigenic. Other minerals in this formation which are also probably authigenic include clinoptilolite, barite and montmorillonite (Figure 9). Tridymite euhedra which were identified during the Leg 9 cruise line the interior walls of some foraminaferal tests. Its abundance is too small to be resolved on the X-ray diffractograms.

Both zeolites, phillipsite and clinoptilolite occur in Leg 9. Site 76, which is located about 100 kilometers northeast of the Tuamotu volcanic Archipelagos, has very abundant phillipsite with lesser amounts of clinoptilolite. These zeolites and the accompanying montmorillonite are authigenic. Palagonite is very abundant in these sediments and is probably supplying the necessary cations and silica for these authigenic silicates. This palagonite is probably derived from basaltic islands to the west. The dominance of the low-silica zeolite phillipsite over the silica-rich zeolite clinoptilolite is to be expected, as the type of zeolites that form from volcanic rocks often bear a close relation to the silica content of the altered volcanic material (Hay, 1966). Likewise at Site 84, where rhyolitic glass is very abundant, the silica-rich zeolite clinoptilolite is the only zeolite detected.

The iron bearing mineral goethite is also present in the reddish-brown sediments at Site 76. Whether or not the goethite is authigenic or detrital is not known. In either case goethite, along with palagonite and probable amorphous iron oxides are giving these sediments their reddish brown color.

Again, as in Leg 8, the ubiquitous occurrence of barite forms an interesting problem. It occurs throughout the eastern equatorial Pacific, across both sides of the East Pacific Rise, and in sediments ranging from Eocene to

Pleistocene in age. Leg 8 and 9 cores may provide an excellent suite of materials to study the origin of barite in deep sea environments.

Dolomite is rare and was only detected in a few Leg 9 samples.

REFERENCES

Bostrom, K. and Peterson, M. N. A., 1966. Precipitates from hydrothermal exhalations on the East Pacific Rise. *Econ. Geol.* 61, 1258.

———, 1969. The origin of aluminum-poor ferromanganoan sediments in areas of high heat flow on the East Pacific Rise. *Marine Geol.* 7, 427.

Cook, H. E., 1971. Iron and manganese rich sediments overlying oceanic basaltic basement, equatorial Pacific, Leg 9, D.S.D.P., (Abst), *Geol. Soc. Am. Spec. Paper.* (in press).

Cook, H. E., and Zemmels, I., 1971. X-ray mineralogy studies–Leg 8, in Sutton, G. H. *et al,* 1971. *Initial Reports of Deep Sea Drilling Project, Volume VIII,* Washington (U.S. Government Printing Office), 901.

Hay, R. L., 1966. Zeolites and zeolitic reactions in sedimentary rocks. *Geol. Soc. Am. Spec. Paper 85.*

Meischner, K. D., 1964. Allodapische kalke, turbidite in riffe-nahen sedimentation-becken. In A. H. Bouma and A. Brouwer *et al. Turbidites.* (Elsevier), 156.

Rex, R. W. and Goldberg, E. D., 1962. Insolubles. **In** *The Sea.* M. N. Hill (Ed.). New York (Interscience) **1**, 295.

Rex, R. W., Eklund, W. A. and Jamieson, I. M., 1971. X-ray mineralogy studies Leg 6, in Fischer, A. G. *et al.* 1971. *Initial Reports of the Deep Sea Drilling Project, Volume IV,* Washington (U.S. Government Printing Office), pp. 691-708.

Tracey, J. I. *et al.,* 1971. *Initial Reports of the Deep Sea Drilling Project, Volume VIII,* Washington (U.S. Government Printing Office).